REACTIONS OF THE IRON(III) HYDROXO DIMER WITH INORGANIC LIGANDS

PhD Thesis

Gábor Lente

Supervisor: Dr. István Fábián

University of Debrecen
Faculty of Science
Debrecen, 2001

REACTIONS OF THE IRON(III) HYDROXO DIMER WITH INORGANIC LIGANDS

PhD Thesis

Gábor Lente

Supervisor: Dr. István Fábián

University of Debrecen
Faculty of Science
Debrecen, 2001

Ezen értekezést a Debreceni Egyetem TTK *Kémiai* Doktori Iskola *koordinácós kémiai* programja keretében készítettem a Debreceni Egyetem TTK doktori (PhD) fokozatának elnyerése céljából.

Debrecen, 2001. augusztus 21

a jelölt aláírása

Tanúsítom, hogy *Lente Gábor* doktorjelölt 1997 – 2001 között a fent megnevezett Doktori Iskola *koordinációskémiai* programjának keretében irányításommal végezte munkáját. Az értekezésben foglalt eredményekhez a jelölt önálló alkotó tevékenységével meghatározóan hozzájárult. Az értekezés elfogadását javasolom.

Debrecen, 2001. augusztus 21.

a témavezető aláírása

Az alma a sötétben is lefelé esik.

The direction apples fall is toward the ground – even in the dark.

Moldova György: Az ideális hadifogoly (1995)

Moldova György: The ideal prisoner of war (1995)

Acknowledgment

Before beginning the scientific part of this dissertation, the author would like to express his acknowledgment to the people who have helped him.

First of all, I would like to thank my supervisor, *Prof. István Fábián*, for working with me patiently since 1994, introducing me into the theory and practice of chemical kinetics, and using his inexhaustible creativity to advance my scientific career.

I would also like to thank

- ☺ *Prof. James H. Espenson* for inviting me to spend a year in his laboratory in Ames, Iowa, for his professional and personal advice.
- ☺ *Dr. Elizabeth Maria Alfonso Magalhães* and *Ms. Zsuzsa Hadady* for taking part in the research summarized in this PhD thesis.
- ☺ *Ms. Katalin Biró* and *Dr. Attila Nemes* for their indispensable practical help.
- ☺ *Dr. David W. Lahti* for his personal and professional help, suggestions and comments on this dissertation.
- ☺ *Dr. Andreja Bakac*, *Dr. Josemon Jacob*, *Prof. David T. Richens*, *Ms. Zsuzsanna Tóth*, and *Dr. Wei-Dong Wang* for their professional and personal support and insightful discussions.
- ☺ *Prof. István Bányai*, *Dr. Attila Bényei*, *Dr. Zoltán Berente*, *Dr. Ilia A. Guzei*, *Prof. Róbert Király*, and *Mr. Béla Rózsa* for help at certain stages of various projects.
- ☺ group members in Debrecen, Hungary from 1994 to 2001: *Mr. Zsolt Balázs*, *Mr. Viktor Bán*, *Mr. Viktor Csordás*, *Mr. Tibor Deczki*, *Mr. Árpád Ferencz*, *Mr. Levente Fodor*, *Ms. Tímea Fodor*, *Ms. Zita Katona*, *Ms. Ildikó Kerezsi*, *Mr. Zsolt Körtvélyesi*, *Ms. Csilla Rácz*, *Mr. Zsolt Szíjgyártó*, *Ms. Dóra Szűcs*, *Mr. János Török (Nico)*, and *Mr. János Török (Sowy)*.
- ☺ group members in Ames, Iowa in 1999: *Dr. Kimberley A. Brittingham*, *Dr. Ruili Huang*, *Mr. William Lam*, *Dr. Peter Metelski*, *Mr. Xiao-Peng Shan*, *Dr. Saša Stanković*, *Dr. Haisong Tan*, *Mr. Douglas Tak Yiu*, and *Dr. Ying Wang*.

I would also like to thank a number of Hungarian public foundations, Magyar Vidékért Alapítvány, Universitas Alapítvány, a Magyar Tudományos Akadémia Debreceni Akadémiai Bizottsága, Tehetséges Debreceni Fiatalokért Alapítvány, Bognár Rezső Alapítvány, Magyar-Amerikai Közös Tudományos Alap, for their financial support throughout the years I spent as an undergraduate and PhD student.

Finally, I would like to thank my family, especially my wife, Kata, my parents and my brother, Zsolt, for their patience and encouragement.

Table of Contents

1. Introduction

Iron is the most abundant transition element in the solar system and on the earth. One of its stable nuclei (^{56}Fe) is the most stable nucleus of the periodic table because it has the highest bonding energy per nucleon. Therefore, the formation of iron was energetically quite favorable during the nucleogenesis explaining its abundance in the universe. Iron is the fourth most abundant element (after oxygen, silicon and aluminum) in the crustal rocks of the earth (6.2 %). It is believed to be the main constituent of the core of the earth and is the major component of 'siderite' meteorites. About 0.5% of lunar soil is known to be metallic iron, which gives an estimate of ~ 10^{12} tons of iron on the surface of the moon alone. In the oxidative atmosphere of the earth iron mostly occurs in the oxidation state of +3.

Iron has been known to humankind for at least six millennia. The first man-made objects were created from metallic iron recovered from meteorites. Iron production by smelting began sometime in the third millennium BC in the Hittita empire in Asia Minor, but the secret of the technology was guarded so carefully that iron production only became widespread around 1200 BC. The following historical period, Iron Age, was named after the element. Besides making tools and weapons, the metal has been used as a construction material for a long time. The iron pillar (weight: 6.5 tons, height: 6.7 meters) close to the famous Qutab Minar in the courtyard of the Quwwat-ul-Islam mosque in Delhi, India, was transported to its present place in the fourth century AD, although it may have been built a thousand years before. It has survived without any signs of rusting, which is more than remarkable especially in the humid local climate. This phenomenon is still not completely understood. The immense cultural impact of the metal is also shown by the fact that it is one of the few chemical elements for which words of different origin exist in various (not closely related) languages implying that this element was independently discovered and used by different ancient nations.* Today the annual world production of iron is close to 10^9 tons.

* A few examples: ferrum (Latin), Eisen (German), железо 'zhelezo' (Russian), σίδηρος 'sidiros' (Greek), rauta (Finnish), vas (Hungarian), járn (Icelandic), burdina (Basque), demir (Turkish), chuma (Swahili), khilla (Quechuan), besh (Navajo), rino (Maori), الصلب 'ḥadiid' (Arabic), 鉄 'tetsu' (Japanese), 鐵 'tie' (Chinese), अयसः 'ayasaH' or लोह 'loha' (Sanskrit).

Iron is classified as essential in biological systems. It has been a key metal in the evolution of life from primitive bacteria and algae to higher organisms. A human being contains as much as 3–4 g of iron on average in various forms including hemoglobin in blood cells, ferritin and transferrin for iron storage and transport, the efficiency of which is spectacularly demonstrated by the very long biological half life of the element (8 years, much longer than the corresponding value of 9 months for bone-forming calcium). The major function of iron in these proteins is often some kind of electron transfer or the activation of small molecules, especially dioxygen, which is due to its advantageous redox chemistry. Iron(III) is often found in biological systems in oxo- or hydroxo-bridged di- or oligonuclear structures. Numerous enzymes with dinuclear iron(III) centers have been described with various functions in living organisms (Table 1).[1-3] One of the most important such enzymes is methane monooxygenase, the function of which is to insert an oxygen atom into a C–H bond of an alkane at ambient temperatures. This function attracts considerable industrial attention as well. Structural motifs found in these enzymes can be used to design protein-free dinuclear iron(III) catalysts that are effective in various processes.[4-8] Understanding the way these enzymes and catalysts work requires fundamental information on the dinuclear iron(III) core.

The complexes of iron(II) and iron(III) have played major roles in understanding the mechanisms of substitution and redox processes.[9-14] The first studies were usually motivated by basic interest in fundamental aqueous processes. Today the biological relevance is probably the main driving force of research in this field. Iron(III) is known to feature a marked preference for O-donor as opposed to N-donor ligands. Due to its high-spin d^5 configuration, the crystal field stabilization energy does not favor any particular stereochemistry, and iron(III) complexes with coordination numbers from 3 to 8 are known.[9]

Almost all cations with a charge +3 or higher give rise to polynuclear species in aqueous solution over a characteristic pH range. This hydrolytic polymerization is characteristic of aqueous iron(III) solutions as well. It is well established that the mononuclear hydrolytic species are important in the kinetics and mechanism of the substitution and redox reactions of iron(III), and are often much more reactive than the aqua ion itself. It seems to be quite reasonable that polynuclear hydrolytic complexes may also have similar roles, but this field received much less attention compared to the investigation of mononuclear forms. Reliable information on aqueous dinuclear iron(III) forms and their reactivity patterns could be beneficial for

Table 1. Diiron oxygen proteins.

enzyme	source	function
class I ribonucleotide reductase	bacteria, bacteriophages, some eukaryotic cells	reduction of ribonucleotides to deoxyribonucleotides
methane monooxygenase	methanotrophic bacteria	conversion of methane to methanol
purple acid phosphatases	mammals	phosphatase activity, details unclear
soluble stearoyl-acyl carrier protein Δ^9 desaturase	higher plants, e.g. cucumber, spinach, avocado	catalyst of the first step in lipid desaturation
ferritin[a]	mammals, plants, bacteria	iron storage
hemerythrin, myohemerythrin	marine invertebrates	oxygen transfer
rubrerythrin, nigerythrin	anaerobic bacteria	possible catalyst of reactions involving peroxides and oxygen, details unclear
nitric oxide reductase	bacteria	reduction of NO to N_2O

a: contains multinuclear iron centers as well

the ongoing studies on the biological role of iron(III) in addition to holding considerable interest for the mechanistic research of inorganic reactions. Studies in this field may shed light on the formation of dinuclear iron(III) cores and contribute to the understanding of the basic kinetic features of di- and multinuclear iron(III) complexes.

2. Research Objectives

The major goal of the present study was to characterize the kinetics and equilibrium of direct ligand substitution reactions of the aqueous iron(III) hydroxo dimer, $Fe_2(\mu\text{-}OH)_2(H_2O)_8^{4+}$,* with simple inorganic ligands and draw structural and mechanistic conclusions from the results.

In order to achieve this goal, a main objective was to identify the inorganic ligands that react with the hydroxo dimer directly and to study the identified reactions in detail. Exact description of the equilibria in aqueous iron(III) solution is prerequisite to these investigations. Some of the literature results are contradictory on the equilibrium and kinetics of the hydrolytic processes and a detailed study was designed to resolve these contradictions.

A further objective was to explore the possible role of the iron(III) hydroxo dimer in redox reactions between iron(III) and inorganic species. A detailed study of the redox reaction was planned in the iron(III) – sulfur(IV) system because of its outstanding significance.

* Iron(III) complexes are assumed to be octahedral in this work and coordinated water molecules will not be shown in the formulas for clarity throughout the rest of the text unless they have particular significance.

3. Literature Overview

The hydrolysis of iron(III) has been studied for a long time by various methods and researchers. The results have been reviewed several times.[15-20]

The structure and composition of mononuclear forms has been characterized with a large variety of techniques. The equilibrium between mononuclear forms was studied by pH-potentiometry[21-23] and spectrophotometry,[24-31] and the structure of the aqua complex $Fe(H_2O)_6^{3+}$ was characterized by single crystal X-ray diffraction (XRD) in a nitrate salt[32] and alums.[33,34] Extended X-ray absorption fine structure (EXAFS),[35] neutron diffraction,[36] neutron scattering,[37] and solution X-ray scattering[38] studies on the mononuclear iron(III) forms have all been reported. Theoretical investigations have also been carried out to describe the interaction between iron(III) centers and the surrounding oxygen atoms in simple complexes.[39-42] Isotope effects,[29] pressure and ionic strength effects[43] on the mononuclear equilibrium were studied as well as the photodissociation of the hydrolytic species,[44-46] and cohydrolysis of $Fe(H_2O)_6^{3+}$ with divalent metal ions.[47]

General studies on the hydrolytic oligomerization and/or precipitation of iron(III) showed that very slow and practically irreversible processes may begin even at relatively low pH (~ 3).[48-52] Some of these processes last very long excluding the possibility of reliable equilibrium studies. This phenomenon is generally referred to as ageing. Indeed, the ageing of one such iron(III) solution was monitored over a period of 15 years.[52]

Investigations on the dinuclear hydrolytic species have not been free of ambiguity. The stoichiometry $Fe_2(OH)_2^{4+}$ has been established beyond any reasonable doubt based on pH-potentiometric[20-22] and UV-vis spectrophotometric[27,30] studies independently.* However, the structure of this species could be either dihydroxo-bridged, $(H_2O)_4Fe(\mu\text{-}OH)_2Fe(H_2O)_4^{4+}$, or monooxo-bridged, $(H_2O)_5Fe(\mu\text{-}O)Fe(H_2O)_5^{4+}$. The difference between these two structures is only a water molecule, thus they are indistinguishable by composition. The magnetic properties of the dinuclear species were also the subject of intense scientific discussion. Claims for diamagnetic[26] and paramagnetic[53] behavior were both made. This debate seems to have reached a conclusion with agreement on a paramagnetic $Fe_2(OH)_2^{4+}$ with some

* The formula $Fe_2(OH)_2^{4+}$ is adapted for the dinuclear hydrolytic species in this work despite the contradictions about the structure. The formula is meant to indicate the composition only.

spin-spin interaction between the metal centers. The question of dihydroxo- or monooxo-bridging structure still lacks decisive evidence, although the dihydroxo formulation has been strongly favored by most solution chemists, one of the most convincing arguments being the existence of the well characterized, inert, dihydroxo-bridged chromium(III) analog $Cr_2(OH)_2^{4+}$.[54-58]

Oligomeric species, such as $Fe_3(OH)_4^{5+}$[22] or $Fe_{12}(OH)_{34}^{2+}$[59] were also reported in the literature. Some of these oligomeric species, especially the tetrahydroxo trinuclear complex, may be present in equilibrium at very high total iron(III) concentrations, but the detection of higher oligomers could also be a computational artefact arising from data sets not in true equilibrium. It is notable that such higher oligomers are always postulated based on pH-potentiometry, but no UV-vis spectrophotometric evidence has been reported for them thus far. A reason for this could well be the different sensitivity of the two methods, but it should be kept in mind that the pH-potentiometric studies usually involve titration of an iron(III) solution with base and local inhomogenities, particularly under less acidic conditions, may initiate irreversible processes during this procedure. This problem was sometimes circumvented by the use of $NaHCO_3$ solution as a titrant, which seems to be more suitable for pH-potentiometric titration of iron(III) solutions.[22] However, this technique adds the problem of possible incomplete removal of the carbon dioxide formed. In any case, the applicability of pH-potentiometry is limited because iron(III) solutions cannot usually be brought above 2.7–3.0 without initiating irreversible processes.

The solution structure of $Fe_2(OH)_2^{4+}$ was characterized with EXAFS in the late 70s and the structure shown in Scheme 1 was proposed.[60] The distance between the two iron(III) centers was calculated to be 291 pm, with an Fe–O–Fe angle of 101°. However, the authors failed to realize that only a few percent of the total iron concentration was in the form $Fe_2(OH)_2^{4+}$ in their solutions. The discrepancies in this work were pointed out,[61] and the criticism led to a re-evaluation and full retraction of the EXAFS study.[62] However, the fact that EXAFS should be quite sensitive to the

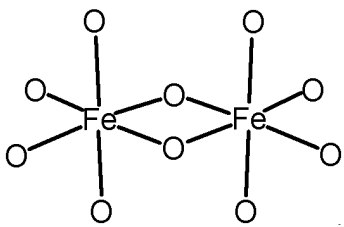

Scheme 1. Proposed structure for the iron(III) hydroxo dimer (hydrogens are excluded for clarity)

shortest Fe–Fe distance in solution because of the high product of the atomic numbers seems to have been ignored in this dispute. In addition, the EXAFS structural data are in excellent agreement with XRD studies on $Fe_2(\mu\text{-}OH)_2$ cores in the dihydroxo-bridged diiron(III) complexes $Fe_2(\mu\text{-}OH)_2(Dipic)_2$,[63] $Fe_2(\mu\text{-}OH)_2(Chel)_2$,[63] and $Fe_2(\mu\text{-}OH)_2(Sal)_2 \cdot 2H_2O \cdot 2py$,[64] and on the analogous trivalent metal cores $Cr_2(\mu\text{-}OH)_2(H_2O)_8^{4+}$,[55] and $Al_2(\mu\text{-}OH)_2(H_2O)_8^{4+}$ [65] (formulas for ligands are given in Scheme 2). A second re-evaluation of the original EXAFS study,[60] or preferably a complete re-investigation is thus needed.

A combined Mössbauer and IR spectroscopy study led to postulating a diamagnetic, monooxo-bridged structure for $Fe_2(OH)_2^{4+}$.[66] However, this study was

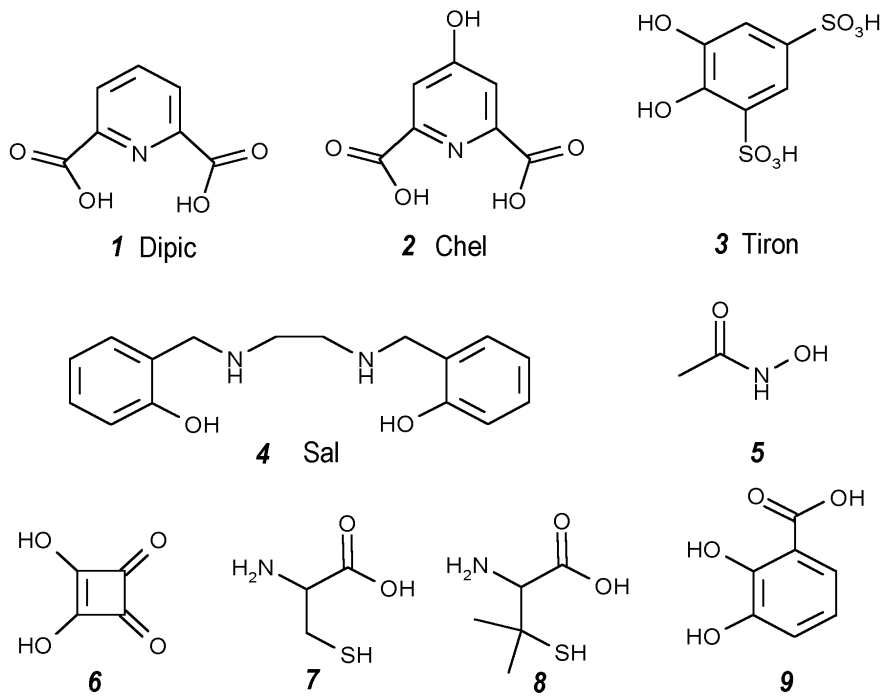

Scheme 2. Chemical structures of organic ligands referred to in the text. ***1*** Dipic = 2,6-pyridinedicarboxylic acid, ***2*** Chel = 4-hydroxy-2,6-pyridinedicarboxylic acid, ***3*** Tiron = 1,2-dihydroxy-3,5-benzenedisulfonic acid ***4*** Sal = *N*,*N*'-ethylenebis(salicylamine), ***5*** acetohydroxamic acid, ***6*** squaric acid = 3,4-dihydroxy-3-cyclobutene-1,2-dione, ***7*** cysteine, ***8*** penicillamine, ***9*** 2,3-dihydroxybenzoic acid

seriously flawed. The authors used direct addition of base to the iron(III) solutions and did most of their experiments in basic solution, a practice that should clearly be avoided because of the tendency of iron(III) to form colloidal hydroxide phases irreversibly. The formation of the dinuclear species is assumed to be guaranteed by setting a suitable Fe/OH ratio without considering the equilibrium features. In addition, the Mössbauer spectra were recorded in frozen solutions, and few considerations were offered on the significance of the results for the solution structure. Finally, little effort was made to identify what parts of the signal came from mononuclear and multinuclear forms of iron(III). Further Mössbauer studies led to diverse conclusions.[67-70] One study proposed an equilibrium between the dihydroxo- and monooxo-bridged forms with the former being somewhat dominant in solution.[69] Another published work interpreted the Mössbauer data assuming the dihydroxo-bridged structure only.[70]

A later combined EXAFS and Mössbauer study on a neutralized Nafion membrane was interpreted in terms of a monooxo-bridged structure with an Fe–O–Fe angle of 155° and a Fe–Fe distance of 342 pm.[71] Although the mononuclear and dinuclear forms were clearly distinguished in this work, the experimental procedure was similar to the one in the mentioned combined Mössbauer-IR study[66] and could be a significant source of error. It is again questionable whether the data are conclusive for solution structure. The bridging Fe–O distance in the dinuclear species was calculated to be 30 pm shorter than the non-bridging Fe–O distances in the same species, which is a suspiciously unusual finding. In fact, data obtained by Mössbauer spectroscopy resulted in more confusion than insight probably because the method itself is unsuitable for answering these structural questions.

Magnetic measurements suggested that there is some spin-spin interaction between the high spin iron(III) centers in the dinuclear species. An early study found $Fe_2(OH)_2^{4+}$ diamagnetic.[26] However, a more careful reinvestigation of the system reached the opposite conclusion: $Fe_2(OH)_2^{4+}$ is paramagnetic with a magnetic moment roughly equivalent to 2 unpaired electrons per iron center.[53] This is also in line with magnetic studies on model compounds featuring the dihydroxo-bridged core with organic ligands.[63,72,73] Considerations based on the magnetic properties also lent some support to the dihydroxo-bridged formulation for $Fe_2(OH)_2^{4+}$. The value of $\mu_{eff} \sim 3.7$ BM (Bohr Magneton) is much larger than the values measured for monooxo-bridged diiron(III) complexes, but similar to those of dihydroxo-bridged complexes. In addition, IR spectroscopic investigations confirmed the absence of a characteristic

ν(Fe–O–Fe) band,[53] which is arguably the strongest piece of evidence against the monooxo-bridged structure known to date.

It is now understood that the contradictions concerning the properties of $Fe_2(OH)_2^{4+}$ largely arise from the fact that it is never a dominant species in solution. It amounts to no more than 10–15% of the total iron concentration, and it is always accompanied by large amounts of mononuclear forms, the properties of which are often quite similar to the dinuclear species. Thus, any measured physical property of an iron(III) solution has contributions from mono- and dinuclear forms. The contribution of the dinuclear form is not always easy to identify, and is often small compared to that of the mononuclear forms because of the unfavorable concentration ratio. Another problem is imposed by the lability of iron(III) complexes. Any procedure which is necessary to carry out structural studies, including freezing or crystallization, could result in an immediate change in speciation or formation of new species. It should also be added that experimental limitations, such as the significance of using special chloride-free solutions and avoiding the direct addition of base to test solutions, were not recognized in many of the earlier studies.

In summary, the available structural information is more in line with the dihydroxo-bridged structure, a conclusion also reached in a review on dinuclear oxo-bridged iron(III) complexes.[74] In our studies the properties of $Fe_2(OH)_2^{4+}$ have been interpreted assuming the dihydroxo-bridged structure exclusively.

A vast amount of kinetic information on the mononuclear forms of iron(III) is available from the literature. The kinetics of substitution reactions between mononuclear forms of iron(III) and a large number of inorganic and organic ligands were studied.[75-99] Temperature and pressure dependent investigations were also reported.[90-92] Water exchange on the metal center was studied with ^{17}O NMR even under high pressures.[93-95] The electric field jump relaxation kinetic technique yielded some information on the deprotonation kinetics of mononuclear forms.[96]

Very limited information is available on the reactions of the hydroxo dimer. Its dissociation into mononuclear forms was studied by several groups,[100-105] and a mechanism comprising two pathways was proposed.[100] The shortcomings of this mechanism will be discussed in detail later (section 5.1.2., page 25).

Direct reactions of the hydroxo dimer were postulated with four organic ligands (Table 2).[106-108] The formulas of the ligands are given in Scheme 2 (page 9). In these reactions Fe_2L type complexes are formed and their formation constants could be estimated. Iron(III) oxidizes squaric acid, penicillamine, and cysteine, thus

Table 2. Complexation between the hydroxo dimer and organic ligands. $T = 25.0$ °C; $\mu = 1.0$ M ($NaClO_4$).

ligand	reaction	log K	ref
squaric acid	$Fe_2(OH)_2^{4+} + L^{2-} = Fe_2(OH)_2L^{2+}$	5.18	106
tiron	$Fe_2(OH)_2^{4+} + H_2L = Fe_2(OH)_xLH_x^{4+}$	3.80	107
cysteine	$Fe_2(OH)_2^{4+} + H_3L = Fe_2(OH)_2L^{3+} + 2H^+$	−1.15	108
penicillamine	$Fe_2(OH)_2^{4+} + H_3L = Fe_2(OH)_2L^{3+} + 2H^+$	−0.42	108

the dinuclear complexes are formed as intermediates with these ligands. It could be shown that the dominant final product in the tiron system was a mononuclear iron(III) complex and the corresponding Fe_2L complex barely exists when the equilibrium is reached.[107] Several possibilities were considered for the structure of Fe_2L complexes, but none of them could find any support other than chemical intuition. A fortunate aspect of this research was the fact that Fe_2L complexes with those four ligands have strong characteristic absorption bands in the visible wavelength range, and they could be studied without interference from other colored species.[106-108] It was also concluded that $[Fe^{3+}]^2$ terms established earlier in the rate equations of iron(III) reactions is due to the reactivity of the hydroxo dimer.[107] Earlier, it was proposed that the hydroxo dimer reacts with acetohydroxamic acid[109] and 2,3-dihydroxybenzoic acid,[110] but mononuclear complexes were postulated as the direct products of these reactions. The second-order rate constants for the reactions of $Fe_2(OH)_2^{4+}$ with various protonated forms of the ligands are in the range of $10^3 - 10^5$ $M^{-1}s^{-1}$ at 25 °C.

While the present work was in progress, two articles were published where the authors postulated direct reactions with the hydroxo dimer.[111,112] However, their results are questionable in that fast pre-equilibrium or steady state approaches are used for the hydroxo dimer. These assumptions are not justified by independent data on the formation and dissociation kinetics of $Fe_2(OH)_2^{4+}$.[100-105] The authors seem to be unaware of this error, they even believed to find support from a study[100] that actually directly contradicts their interpretation.

The presence or absence of the hydroxo dimer as a product was occasionally used as evidence in favor of or against a particular mechanism where iron(III) is produced in redox reactions. For example, aqueous oxidation of iron(II) by ozone is thought to involve an iron(IV) (ferryl) intermediate, FeO^{2+}, which reacts with Fe^{2+}

very rapidly to give $Fe_2(OH)_2^{4+}$.[113] A similar mechanism was proposed for the iron(II) – hypochlorous acid reaction where $Fe_2(OH)_2^{4+}$ was formed as an immediate product.[105] The absence of the formation of $Fe_2(OH)_2^{4+}$ led to the conclusion that the oxidations of iron(II) by H_2O_2 and ClO_2^- involve one-electron steps.[105,114]

A very large number of oxo- or hydroxo-bridged di- and multinuclear iron(III) complexes are known in the solid state with various spectral and magnetic properties.[74,115-130] Although some of these species may be related to the hydroxo dimer in some ways, the existence of these multinuclear structures is typically the consequence of using multidentate, chelating, and bridging ligands. It is also not quite clear how relevant the solid state structures are for aqueous species. The presence of such multinuclear complexes is not proved in the solution phase.

It is notable that perchlorate ion is also thought to be coordinated to iron(III) centers in certain cases based on internuclear distances measured in the solid state by XRD.[131] Similar interactions are occasionally proposed in solution at high concentrations of the perchlorate medium (e.g. 3.0 M $NaClO_4$) either directly[132] or indirectly to explain the unusual sensitivity of the equilibrium constants to ionic strength.[59] This interaction is sometimes termed outer sphere complexation.[132] However, the proposal is based on unconvincingly small UV-vis spectroscopic changes. It is also doubtful if outer sphere complexation is a meaningful concept in this case, as the H_2O/ClO_4^- ratio is ~ 16 in 3.0 M $NaClO_4$, and at least one perchlorate ion should be present in the outer coordination sphere of the metal ion on a purely statistical basis even if the electrostatic forces are ignored between the oppositely charged iron(III) and perchlorate ions. In addition, none of these studies reported that appropriate precautions were made in order to avoid specific effects of chloride ion which could very well be present as a contaminant. Chloride ion is a common impurity in perchlorate salts, including iron(III) and sodium perchlorate. It is also known to be a fairly good complexing agent toward iron(III) and the complex $FeCl^{2+}$ has a characteristic UV-vis absorption band.[24] Even if the interaction with perchlorate is real, it has never been reported in 1.0 M $NaClO_4$, the medium used in this study. A recent review on inorganic perchlorato complexes reported very few examples of purely inorganic iron(III) perchlorato complexes.[133]

4. Experimental Methods

4.1. Chemicals

Chemicals used in this study were of analytical reagent grade and purchased from various commercial suppliers. Low chloride iron(III) perchlorate (Aldrich, color: very pale violet) was used without further purification. The iron(III) concentration of the stock solutions was determined by the iodometric method, the free acid concentration was determined by acid-base titration following ion exchange.[76,134] No ageing effects were observed in the iron(III) stock solutions during the entire study, i.e. the results were the same using freshly prepared and a few weeks old samples. Samples were always prepared from the stock solutions with dilution and/or acidification. Addition of base to iron(III) solutions to adjust the pH was completely avoided.

High purity concentrated $HClO_4$ was purchased from Carlo Erba and Reanal. Dilute perchloric acid solutions were standardized by acid-base titration. High purity $NaClO_4$ (Fluka) was recrystallized from water before use or prepared form Na_2CO_3 and $HClO_4$ according to a literature method.[135] All solutions were prepared with doubly deionized and ultrafiltered water obtained from MILLI-Q RG (Millipore) water purification system. Experiments were carried out at 10.0 ± 0.1 and 25.0 ± 0.1 °C, the ionic strength was set to 1.0 M with $NaClO_4$.

Other chemicals used in this work included $Na_2B_4O_7 \cdot 10H_2O$, $NaHCO_3$, NaN_3, $NaNO_2$, $NaNO_3$, $NaH_2PO_2 \cdot H_2O$, H_3PO_3, $Na_2HPO_3 \cdot 5H_2O$, $Na_2HPO_4 \cdot 2H_2O$, As_2O_3, $Na_2HAsO_4 \cdot 7H_2O$, NaSCN, $Na_2S_2O_3 \cdot 5H_2O$, $Na_2S_2O_4$, Na_2SO_3, $Na_2SO_4 \cdot 10H_2O$, $K_2S_2O_8$, H_2SeO_3, H_2SeO_4, $NaClO_2$, $NaClO_3$, NaCl, $NaBrO_3$, NaBr, $NaIO_3 \cdot H_2O$, $NaIO_4$, CrO_3, $Na_2MoO_4 \cdot 2H_2O$, $Na_2WO_4 \cdot 2H_2O$, $NaCH_3COO$, 4,5-dihydroxy-1,3-benzenedisulfonic acid disodium salt (tiron), and citric acid. Stock solutions of arsenic(III) were prepared by dissolving a weighed quantity of primary standard As_2O_3 in NaOH and neutralizing this solution with $HClO_4$.[136] All other ligands were soluble in pure water. The stock solution prepared from $K_2S_2O_8$ was converted to a solution of $H_2S_2O_8$ by cation exchange. Stock solutions prepared from $Na_2HPO_4 \cdot 2H_2O$, $Na_2HAsO_4 \cdot 7H_2O$, H_3PO_3, Na_2SO_3, and H_2SeO_3 were standardized by acid-base titration before use to confirm that direct measurements based on weighing were suitable for preparing stock solutions with known concentrations.

4.2. Equilibrium Studies

Equilibrium studies involved the use of UV-vis spectroscopic and pH-potentiometric methods. UV-vis spectra were recorded on a HP-8543 diode array and a Unicam Helios-α scanning spectrophotometer. Quartz cells with optical path lengths of 1 cm, 2 mm and 1 mm were used. A GK2401C combination electrode (filled with NaCl as an inner electrolyte) was used for pH-potentiometric measurements with a PHM85 pH-meter (Radiometer). Buffers used for calibration were in agreement with IUPAC recommendations.[137] The pH-meter readings were converted into $[H^+]$ in the pH range 2–12 using the method published by Irving.[138] In some cases, it was necessary to extend pH-potentiometric measurements to the pH range 1–2 with special point-by-point calibrating functions.[139]

4.3. Kinetic Studies

The HP- 8543 diode array spectrophotometer was used in the kinetic mode for some experiments with manual mixing in a divided quartz cell (optical path length 2 × 0.435 cm). An Applied Photophysics RX2000 Rapid Kinetics Spectrometer Accessory with a pneumatic drive unit, operating based on the principles of the stopped flow method, was also used connected to the HP spectrophotometer to obtain spectral data as a function of time. The minimum time needed to record a single full spectrum with the HP spectrophotometer was 0.1 s.

It should be added that the shape of the kinetic traces were dependent on the pH of the reactant iron solutions used in the experiments (prior to mixing) as well as the pH of the final reaction mixtures. This observation will be interpreted later (section 5.1.2., page 25 and section 5.2., page 30). The pH of the original iron solutions (pH_{Fe}) and the pH of the final mixtures (pH) will both be given in figure captions to indicate the experimental conditions unambiguously.

4.3.1. Stopped Flow Method

The overwhelming majority of kinetic measurements were performed with an Applied Photophysics SX-18 MV Stopped Flow Reaction Analyser using 10 and 2 mm optical path lengths. A photomultiplier tube with a time resolution of ~ 5 μs was used as a detector for most of the measurements. A PD.1 Photodiode Array Accessory (PDA) was also used in a few experiments. The intensity of the light source in the spectral region of interest made it necessary to use integrating time of 10 ms for the PDA. The baseline calibration was usually repeated every 5 - 6 hours of continuous operation for both detectors. The stopped flow instrument was used in both conventional (two-component) and sequential mode. The general flow scheme of the instrument is shown in Figure 1.

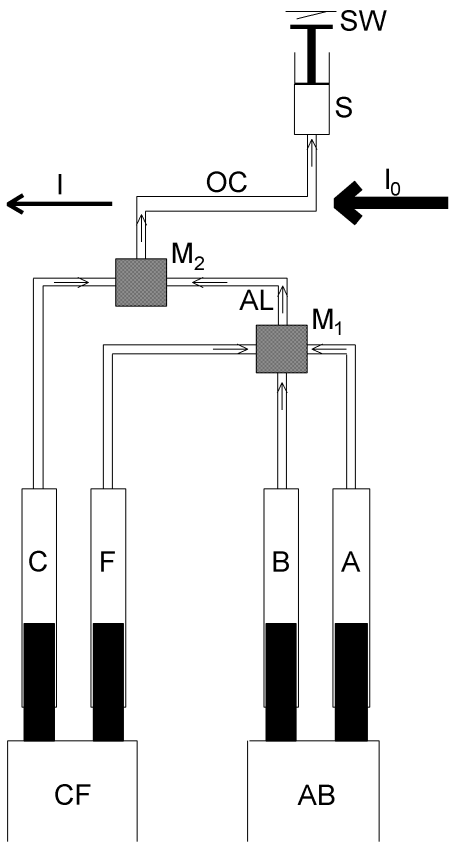

Figure 1. Flow scheme of the stopped flow instrument. A, B, C, F: syringes; AB, CF: rams; AL: ageing loop; M_1, M_2: mixers, OC: optical cell; S: stop syringe; SW microswitch; I_0: incident light beam; I: exiting light beam.

In a conventional stopped flow experiment, syringes C and F are filled with the reagents. Ram CF pushes the plungers of the syringes pneumatically, thus forces the reagents through mixer M_2, fills the cell (OC) and the stop syringe (S). When the plunger of the stop syringe reaches the microswitch (SW), the resulting trigger signal starts the detection.

The sequential stopped flow technique is suitable for studying the reactions of unstable species. In this mode, syringes A and B are filled with solutions that generate the unstable species of interest, syringe C is filled with the other reagent, and syringe F is filled with a flush liquid, usually the medium of the reaction. At first, ram AB pushes the plungers and fills the ageing loop (AL) through mixer M_1 with a 1:1 mixture of solutions A and B. Ram AB has a fixed moving distance, thus the flow is stopped before the stop syringe (S) is filled up totally. After a pre-set interval, in a conventional stopped flow phase ram CF mixes the content of the ageing loop with reagent C through mixer M_2 thus starts the reaction between the *in situ* prepared reactant and C, fills up the stop syringe (S) and starts the detection. As seen, solution F is only used to push the content of the ageing loop from mixer M_1 to mixer M_2. The system is calibrated so that the flow stops before the flush solution reaches mixer M_2. It should be added that sequential stopped flow experiments are very time consuming, especially at low temperature. When it was possible, conventional stopped flow measurements were performed with reagents freshly prepared prior to the kinetic run.

The stopped flow instrument was calibrated and its performance was regularly tested. The working characteristics were determined experimentally. The dead time (t_d) is arguably the most important parameter of the stopped flow instrument. This is defined as the time during which the reaction proceeds undetected, or in a more technical definition, as the time required for the reaction mixture to reach the optical cell (OC) from mixer M_2. The dead time thus imposes a practical limit on the rate of reactions measurable by the stopped flow instrument. Processes complete within the dead time will be referred to as *instantaneous* reactions in the following sections.* During the time interval of the work reported in this thesis, the dead time was determined four times using a literature method.[140] Its value was between 1.09 and 0.89 ms with a standard error of ± 0.02 ms in each determination.

* The term '*instantaneous*' is used in this context to indicate that no kinetic information can be obtained by the stopped flow method. The kinetics of reactions called instantaneous here could be measurable by other methods with better time resolution.

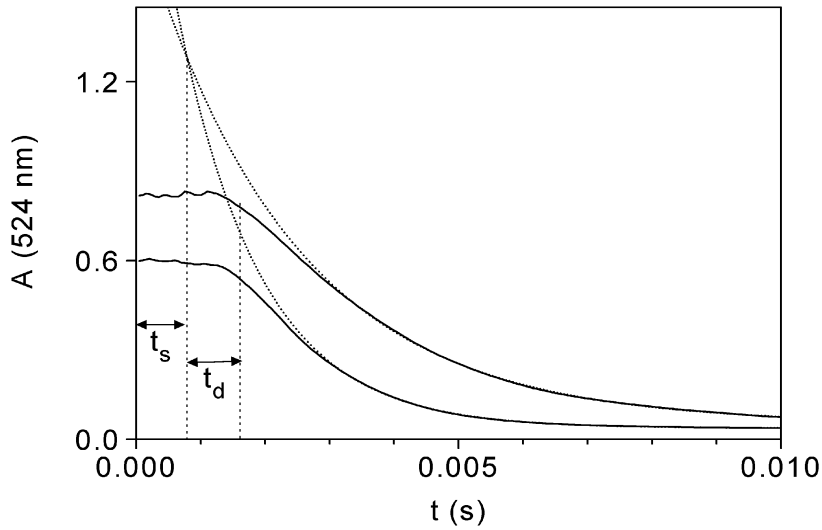

Figure 2. Typical stopped flow absorbance traces in the dichloro-indophenol (DCIP) – ascorbic acid system used for calibration. Dotted lines represent exponential fits to the evaluable parts of the curves (> 3 ms). [DCIP] = 0.5 mM; [asc] = 20.0 mM and 10.0 mM; pH = 1.70; T = 25.0 °C; μ = 0.2 M (NaCl); optical path length 1 cm.

The time shift (t_s) is another important parameter. This is due to the fact that the detection does not start exactly at the time of mixing in a stopped flow experiment. When an estimation of the actual initial absorbance is needed, the measured kinetic curve should be extrapolated back to the time point defined by the time shift. A method to determine the time shift was developed earlier.[141] Its value was between 0.69 and 0.85 ms (standard error: ± 0.04 ms) in four separate calibrations in agreement with the value of ~ 1 ms given by the instruction manual.[142] It should be noted that in principle t_d is dependent on the speed at which the plungers move and consequently on the pressure of the pneumatic drive system. Because the instrument always operates at constant drive pressure, t_d is also considered to be constant in this work.

The effect of dead time and time shift on the kinetic curves are shown in Figure 2. This figure displays kinetic curves detected in the dichloro-indophenol – ascorbic acid system used for calibration.[140] Stopped flow curves always have a flat, horizontal region at the beginning (first ~ 1.5 ms in Figure 2). This is because the flow is not stopped in that region, and consequently the measured absorbance reflects

the principles of continuous flow measurements. There is a poorly defined region unsuitable for data treatment between ~ 2 and 3 ms, most probably due to the mechanical shock caused by stopping the flow of reagents.

The occurrence of a reaction within the dead time can conveniently be tested.[143] This test involves a comparison of the initial absorbance value (extrapolated if needed) with the sum of the independently known initial absorbance contributions of the reagents. A difference between the two values that is larger than experimentally acceptable confirms the existence of at least one instantaneous reaction. Such an observation will be referred to as initial absorbance jump throughout this dissertation.

Several improvements on the calibration and performance of stopped flow instruments can be found in the literature, most of them seeking the extension of the stopped flow method to measure higher rate constants.[143-148] Carefully selected conditions allow the direct determination of second-order rate constants as large as 10^8 $M^{-1}s^{-1}$ in some cases.[144] The effect of mixing inhomogenities is being studied and inhomogenity within the cell can also be taken into account.[148] The use of these improved methods is only important at high reaction rates (pseudo first-order rate constant over 500 s^{-1}). The applicability of the correction methods and their interpretation led to thorough discussions between the researchers working in this field. In this study, it was possible to avoid the problem of high reaction rates through lowering the temperature, and none of the correction methods needed to be used.

Stopped flow experiments also have an upper time limit, although this is rarely mentioned in the literature. The flow scheme in Figure 1 (page 17) shows that the cell is open to the reagent and stop syringes during the measurement. Thus, linear diffusion may corrupt the kinetic curves on longer time scales. Experimental methods to test this possible source of error have been developed and it was shown that the stopped flow instrument used in this study is suitable for recording kinetic curves reliably up to 200 s.[149] Kinetic traces recorded by the stopped flow method over longer time scales will only be shown as illustrations in this dissertation, such curves were not used for the quantitative evaluation of the kinetic models.

4.4. Data Analysis

The software package PSEQUAD was used to evaluate equilibrium data.[150] The software package SX-18 MV provided with the stopped flow instrument was used for simple evaluation of kinetic curves. The software package SCIENTIST was used for general linear and nonlinear least squares fitting.[151]

Acceptable evaluation of kinetic data was not always possible using the traditional kinetic methods based on pseudo first-order rate constants. In these cases, direct fitting to an appropriate kinetic model was used. The kinetic model was represented by simultaneous ordinary differential equations, which were integrated using methods suitable for handling *stiff* systems with the differential equation solvers of the software packages SCIENTIST[151] and ZiTa.[152] Free parameters were estimated by minimizing the difference between the calculated and measured absorbance – time traces using the nonlinear least squares fitting algorithms in the softwares mentioned. Parameters known from independent sources were fixed, i.e. their values were not allowed to float throughout the minimizing procedure. Forced values were used for certain parameters. This means that the values of these parameters were not known independently, but they could be calculated from free and fixed parameters using an explicit expression, such as the relationship between forward and reverse rate constants and the corresponding equilibrium constant.

Table 3. Summary of data used for kinetic analysis at 10.0 °C.

system	[Fe(III)] (mM)	[L] (mM)	pH	number of kinetic traces [a,b]
P(I)	2.6 – 10	0.1 – 1.5	0.5 – 1.9	33
P(III)	2.6 – 10	0.1 – 1.5	0.3 – 1.9	20
P(V)	3 – 35	0.02 – 2.0	0.7 – 1.9	23 [c]
As(V)	2.0 – 60	0.04 – 1.0	0.7 – 2.3	40
S(IV)	5.0 – 35	0.3 – 1.5	1.1 – 1.9	48 [d]
S(IV) [e]	33 – 70	0.3 – 2.0	0.9 – 1.6	21
Se(IV)	2.6 – 10	0.1 – 1.5	0.3 – 2.1	32

a: at least 400 individual points on a each kinetic trace; b: each trace is the average of at least 5 replicate runs; c: 340 and 370 nm simultaneously; d: 340 and 430 nm simultaneously; e: 25.0 ° C

Estimated values for fitted parameters are quoted with one σ as a standard error throughout this work. Calculated values of forced parameters are given without standard errors. Error bars on graphs are only shown if they are very significantly different for various points inside the same graph. The data sets summarized in Table 3 were used for detailed kinetic analysis in the iron(III) – ligand systems.

Singular value decomposition for matrix rank analysis (MRA)[153-160] was carried out by the software Matlab.[161] As matrix rank analysis results are of secondary importance in this work, and were only used to obtain supporting evidence, residual methods were not used.[159] Statistical tests on the significance of singular values were not used for the same reason.

This study makes extensive use of initial rates, which were always determined as initial rates of absorbance change based on stopped flow traces. The effect of dead time was taken into consideration, appropriate polynomial or exponential extrapolating functions were used.[162] Although absorbance is a dimensionless physical quantity, the unit abbreviated as AU (absorbance unit) will be employed in a few cases in this work to emphasize the use of absorbance values for calculating certain quantities, most importantly initial rates.

5. Results and Discussion

5.1. Hydrolysis of Iron(III)

5.1.1. Equilibria

In agreement with literature results,[21,22,27] our UV-vis measurements indicated that the following equilibria need to be taken into account in dilute, acidic solutions of iron(III) under the conditions pH = 0.3–2.5, [Fe(III)] < 0.1 M:

$$Fe^{3+} = FeOH^{2+} + H^+ \qquad K_1 = \frac{[FeOH^{2+}][H^+]}{[Fe^{3+}]} \qquad (1)$$

$$Fe^{3+} = Fe(OH)_2^+ + 2H^+ \qquad K_2 = \frac{[Fe(OH)_2^+][H^+]^2}{[Fe^{3+}]} \qquad (2)$$

$$2Fe^{3+} = Fe_2(OH)_2^{4+} + 2H^+ \qquad K_3 = \frac{[Fe_2(OH)_2^{4+}][H^+]^2}{[Fe^{3+}]^2} \qquad (3)$$

The equilibrium constants determined in the present study are summarized in Table 4. Some literature data are also given for comparison. We could not determine K_2 directly in our spectrophotometric studies, similarly to other studies.[24-31] This is because $Fe(OH)_2^+$ is not present in appreciable concentrations at pH < 2.5 and thus gives a negligible contribution to the UV-vis spectra. However, it was also confirmed by our studies that the dihydroxo complex may have a significant

Table 4. Equilibrium constants for the hydrolysis of iron(III). μ = 1.0 M ($NaClO_4$).

K_1	K_2	K_3	T (°C)	Method	ref
−3.03 ± 0.05	−6.7 [b]	−2.98 ± 0.02	10.0	UV-vis	a
−2.72 ± 0.04	−6.29 [c]	−2.86 ± 0.03	25.0	UV-vis	a
−2.73	−6.29	−3.20	25.0	pH	22
−2.80	–	−2.72	25.0	UV-vis	27
−3.05 [d]	−6.33 [d]	−2.92 [d]	25.0	pH	21

a: this work; b: estimated based on the value measured at 25.0 °C and the standard enthalpy of reaction; c determined by Khoe et al. (ref. 22); d: μ = 3.0 M ($NaClO_4$); UV-vis: UV-vis spectrophotometry; pH: pH-potentiometry

contribution to the overall kinetics in the reactions of iron(III). In these cases, we used the K_2 value determined by Khoe and coworkers[22] with pH-potentiometry at 25.0 °C. A value calculated from the equilibrium constant at 25.0 °C and the estimated standard enthalpy of reaction was used at 10.0 ° C.[163,164] We could find no evidence for further hydrolytic species under our conditions. Matrix rank analysis (section 5.6., page 41) proved that the number of absorbing species is 3 in the iron(III) hydrolytic experiments in agreement with the interpretation presented above.

For the purposes of the kinetic studies the overall mononuclear iron concentration [Fe_{mn}] is introduced here:

$$[Fe_{mn}] = [Fe^{3+}] + [FeOH^{2+}] + [Fe(OH)_2^{+}] \quad (4)$$

The calculated UV-vis spectra of Fe^{3+}, $Fe(OH)^{2+}$, and $Fe_2(OH)_2^{4+}$ are shown in Figure 3.* It is seen that $Fe_2(OH)_2^{4+}$ is the dominant absorbing species in the near UV region. Calculations show that it is typically responsible for 60–90% of the overall absorbance around 340 nm. This gives rise to an interesting point: the variation in the absorbance at around 340 nm corresponds primarily to the

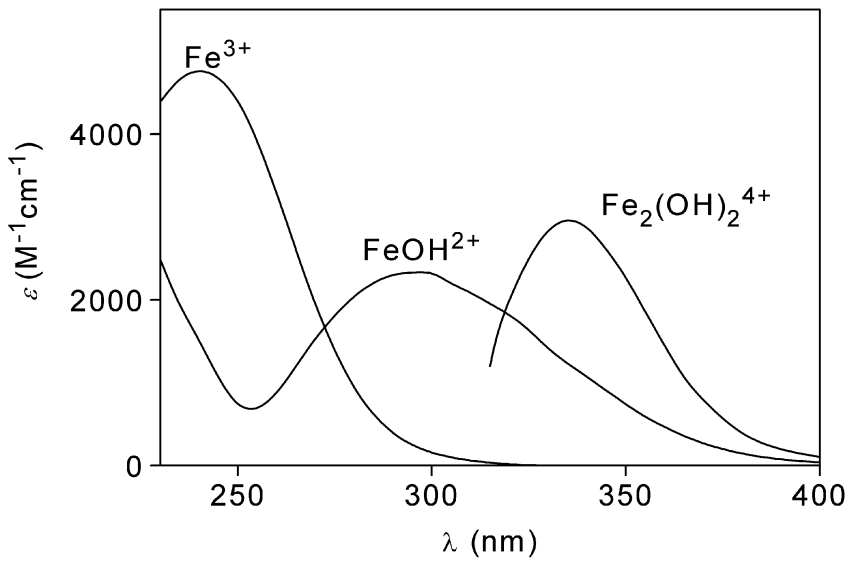

Figure 3. Calculated UV-vis spectra of iron(III) aqua- and hydroxo complexes. T = 10.0 ° C; μ = 1.0 M ($NaClO_4$).

* Contrary to common beliefs, $Fe(H_2O)_6^{3+}$ has only a very pale violet color. The familiar yellow color of iron(III) solutions is always due to the presence of hydrolyzed forms or the chloro complex, $FeCl(H_2O)_5^{2+}$. It should also be noted that iron(III), because of its d^5 electronic configuration, has no spin-allowed d-d transitions and all the absorption bands in this study are charge transfer bands.

Table 5. Molar absorbances for hydrolytic iron(III) species. T = 10.0 °C; μ = 1.0 M ($NaClO_4$)

$Fe_2(OH)_2^{4+}$	340 nm	2760 ± 180 $M^{-1}cm^{-1}$
$Fe_2(OH)_2^{4+}$	370 nm	630 ± 40 $M^{-1}cm^{-1}$
$Fe_2(OH)_2^{4+}$	430 nm	45 ± 5 $M^{-1}cm^{-1}$
$FeOH^{2+}$	340 nm	700 ± 50 $M^{-1}cm^{-1}$
$FeOH^{2+}$	370 nm	160 ± 10 $M^{-1}cm^{-1}$
$FeOH^{2+}$	430 nm	0

concentration change of the hydroxo dimer in aqueous iron(III) solutions providing an ideal way for monitoring the reactions of $Fe_2(OH)_2^{4+}$ (cf. page 11). Molar absorbances for $Fe_2(OH)_2^{4+}$ and $FeOH^{2+}$ at specific wavelengths used in the kinetic evaluation are listed in Table 5.

5.1.2. Kinetics

Reactions 1 and 2 are very fast; these proton transfer reactions are likely to be diffusion controlled or nearly so. Literature results show that reaction 1 is too fast to be measured with electric field jump relaxation, whereas the same method yielded 6.1×10^4 s^{-1} and 8.0×10^9 $M^{-1}s^{-1}$ for the forward and reverse rate constants for the reaction $FeOH^{2+} = Fe(OH)_2^{+} + H^{+}$ at 25 °C and low ionic strength.[96] Reactions 1 and 2 can thus be treated as fast equilibria for the purposes of the present study.

The dissociation and formation of $Fe_2(OH)_2^{4+}$ can conveniently be studied by the stopped flow method. When iron(III) solutions are diluted or acidified, first-order kinetic traces are observed in a wide range of metal ion concentrations. For the interpretation of these observations, two opposite effects need to be considered. When an iron(III) sample is diluted in these experiments, the total concentration of iron(III) drops to half of its original value and simultaneously the pH increases by 0.3. The concentration change favors the dissociation of $Fe_2(OH)_2^{4+}$ while the pH change alone would lead to the formation of more hydroxo dimer. The net effect is usually a small increase in the concentration of the hydroxo dimer. When the iron(III) sample is mixed with acid, both the concentration and pH jumps lead to the dissociation of the hydroxo dimer.

The first-order kinetic curves were interpreted by Sommer and Margerum in a detailed kinetic study as follows:[100]

$$Fe_2(OH)_2^{4+} = 2Fe_{mn}$$

$$v_H = k_H[Fe_2(OH)_2^{4+}] + k_{-H}[Fe_{mn}]^2 \quad (5)$$

In this equation, k_H and k_{-H} are pH-dependent rate constants. With standard relaxation treatment of the kinetic data (i.e. a concentration jump experiment) it can be shown that this process will lead to pseudo first-order kinetic behavior under all real conditions and the pseudo first-order rate constant, k_{hdr}, is expressed as:

$$k_{hdr} = k_H + 4k_{-H}[Fe_{mn}] \quad (6)$$

Strictly speaking, $[Fe_{mn}]$ should refer to equilibrium concentration in this formula. However, this concentration changes only very slightly and the variation in $[Fe_{mn}]$ is practically negligible throughout the process, because only a small portion of iron(III) is present as the hydroxo dimer. Based on the pH-dependence of k_{hdr}, Sommer and Margerum proposed a mechanism with 2 pathways to interpret the observations.[100] The first pathway is a direct dissociation of the dimer into two monohydroxo monomers:

$$Fe_2(OH)_2^{4+} = 2FeOH^{2+}$$

$$v_7 = k_7[Fe_2(OH)_2^{4+}] - k_{-7}[FeOH^{2+}]^2 \quad (7)$$

The second pathway is proton-assisted:

$$Fe_2(OH)_2^{4+} + H^+ = FeOH^{2+} + Fe^{3+}$$

$$v_8 = k_8[Fe_2(OH)_2^{4+}][H^+] - k_{-8}[FeOH^{2+}][Fe^{3+}] \quad (8)$$

The following formula can be given for k_{hdr} based on equations 7–8:

$$k_{hdr} = k_7 + k_8[H^+] + \frac{4[Fe_{mn}]K_1}{(K_1 + [H^+])^2}(k_{-7}K_1 + k_{-8}[H^+]) \quad (9)$$

Sommer and Margerum determined the rate constants k_7, k_8, k_{-7}, k_{-8}, and proposed a mechanism for the reaction (Scheme 3, page 29, upper two rows).[100] They also noted some discrepancy between the equilibrium and kinetic data, i.e. the fitted values of k_{-7} and k_{-8} were about 5 times higher than the ones calculated from the fitted forward rate constants, k_7 and k_8, and the independently determined equilibrium constants, K_1 and K_3.

Equation 9 predicts that the rate constants should increase linearly with increasing $[Fe_{mn}]$ at constant pH, and the intercepts (k_H) should decrease with increasing pH. Figure 4 shows our results in a somewhat extended pH range. The intercepts clearly increase with increasing pH at pH > 1.8 indicating that an additional step should be taken into account. This step is inversely proportional to the hydrogen

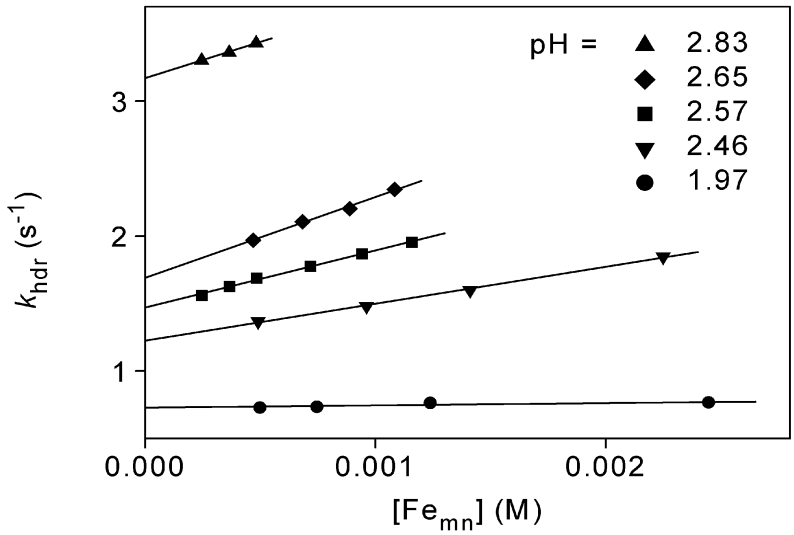

Figure 4. Experimental rate constants as a function of mononuclear iron(III) concentration. T = 25.0 °C; μ = 1.0 M ($NaClO_4$).

ion concentration and formulated as a fast proton loss from $Fe_2(OH)_2^{4+}$ followed by the dissociation of the dinuclear species in the rate determining step:

$$Fe_2(OH)_2^{4+} = H^+ + Fe_2(OH)_3^{3+}$$

$$Fe_2(OH)_3^{3+} = FeOH^{2+} + Fe(OH)_2^{+}$$

$$v_{11} = k_{11}[Fe_2(OH)_2^{4+}]/[H^+] - k_{-11}[FeOH^{2+}][Fe(OH)_2^{+}] \quad (11)$$

With the addition of this new pathway the pseudo first-order rate constant k_{hdr} can be expressed as:

$$k_{hdr} = k_7 + k_8[H^+] + \frac{k_{11}}{[H^+]} + \frac{4[Fe_{mn}]K_1}{(K_1 + [H^+] + K_2/[H^+])^2}\left(k_{-7}K_1 + k_{-8}[H^+] + \frac{k_{-11}K_2}{[H^+]}\right) \quad (12)$$

Rate constants determined in this work are shown in Table 6. The contributions of the k_{-7} and k_{-8} terms were found to be marginal, and these constants were replaced by $k_7K_3/(K_1)^2$ and k_8K_3/K_1 based on microscopic reversibility. The fit of the data based on the new and old models is compared in Figure 5. The consistency of the model can be tested by calculating $K_3/(K_1K_2)$ from the independently determined kinetic data as

Table 6. Rate constants determined for the decomposition and formation of the iron(III) hydroxo dimer. μ = 1.0 M ($NaClO_4$).

	25.0 °C	10.0 °C	25.0 °C [a]
k_7	0.35 ± 0.02 s^{-1}	0.059 ± 0.004 s^{-1}	0.4 s^{-1}
k_8	3.5 ± 0.1 $M^{-1}s^{-1}$	1.08 ± 0.02 $M^{-1}s^{-1}$	3.1 $M^{-1}s^{-1}$
k_{11}	(3.6 ± 0.2) × 10^{-3} Ms^{-1}	(5.8 ± 0.7) × 10^{-4} Ms^{-1}	–
k_{-7}	1.3 × 10^2 $M^{-1}s^{-1}$ [b]	71 $M^{-1}s^{-1}$ [b]	6.7 × 10^2 $M^{-1}s^{-1}$
k_{-8}	2.5 $M^{-1}s^{-1}$ [c]	1.2 $M^{-1}s^{-1}$ [c]	6.6 $M^{-1}s^{-1}$
k_{-11}	(6.7 ± 1.8) × 10^3 $M^{-1}s^{-1}$	3.3 × 10^3 $M^{-1}s^{-1}$ [d]	–

a: values determined by Sommer and Margerum at μ = 3.0 M ($NaClO_4$) (ref. 100); b: calculated as $k_7K_3/(K_1)^2$; c: calculated as k_8K_3/K_1; d: calculated as $k_{11}K_3/(K_1K_2)$

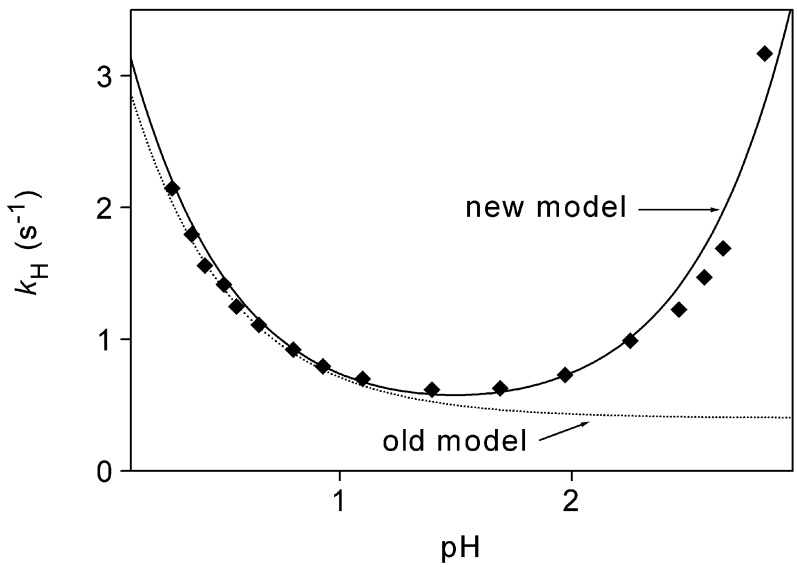

Figure 5. k_H as a function of pH. Solid line: best fit to equation 12; dotted line: best fit to equation 9. T = 25.0 °C; μ = 1.0 M ($NaClO_4$).

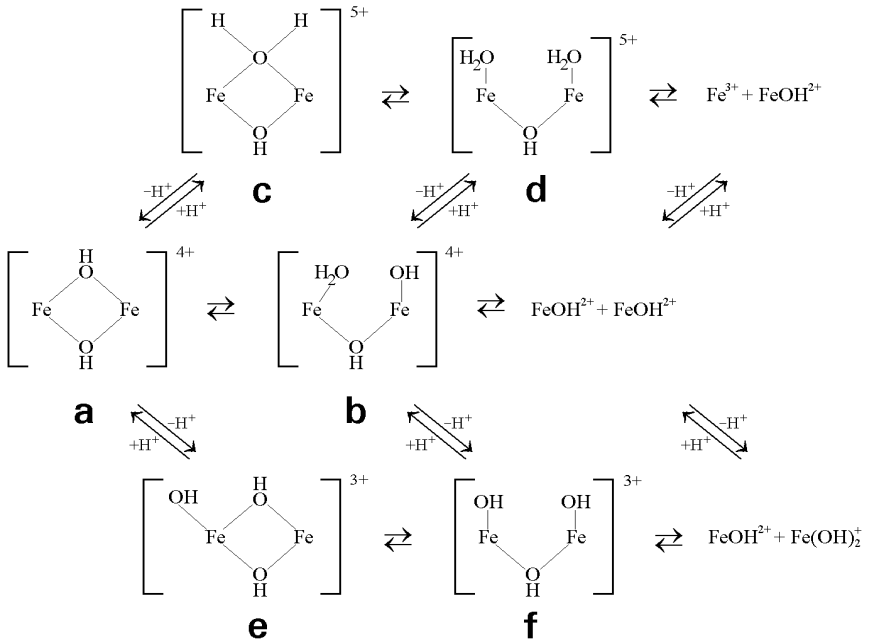

Scheme 3. Proposed mechanism for the decomposition and formation of the iron(III) hydroxo dimer.

k_{-11}/k_{11}. The agreement is excellent, as the expression is calculated to be 1.4×10^6 M^2 from the equilibrium data and 1.8×10^6 M^2 from the forward and reverse rate constants. In accordance with these results, we propose the mechanism shown in Scheme 3 for the hydrolytic reactions of iron(III). This is a straightforward extension of the scheme postulated by Sommer and Margerum.[100] Formally, various rate determining steps can be consistent with the experimentally confirmed rate law. However, it is very likely that whenever one of the two hydroxide ion bridges is broken in the dimer, the two iron(III) moieties dissociate very quickly. Protonation and hydrolysis can break the symmetry of the dimeric structure and accelerate the dissociation of $Fe_2(OH)_2^{4+}$. These considerations imply that the rate determining steps are ***a*** ⇌ ***b***, ***c*** ⇌ ***d***, and ***e*** ⇌ ***f***.

The new pathway implies the formation of $Fe_2(OH)_3^{3+}$ at low, presumably steady state concentration levels. The possible kinetic role of the putative $Fe_2(OH)_3^{3+}$ complex was also proposed for the interpretation of pH-dependent data in complex formation reactions with tiron.[107]

5.2. Test to Confirm the Ligand Substitution Reactions of the Hydroxo Dimer

Preliminary experiments showed that some of the inorganic ligands might react directly with the hydroxo dimer. We developed a simple and quick test to distinguish between ligand substitution reactions of the hydroxo dimer and mononuclear iron(III) species.

The test is based on a comparison of the initial rates measured in two complementary kinetic runs, which are designed to give the same final composition for the reaction mixture. In Type 1 experiments a moderately acidic iron(III) solution ([Fe(III)] = 13.7 mM, $[H^+]$ = 18.6 mM) is mixed with a more acidic solution of the ligand ([L] = 1.0 mM, $[H^+]$ = 49.9 mM). In Type 2 experiments the difference between the acidities of the solutions is considerably smaller ([Fe(III)] = 13.7 mM, $[H^+]$ = 28.7 mM; and [L] = 1.0 mM, $[H^+]$ = 39.8 mM). It can be shown that the initial concentration of $Fe_2(OH)_2^{4+}$ is higher in the first experiment, but all other concentrations including the pH are practically the same. The conditions were chosen so that the initial concentration of $Fe_2(OH)_2^{4+}$ in Type 1 experiments ($[Fe_2(OH)_2^{4+}]_{0,1}$ = 0,20 mM) is exactly twice of that in Type 2 experiments ($[Fe_2(OH)_2^{4+}]_{0,2}$ = 0.10 mM).

Kinetic traces for Type 1 and 2 experiments with two ligands (iodate and arsenate ions*) and without any ligands are shown in Figure 6. Type 1 experiments have higher initial absorbances because the initial concentration of the strongly absorbing $Fe_2(OH)_2^{4+}$ is higher. Type 1 and Type 2 curves have the same final absorbance readings in agreement with the fact that the same final solutions are obtained and the equilibria between the mononuclear and dinuclear forms of iron(III) are reached at the end. As shown in Figure 5, there is also a slow absorbance change in the absence of ligands (hydrolytic experiment), i.e. when the initial iron(III) solution is acidified and diluted. This is due to the dissociation of some $Fe_2(OH)_2^{4+}$ into mononuclear forms (cf. section 5.1.2, page 25).

In the most general case, when both the mononuclear and dinuclear forms of iron(III) react with the ligand, the initial rate of absorbance change can be expressed as:

* The terms sulfite ion, sulfate ion, arsenate ion, etc. are used in a general sense throughout the text to refer to all protonated forms together. The difference between the individual protonated forms will be made only when it is necessary for the clarity of the presentation.

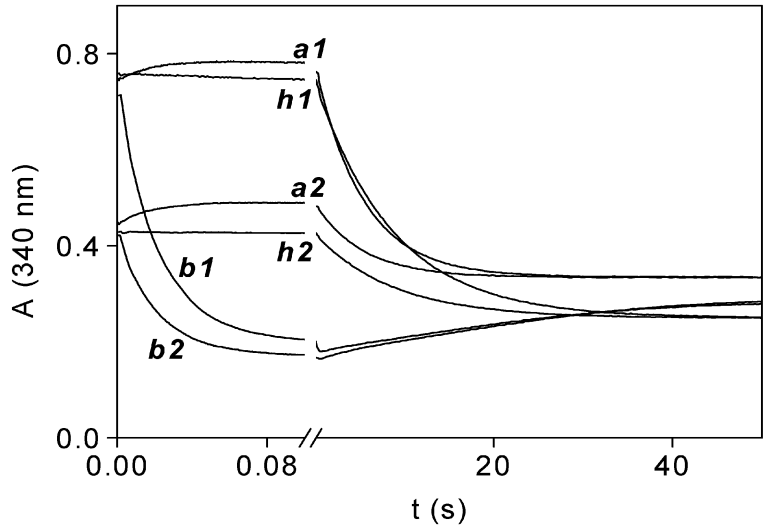

Figure 6. Representative kinetic traces for Type 1 and 2 experiments. Type 1 (***a1***, ***b1***, ***h1***): an iron solution containing [Fe(III)] = 13.7 mM and $[H^+]$ = 18.6 mM mixed with a ligand solution containing [L] = 1.0 mM, $[H^+]$ = 49.9 mM. Type 2 (***a2***, ***b2***, ***h2***): an iron solution containing [Fe(III)] = 13.7 mM and $[H^+]$ = 28.7 mM mixed with a ligand solution containing [L] = 1.0 mM and $[H^+]$ = 39.8 mM. Ligand: ***a1***, ***a2***: IO_3^-; ***b1***, ***b2***: $H_2AsO_4^-$; ***h1***, ***h2***: hydrolytic experiment without ligand. T = 10.0 °C; μ = 1.0 M ($NaClO_4$); optical path length 1 cm.

$$v_i = \frac{dA}{dt}(0) = \Delta\varepsilon_M k_M [Fe_{mn}]_0^{\alpha} [L]_0^{\beta} + \Delta\varepsilon_D k_D [Fe_2(OH)_2^{4+}]_0^{\gamma} [L]_0^{\delta} + \\ + \Delta\varepsilon_H (k_H [Fe_2(OH)_2^{4+}]_0 - k_{-H} [Fe_{mn}]_0^2) \quad (13)$$

where k_M, k_D, k_H and k_{-H} are pH-dependent rate constants; $\Delta\epsilon_M$, $\Delta\epsilon_D$ and $\Delta\epsilon_H$ are the differences between the molar absorptions of products and reactants; α, β, γ, and δ are orders of reactions with respect to the specific component. Note that the ligand may exist in various protonated forms which are assumed to be in fast equilibria. The initial rate v_i can be corrected with the contribution of the hydrolytic path known from independent experiments:

$$v_i' = v_i - \Delta\varepsilon_H (k_H [Fe_2(OH)_2^{4+}]_0 - k_{-H} [Fe_{mn}]_0^2) = \\ = \Delta\varepsilon_M k_M [Fe_{mn}]_0^{\alpha} [L]_0^{\beta} + \Delta\varepsilon_D k_D [Fe_2(OH)_2^{4+}]_0^{\gamma} [L]_0^{\delta} \quad (14)$$

The ratio (r) of the corrected initial rates from Type 1 and 2 experiments is expressed as follows:

$$r = \frac{v_{i1}'}{v_{i2}'} = \frac{\Delta\varepsilon_M k_M [Fe_{mn}]_0^{\alpha} [L]_0^{\beta} + \Delta\varepsilon_D k_D [Fe_2(OH)_2^{4+}]_{0,1}^{\gamma} [L]_0^{\delta}}{\Delta\varepsilon_M k_M [Fe_{mn}]_0^{\alpha} [L]_0^{\beta} + \Delta\varepsilon_D k_D [Fe_2(OH)_2^{4+}]_{0,2}^{\gamma} [L]_0^{\delta}} \quad (15)$$

The value of *r* can be used as a sensitive parameter to confirm the reactions of the hydroxo dimer. There are two limiting cases. When the second term is negligible both in the numerator and denominator, *r* will be 1.0 because $[Fe_{mn}]$ and [L] are practically the same in Type 1 and Type 2 experiments. When the reaction is much faster with the hydroxo dimer, the first term will be negligible and the ratio will be 2^{γ}. When the two terms are comparable, a value between 1.0 and 2^{γ} is expected. It follows that any *r* value significantly different from 1.0 indicates that a direct reaction occurs between $Fe_2(OH)_2^{4+}$ and the ligand.

The test was used with a number of inorganic ligands. Initial rates were determined in stopped flow experiments; the corresponding values of *r* are listed in Table 7. The 340 nm absorption maximum of $Fe_2(OH)_2^{4+}$ was found to be an ideal wavelength for this study. In some cases, the initial rates could not be determined very accurately at this wavelength, and other wavelengths were also used. Ligands which are not stable in acidic solution (carbonate, nitrite, thiosulfate, dithionite, sulfite, and chlorite ions) were tested using the sequential stopped flow technique. In these experiments, the acidic solution of the ligand was generated inside the ageing loop of the stopped flow instrument and used 0.2 s after generation.

Tiron (1,2-dihydroxy-3,5-benzenedisulfonic acid) was reported earlier to react directly with $Fe_2(OH)_2^{4+}$.[107] This conclusion is confirmed by the test presented here. In addition, 9 inorganic ligands (hypophosphite, phosphite, phosphate, arsenite, arsenate, dithionite, sulfite, selenite, and periodate ions) and citric acid are also shown to react with the hydroxo dimer.

Periodate ion seems to be exceptional because the test predicts second-order dependence with respect to $Fe_2(OH)_2^{4+}$ as indicated by the *r* value around 4. The *r* value obtained for arsenite ion (2.96) is practically the same as the ratio of the initial rates measured in hydrolytic experiments (first four rows in Table 7). This will be discussed later in this dissertation (section 5.7.7., page 69). The rest of the ligands seem to react with the hydroxo dimer in reactions that are first-order with respect to $Fe_2(OH)_2^{4+}$.

It should be noted that hypophosphite, arsenite, dithionite, thiosulfate, sulfite, and chlorite ions are involved in redox processes with iron(III), but the contributions of these reactions to the initial rates are negligible under the conditions applied here (section 5.4., page 37).[75,134,165] In several cases including acetate, chlorate, nitrate and

Table 7. Summary of r values with various ligands. T = 10.0 °C; μ = 1.0 M ($NaClO_4$); optical path length 1 cm.

ligand	λ (nm)	v_{i1} (AU·s^{-1})	v_{i2} (AU·s^{-1})	r
hydrolysis	340	−0.053 ± 0.001	−0.019 ± 0.001	
	370	−0.015 ± 0.001	−0.005 ± 0.001	
	430	−0.0008 ± 0.0001	−0.0003 ± 0.0001	
	460	−0.0005 ± 0.0002	$0 > v_{i2} > -0.0002$	
SCN^-	340	0.053 ± 0.004	0.103 ± 0.003	0.87 ± 0.07
	460	1.34 ± 0.01	1.35 ± 0.01	0.99 ± 0.01
N_3^-	340	0.146 ± 0.006	0.191 ± 0.003	0.95 ± 0.03
	460	0.602 ± 0.003	0.616 ± 0.003	0.98 ± 0.01
Cl^-	340	0.3 ± 0.1	0.4 ± 0.1	0.8 ± 0.3
	370	0.18 ± 0.02	0.17 ± 0.01	1.1 ± 0.1
ClO_2^-	340	0.25 ± 0.03	0.31 ± 0.03	0.9 ± 0.1
IO_3^-	340	2.6 ± 0.4	2.6 ± 0.2	1.0 ± 0.2
SO_4^{2-}	340	3.88 ± 0.05	4.04 ± 0.09	0.97 ± 0.02
$HCrO_4^-$	340	0.75 ± 0.03	0.88 ± 0.04	0.89 ± 0.05
Mo(VI)[a]	340	29.7 ± 0.2	32.2 ± 0.5	0.92 ± 0.02
W(VI)[a]	340	0.211 ± 0.009	0.25 ± 0.01	0.98 ± 0.05
	370	0.071 ± 0.002	0.076 ± 0.002	1.06 ± 0.04
HSO_3^-	340	−11.8 ± 0.3	−5.9 ± 0.2	2.00 ± 0.08
	430	1.31 ± 0.02	0.67 ± 0.04	2.0 ± 0.1
$HS_2O_4^-$	340	−16 ± 2	−8 ± 1	2.0 ± 0.4
SeO_3^{2-}	340	−29 ± 1	−13.3 ± 0.9	2.2 ± 0.2
$H_2PO_2^-$	340	−62 ± 6	−30 ± 1	2.1 ± 0.2
$H_2PO_3^-$	340	−79 ± 3	−40 ± 3	2.0 ± 0.2
$H_2PO_4^-$	340	−45 ± 2	−24 ± 2	1.9 ± 0.2
	370	−12.5 ± 0.5	−6.2 ± 0.3	2.0 ± 0.1
$H_2AsO_4^-$	340	−28.1 ± 0.5	−15.4 ± 0.7	1.82 ± 0.09
Citric Acid	340	−2.08 ± 0.07	−1.01 ± 0.06	2.0 ± 0.1
Tiron[b]	340	−0.97 ± 0.01	−0.44 ± 0.01	2.18 ± 0.06

Table 7 (continued). Summary of r values with various ligands. T = 10.0 °C; μ = 1.0 M ($NaClO_4$); optical path length 1 cm.

ligand	λ (nm)	v_{i1} (AU·s^{-1})	v_{i2} (AU·s^{-1})	r
IO_4^- [a]	340	−5.6 ± 0.1	−1.37 ± 0.06	4.1 ± 0.2
$As(OH)_3$	340	−0.257 ± 0.001	−0.088 ± 0.001	2.96 ± 0.06
Br^-	340	−0.053 ± 0.001	−0.018 ± 0.001	– [c]
ClO_3^-	340	−0.052 ± 0.001	−0.019 ± 0.001	– [c]
BrO_3^-	340	−0.053 ± 0.001	−0.019 ± 0.001	– [c]
$S_2O_3^{2-}$	340	−0.057 ± 0.001	−0.022 ± 0.002	– [c]
$S_2O_8^{2-}$	340	−0.064 ± 0.001	−0.024 ± 0.001	– [c]
SeO_4^{2-}	340	−0.059 ± 0.001	−0.019 ± 0.001	– [c]
NO_2^-	340	−0.054 ± 0.003	−0.019 ± 0.001	– [c]
NO_3^-	340	−0.053 ± 0.001	−0.018 ± 0.001	– [c]
H_2CO_3	340	−0.050 ± 0.002	−0.019 ± 0.001	– [c]
H_3BO_3	340	−0.064 ± 0.002	−0.023 ± 0.001	– [c]
CH_3COOH	340	−0.058 ± 0.001	−0.020 ± 0.001	– [c]

a: The ligand exists as an equilibrium mixture of mono- and multinuclear species
b: Tiron = 4,5-dihydroxy-1,3-benzenedisulfonic acid (formula given on page in Scheme 2, page 9)
c: Initial rates are practically identical to the ones measured with hydrolysis only

nitrite ions, initial rates are practically identical to the ones measured in the hydrolytic experiments. In these systems the hydrolytic reactions of iron(III) are considerably faster than any complex formation reaction with either mononuclear or dinuclear forms of aqueous iron(III). We obtained no evidence for such complexation under the conditions of the test experiments. However, complex formation reactions between some of these ligands and mononuclear iron(III) species were reported at higher pH and/or higher ligand concentrations.[85,166]

There are two possible cases in which a reaction of the hydroxo dimer would be undetected by the test. The first is when a ligand reacts with both the mononuclear and dinuclear forms of aqueous iron(III) but the reaction with the mononuclear form is several orders of magnitude faster. However, this is an unlikely scenario because appropriate wavelength selection may ensure that the reaction of the hydroxo dimer has a relatively high weight in the initial absorbance change. Thus, at the 340 nm

absorption maximum of the hydroxo dimer (where tests were performed with each ligand) even a small change in its concentration is expected to be detectable. The other possibility is when the hydroxo dimer reacts in an instantaneous process. In this case the reaction of the hydroxo dimer would not contribute to the measured initial rate, and kinetic information for its reaction could not be obtained at all. The occurrence of an instantaneous reaction can be tested by comparing the initial absorbance readings in the presence and absence of a ligand. This analysis showed that an instantaneous reaction of the hydroxo dimer occurred only with sulfate ion as a ligand.

Dithionite ion decomposes in acid and is also oxidized by iron(III) relatively rapidly. These reactions overlap with the complex formation reactions of the hydroxo dimer and, because of the complexity of the overall reaction, further investigations were not planned in the iron(III) – dithionite ion system. A detailed study was planned with periodate ion as a ligand, but remained inconclusive. The test predicts second-order dependence with respect to $Fe_2(OH)_2^{4+}$, and this order of reaction was also confirmed by the initial rate method. However, the kinetic curves showed composite features, and the reaction time was much longer than for any other ligands. Although the speciation in periodate ion solutions has been studied,[167-169] the details are still unclear. In addition, unlike the other systems, the iron(III) – periodate ion reaction could lead to the formation of a multinuclear complex as a final product.[170] The reactions of the remaining 8 ligands with the hydroxo dimer were studied in detail, and the results will be presented in the following sections.

5.3. Protolytic Equilibria of Ligands

The relevant protonation constants of the ligands were determined by standard pH-potentiometric or spectrophotometric methods. These were usually routine measurements with well established techniques and are not discussed here. Results are summarized in Table 8. The values determined here are in reasonable agreement with literature data.[75,171-178] Some of the ligands take part in additional non-protolytic equilibria in aqueous solution. These processes are different from case to case and will be considered under the detailed study of the reaction with the particular ligand. All proton transfer reactions of these ligands are considered to be close to diffusion controlled and were treated as fast equilibria throughout this work.

Table 8. Protonation constants of ligands. μ = 1.0 M ($NaClO_4$).

Reaction	log K	T (°C)	Method	Ref.
$H_2PO_4^- + H^+ = H_3PO_4$	1.39 ± 0.02	10.0	pH	a
	1.76 [d]	25	pH	173
$HPO_4^{2-} + H^+ = H_2PO_4^-$	6.31 ± 0.01	10.0	pH	a
	7.25 [b]	10	pH	176
$HSO_3^- + H^+ = H_2O{\cdot}SO_2$	1.49 ± 0.02	10.0	UV-vis	a
	1.74 ± 0.01	25.0	UV-vis	a
	1.76 [b]	25.0	pH	175
$SO_3^{2-} + H^+ = HSO_3^-$	6.44 ± 0.01	10.0	pH	a
	6.34	25	pH	177
$H_2AsO_4^- + H^+ = H_3AsO_4$	2.05 ± 0.02	10.0	pH	a
	2.25 [b]	18	pH	171
$HAsO_4^{2-} + H^+ = H_2AsO_4^-$	6.19 ± 0.02	10.0	pH	a
	6.77 [b]	18	pH	171
$HSeO_3^- + H^+ = H_2SeO_3$	2.59 ± 0.02	10.0	UV-vis	a
	2.27	25	pH	172
$SeO_3^{2-} + H^+ = HSeO_3^-$	7.55 ± 0.05	10.0	UV-vis	a
	7.78	25	pH	172
$H_2PO_2^- + H^+ = H_3PO_2$	0.87 ± 0.03	10.0	cplx	a
	0.87 [c]	25.0	pH	75
$SO_4^{2-} + H^+ = HSO_4^-$	1.06 ± 0.02	25.0	cplx	a
	1.10 [d]	25	pH	173
$H_2PO_3^- + H^+ = H_3PO_3$	1.01 ± 0.01	10.0	cplx	a
	0.97 [c]	25.0	pH	75
$HPO_3^- + H^+ = H_2PO_3^-$	6.34 ± 0.07	10.0	UV-vis	a
	6.70 [b]	20.0	pH	174
$H_2AsO_3^- + H^+ = H_3AsO_3$	9.23 [b]	18	pH	171

a: this work; b: extrapolated to μ = 0; c: μ = 1.0 M ($LiNO_3$); d: μ = 1.0 M ($NaNO_3$);
pH: pH-potentiometry; UV-vis: UV-vis spectrophotometry; cplx: determined from the equilibrium complexation study with mononuclear iron(III) using UV-vis spectrophotometry

5.4. Possible Redox Reactions

One of the main objectives of this work was to study ligand substitution reactions of the iron(III) hydroxo dimer. Thus, any possible redox reaction between the mildly oxidizing iron(III) and the ligands were seen as unwanted sources of interference with the exception of the iron(III) – sulfite ion system. Sulfite ion is known to reduce iron(III) rapidly.[165] The redox process is of great interest since it is linked to acid rain formation. Thus, the relevance of our substitution studies with respect to the redox reaction between sulfite ion and iron(III) will be discussed in detail in a later section.

Arsenite, hypophosphite, selenite, and phosphite ions were tested for the occurrence of a redox reaction monitoring the buildup of iron(II) at room temperature with a spectrophotometric method using 2,2'-dipyridyl. None of the reactions with the four ions gave measurable amounts of iron(II) up to 45 minutes. As the corresponding ligand substitution reactions were complete within 1 minute at 10.0 °C, it was concluded that redox reactions do not interfere. On extended time scales arsenite and hypophosphite ions produced some iron(II). Iron(II) concentrations corresponding to 0.7% and 3.4% conversions were detected after 16 and 41 hours in the iron(III) – arsenite ion system, respectively. In the iron(III) – hypophosphite system, iron(II) concentrations corresponding to 0.15% and 1.3% conversion were detected after 1.25 and 17.5 hours, respectively. No iron(II) was detected (conversion < 0.1%) in the iron(III) – phosphite and selenite ion systems after 45 hours. Standard electrode potentials[9] suggest that the oxidation of selenite ion by iron(III) is thermodynamically unfavorable, whereas the oxidation of phosphite ion by iron(III) is thermodynamically allowed.

5.5. Formation of Mononuclear Iron(III) Complexes

As the major final product of the reactions studied here is usually some kind of mononuclear iron(III) – ligand complex, it was necessary to characterize their formation in independent equilibrium and kinetic studies. Results in most of these systems were reported in the literature.[75,77,88,179-187] Thus, our investigations were routine redeterminations of relevant equilibrium and rate constants for the particular

conditions applied here. These experiments were carried out at low total iron(III) concentrations where the reactions of the hydroxo dimer were negligible.

5.5.1. Equilibrium

A large number of equilibrium studies on iron(III) complexes with the ligands studied here are available in the literature.[75,77,88,179-184] In some cases, the formation of multinuclear complexes was also reported on the basis on pH-potentiometric measurements at high iron(III) concentrations.[185-187] In the present study, equilibrium constants of the relevant mononuclear complexes were redetermined using UV-vis spectrophotometry. Stability data were also obtained from the kinetic runs using the overall absorbance changes of a given process. Results are summarized in Table 9. Molar absorbances for the mononuclear complexes at specific wavelengths used in the kinetic studies of the reactions involving the hydroxo dimer were also determined

Table 9. Equilibrium constants for mononuclear complexes of iron(III). μ = 1.0 M ($NaClO_4$)

Reaction	log K	T	Method	Ref
$Fe^{3+} + SO_4^{2-} = FeSO_4^+$	2.06 ± 0.01	25.0	UV-vis	a
	2.31 [b]	25.0	UV-vis	88
$Fe^{3+} + H_2PO_2^- = FeH_2PO_2^{2+}$	2.81 ± 0.01	10.0	UV-vis	a
	3.04 [c]	25.0	kin	75
$Fe^{3+} + H_2PO_3^- = FeH_2PO_3^{2+}$	2.69 ± 0.04	10.0	UV-vis	a
	5.0	24	pot.	179
$Fe^{3+} + H_2PO_4^- = FeH_2PO_4^{2+}$	3.11 ± 0.02	10.0	UV-vis	a
	3.49 [d]	25	UV-vis	77
$Fe^{3+} + H_2AsO_4^- = FeH_2AsO_4^{2+}$	2.64 ± 0.02	10.0	UV-vis	a
$Fe^{3+} + HSeO_3^- = FeHSeO_3^{2+}$	3.15 ± 0.01	10.0	UV-vis	a
	3.25	20	UV-vis	180
$Fe^{3+} + HSO_3^- = FeSO_3^+ + H^+$	0.13 ± 0.05	25.0	UV-vis	a
	0.58	25.0	UV-vis	182

a: this work; b: μ = 2.5 M ($NaClO_4$); UV-vis: UV-vis spectrophotometry; pot.: potentiometry; kin: based on kinetic results

and the corresponding values will be given in the detailed discussions of the individual systems.

5.5.2. Kinetics

The reactions of the mononuclear iron(III) species with phosphate,[77] hypophosphite,[75] and sulfate[88] ions were studied previously. In most cases our results were consistent with earlier data. The following scheme was used to evaluate the kinetic experiments:

$Fe^{3+} + HL \rightarrow FeL^{2+} + H^+$

$$v_{16} = k_{16}[Fe^{3+}][HL] - k_{-16}[FeL^{2+}][L^-] \quad (16)$$

$Fe(OH)^{2+} + HL \rightarrow FeL^{2+}$

$$v_{17} = k_{17}[FeOH^{2+}][HL] - k_{-17}[FeL^{2+}] \quad (17)$$

$Fe^{3+} + L^- \rightarrow FeL^{2+}$

$$v_{18} = k_{18}[Fe^{3+}][L^-] - k_{-18}[FeL^{2+}] \quad (18)$$

$Fe(OH)^{2+} + L^- \rightarrow FeL^{2+}$

$$v_{19} = k_{19}[FeOH^{2+}][L^-] - k_{-19}[FeL^{2+}]/[H^+] \quad (19)$$

where $L^- = H_2PO_2^-$, $H_2PO_3^-$, $H_2PO_4^-$, $H_2AsO_4^-$, SO_4^{2-}, or $HSeO_3^-$. Reactions 17 and 18 are kinetically indistinguishable because of proton ambiguity, and only the appropriate combination of rate constants ($k_{17}K_1K_p + k_{18}$) could be determined.[162] Based on this scheme the following formula can be derived for k_{obs} at high ligand excess over Fe_{mn}:

$$k_{obs} = k_M[L]_T + k_{-M} \quad (20)$$

where

$$k_M = \frac{k_{16}K_p[H^+]^2 + (k_{17}K_1K_p + k_{18})[H^+] + k_{19}K_1}{(K_1 + [H^+])(K_p[H^+] + 1)} \quad (21)$$

$$k_{-M} = k_{-16}[H^+] + (k_{-17} + k_{-18}) + k_{-19}/[H^+] \quad (22)$$

where $[L]_T$ is the total ligand concentration ($[L]_T = [L] + [HL]$). This approach was used with sulfate, hypophosphite and selenite ions. Reverse rate constants were forced to give the equilibrium constants determined independently.

Phosphite, phosphate and arsenate ions gave biphasic kinetic curves under these conditions. In the case of the phosphate ion reaction the fast and slow phases

Table 10. Rate constants for the formation of mononuclear iron(III) complexes. T = 10.0 °C; μ = 1.0 M ($NaClO_4$).

complex	k_{16}	$k_{17}K_1K_p + k_{18}$	k_{19}	λ (nm)
$FeSO_4^{+}$ [a]	– [b]	$(2.4 \pm 0.3) \times 10^3$	$(6.6 \pm 0.5) \times 10^4$	310
$FeH_2PO_2^{2+}$	5.9 ± 1.3	13 ± 2	$(1.7 \pm 0.1) \times 10^3$	280
$FeH_2PO_3^{2+}$	– [b]	33 ± 7	$(1.9 \pm 0.1) \times 10^3$	275
$FeH_2PO_4^{2+}$	2.4 ± 1.0	20 ± 4	$(4.7 \pm 0.1) \times 10^3$	275
$FeH_2AsO_4^{2+}$	2.0 ± 0.7	65 ± 10	$(2.5 \pm 0.1) \times 10^3$	275
$FeHSeO_3^{2+}$	– [b]	$(1.71 \pm 0.03) \times 10^3$	$(1.1 \pm 0.1) \times 10^4$	300

a: 25.0 °C; b: too small to be determined

were interpreted as the formation of the mono- and bis-phosphato complexes, respectively.[77] Our data were consistent with these conclusions, and the validity of the model was extended to the arsenate and phosphite ion systems. In the phosphate ion system, the two phases were separated and the experimental rate constants for the first phase (k_{obs}) were fitted to the formula given in equation 20. This was not possible with the other two ions. The molar absorbances of the mononuclear complexes with these ligands were calculated in the equilibrium studies, and rate constants were determined from the initial rate. It can be shown that the initial rate is given by the following expression:

$$v_i = k_M[Fe_{mn}][L]_T =$$

$$= \frac{k_{16}K_p[H^+]^2 + (k_{17}K_1K_p + k_{18})[H^+] + k_{19}K_1}{(K_1 + [H^+])(K_p[H^+] + 1)}[Fe_{mn}][L]_T \qquad (23)$$

The results are summarized in Table 10. The features of the iron(III) – sulfite ion reaction significantly deviate from the general patterns observed in these systems and will be discussed in detail separately (section 5.6.4., page 59).

5.6. Matrix Rank Analysis

MRA was used to determine the number of absorbing species from time dependent spectral data using singular value decomposition.[153-160] In this procedure, all measured spectra in a system are arranged in a matrix format, and the singular values of this matrix are calculated. In an ideal system the number of absorbing species is given by the number of non-zero singular values. In practice, the singular values decrease sharply until the differences become relatively small between the subsequent values. The slightly different small singular values are attributed to experimental error, and the number of absorbing species is given by the number of singular values in the sharply decreasing region.

Singular values calculated based on the experiments in the studied systems are shown in Table 11, Table 12, and Table 13. These experiments were carried out

Table 11. Matrix rank analysis in various iron(III) – ligand systems. 11 wavelengths with an interval of 10 nm were used in the 300–400 nm wavelength range. T = 10.0 °C; μ = 1.0 M ($NaClO_4$).

system	iron(III)[a]	P(I)	P(III)	Se(IV)	As(V)
number of spectra	800	790	790	1978	637
Singular values in decreasing order. Underlined singular values represent absorbing species.	35.4281	38.7877	43.8905	44.0319	35.1963
	5.4540	3.3629	3.3636	2.4640	3.4179
	0.6646	0.9780	1.4313	2.1991	1.0511
	0.0178	0.1155	0.1238	0.3329	0.0932
	0.0127	0.0263	0.0296	0.0352	0.0290
	0.0111	0.0157	0.0190	0.0298	0.0141
	0.0094	0.0103	0.0119	0.0207	0.0107
	0.0088	0.0085	0.0084	0.0162	0.0085
	0.0085	0.0082	0.0080	0.0141	0.0074
	0.0083	0.0073	0.0075	0.0132	0.0061
	0.0076	0.0069	0.0071	0.0118	0.0058
Predicted number of absorbing species	**3**	**4**	**4**	**4**	**4**

a: no ligand added

Table 12. Matrix rank analysis in the iron(III) – sulfite ion system. 310–440 nm; 14 wavelengths; T = 25.0 °C; μ = 1.0 M ($NaClO_4$).

System	iron(III)[a]	S(IV)	S(IV)[b]
Number of spectra	2400	3992	3192
Singular values in descending order Underlined singular values represent absorbing species.	84.4145	110.0179	80.8527
	9.5254	11.5029	10.8020
	0.6156	1.5135	1.3786
	0.0978	1.0558	0.8178
	0.0720	0.1828	0.1550
	0.0484	0.0832	0.0614
	0.0446	0.0611	0.0441
	0.0229	0.0415	0.0303
	0.0222	0.0365	0.0230
	0.0165	0.0273	0.0223
	0.0146	0.0220	0.0162
	0.0141	0.0182	0.0146
	0.0130	0.0179	0.0139
	0.0121	0.0166	0.0129
Predicted number of absorbing species	**3**	**5**	**5**

a: no ligand added; b: only spectra recorded in the initial 50 ms were used

under conditions where the reactions of the hydroxo dimer could be studied. Data were collected at [Fe(III)] > [L]. Experiments were also carried out under similar conditions with no ligand added. The number of absorbing species for these aqueous iron(III) solutions is determined to be 3. These absorbing species are Fe^{3+}, $FeOH^{2+}$ and $Fe_2(OH)_2^{4+}$ in agreement with the results from earlier equilibrium studies based on UV-vis spectroscopy. When the wavelength range is somewhat narrowed, and only wavelengths above 330 nm are used, the number of absorbing species is 2 (Table 13). This is also in agreement with the equilibrium study as the absorption of Fe^{3+} is negligible in this range (Figure 3, page 24).

In the presence of ligands the formation of mononuclear complexes was confirmed previously (section 5.5., page 37). All of these mononuclear complexes

Table 13. Matrix rank analysis in the iron(III) – phosphate ion system. T = 10.0 °C; μ = 1.0 M ($NaClO_4$).

System	iron(III)[a]	P(V)
Wavelength Range (nm)	332 – 431	332 – 431
Number of Wavelengths	100	47
Number of Spectra	147	666
Largest singular values in descending order	12.2100	35.3643
	0.3018	3.0512
	0.0082	0.9017
Underlined singular values represent absorbing species.	0.0048	0.1983
	0.0043	0.1789
	0.0030	0.1391
	0.0020	0.1097
Predicted number of absorbing species	**2**	**3**

a: no ligand added

($FeH_2PO_2^{2+}$, $FeH_2PO_3^{2+}$, $FeH_2PO_4^{2+}$, $FeH_2AsO_4^{2+}$, $FeSO_3^{+}$, and $FeHSeO_3^{2+}$) have considerable absorptions in the wavelength range applied in the MRA studies. In the hypophosphite, phosphite, phosphate, arsenate, and selenite ion systems evidence shows that no further absorbing species is formed. The combination of these data with the results of the test method (section 5.2., page 30) confirm that potential di- and multinuclear complexes have negligible contribution to the absorbance in these systems.

The iron(III) – sulfite ion system (Table 12) features 5 absorbing species, i.e. 2 colored iron(III) sulfito complexes. One of these complexes is the mononuclear complex $FeSO_3^{+}$, the other will be shown to be the dinuclear complex $Fe_2(OH)(SO_3)^{3+}$ (section 5.7.4., page 55). The data also prove that these sulfito complexes are formed during the initial 50 ms of the reaction, and no new absorbing species are formed at longer reaction times.

5.7. Detailed Kinetic Studies on the Reactions of the Hydroxo Dimer

Detailed studies were based on the following strategy. First, the initial rate method was used in each system to confirm the rate equation for the fastest process, which was usually a reaction of the hydroxo dimer and first-order with respect to both the ligand and $Fe_2(OH)_2^{4+}$. The first phase was studied separately from subsequent phases wherever it was feasible. In these cases, the concentration dependence of the amplitude of the absorbance change were used to subtract stoichiometric information for the first phase. On the basis of the pH-dependence of the observed rate constants, the kinetically significant pathways were identified and the corresponding rate constants were calculated. The overall reactions were evaluated and additional parameters were determined by fitting the absorbance traces to the appropriate kinetic model. As it will be confirmed in the next sections, most of the reactions could be interpreted in terms of the following scheme:

$$Fe_2(OH)_2^{4+} + L = Fe_2L$$

$$v_D = k_D[Fe_2(OH)_2^{4+}][L]_T - k_{-D}[Fe_2L] \quad (24)$$

$$Fe_2L = FeL + Fe_{mn}$$

$$v_S = k_S[Fe_2L] - k_{-S}[FeL][Fe_{mn}] \quad (25)$$

$$Fe_{mn} + L = FeL$$

$$v_M = k_M[Fe_{mn}][L]_T - k_{-M}[FeL] \quad (26)$$

$$Fe_2(OH)_2^{4+} = 2Fe_{mn}$$

$$v_H = k_H[Fe_2(OH)_2^{4+}] - k_{-H}[Fe_{mn}]^2 \quad (27)$$

All rate constants known from independent studies (usually k_D, k_M, k_{-M}, k_H, and k_{-H}) were fixed in these calculations. The values of k_{-D} and k_S were fitted, whereas the expression $k_{-S} = k_S k_D k_{-M} k_{-H}/(k_{-D} k_M k_H)$ was forced to fulfil microscopic reversibility. It should be noted that equations 24–27 represent a general scheme and each reaction may occur in parallel paths. As expected, none of the rate constants were dependent on the initial iron(III) (mono- or dinuclear) or ligand concentrations, while some of them were pH-dependent. This pH-dependence was utilized to distinguish the competing pathways involving different protonated forms of the ligand. The pH-dependence also revealed stoichiometric information for the given reaction. For example, when k_{-D} was found to be independent of pH, it was concluded that no proton release occurs in reaction 24, and the formula of Fe_2L should be the sum of the two reactants.

Absorbing species were included in the calculations with molar absorbances determined prior to the fitting procedure. Molar absorbances for the hydroxo iron(III) species were determined during the equilibrium study (Table 5, page 25). Molar absorbances for mononuclear iron(III) – ligand complexes (FeL) were also determined independently (section 5.5.1., page 38).

5.7.1. Phosphite Ion

Kinetic curves measured in the iron(III) – phosphite ion system are shown in Figure 7. As shown, a fast absorbance decrease (phase I, ~ 0.1 s) is followed by a much slower increase (phase II, ~ 50 s). The initial absorbance was practically the same in the presence and absence of phosphite ion suggesting that no instantaneous reaction occurs between the reactants. The substantial absorbance decrease in phase I can only be interpreted by the disappearance of $Fe_2(OH)_2^{4+}$. The observations confirm a relatively fast reaction between the hydroxo dimer and the ligand. Because

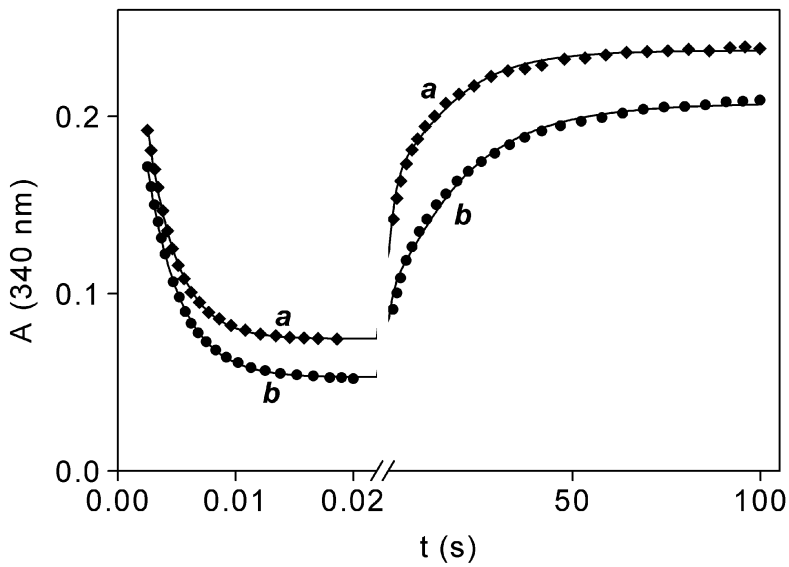

Figure 7. Measured and fitted kinetic curves in the iron(III) – phosphite ion system. Markers: measured points. Solid lines: fitted curves. [Fe(III)] = 2.59 mM; [P(III)] = 1.50 mM; pH = 1.58 (***a***), 1.36 (***b***); pH_{Fe} = 2.00 (***a***, ***b***); T = 10.0 °C; μ = 1.0 M ($NaClO_4$); optical path length 1 cm. Only about 10% of the measured points are shown for clarity.

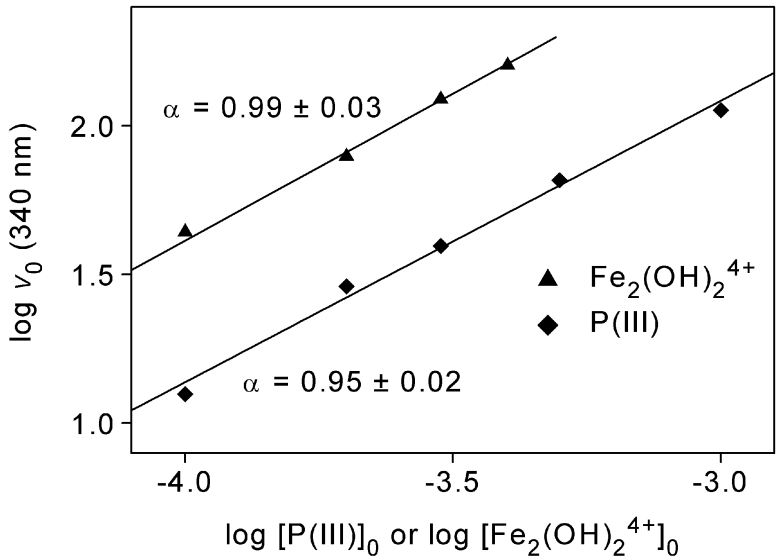

Figure 8. Initial rate method in the iron(III) – phosphite ion system. $[Fe_2(OH)_2^{4+}]_0$ = 0.40 mM and pH =1.70 (phosphite dependence); [P(III)] = 0.50 mM and pH = 1.65 (iron dependence); T = 10.0 °C; μ = 1.0 M ($NaClO_4$); v_0 unit: $AU \cdot s^{-1}$; concentration unit: M.

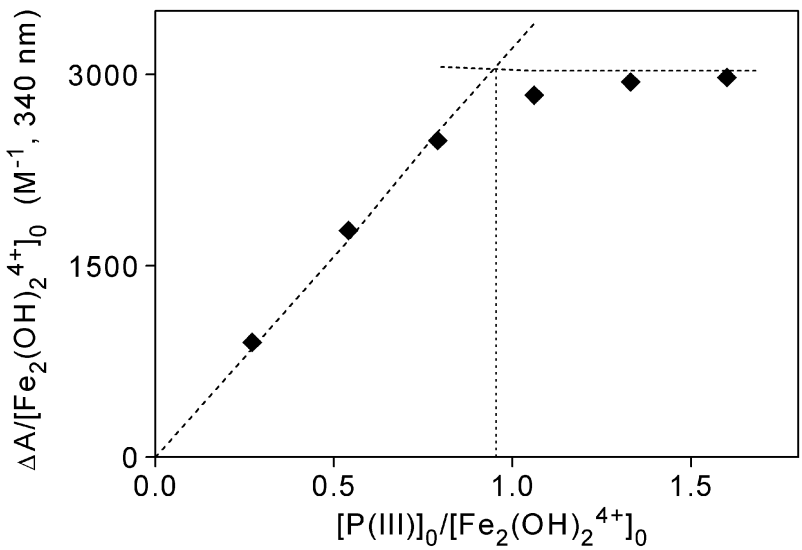

Figure 9. Normalized absorbance change in phase I as a function of the ligand/hydroxo dimer concentration ratio in the iron(III) – phosphite ion system. pH = 1.24; T = 10.0 °C; μ = 1.0 M ($NaClO_4$); optical path length 1 cm.

redox reactions between the reactants can be excluded (section 5.4., page 37) this is a further piece of evidence for a complex formation reaction with $Fe_2(OH)_2^{4+}$.

The reaction was shown to be first-order with respect to both phosphite ion and $Fe_2(OH)_2^{4+}$ by the initial rate method (Figure 8). Figure 8 also serves to indicate the general quality of initial rate studies throughout this work. Graphs for this kind of analysis will only be shown in the following systems if they are considered to be particularly important.

The stoichiometry of phase I could be confirmed measuring the absorbance change in this step as a function of reactant concentrations (Figure 9). It is concluded that the product is a 1:1 complex of $Fe_2(OH)_2^{4+}$ and phosphite ion and this complex has no absorption at 340 nm. The composition and the rate law are in agreement with reaction 24 of the general model (page 44).

The pH-dependence of phase I could be studied under pseudo first-order conditions. Phosphite ion was used in 15-times excess over the hydroxo dimer, and the second-order rate constants k_D were calculated from the experimental pseudo first-order rate constants. The pH-dependence of k_D is shown in Figure 10 and can be interpreted with the following two pathways:

$$Fe_2(OH)_2^{4+} + H_3PO_3 = Fe_2(OH)(HPO_3)^{3+} + H^+$$

$$v_{28} = k_{28}[Fe_2(OH)_2^{4+}][H_3PO_3] - k_{-28}[Fe_2(OH)(HPO_3)^{3+}][H^+] \qquad (28)$$

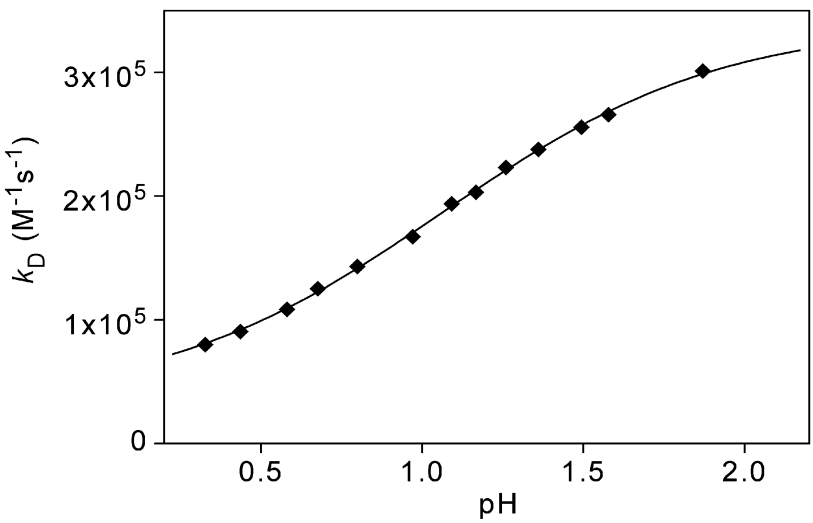

Figure 10. pH-dependence of k_D in the iron(III) – phosphite ion system. T = 10.0 °C; μ = 1.0 M ($NaClO_4$).

$$Fe_2(OH)_2^{4+} + H_2PO_3^- = Fe_2(OH)(HPO_3)^{3+}$$

$$v_{29} = k_{29}[Fe_2(OH)_2^{4+}][H_2PO_3^-] - k_{-29}[Fe_2(OH)(HPO_3)^{3+}] \quad (29)$$

The following formula can be derived for k_D:

$$k_D = \frac{k_{29} + k_{28}K_p[H^+]}{1 + K_p[H^+]} \quad (30)$$

where K_p is the protonation constant of dihydrogenphosphite ion ($K_p = [H_3PO_3]/[H_2PO_3^-]/[H^+]$). The values of k_{28} and k_{29} were determined from this equation and were fixed in the final fittings. A similar derivation for k_{-D} gives:

$$k_{-D} = k_{-28}[H^+] + k_{-29} \quad (31)$$

In fact, k_{-D} values were too small and could not be determined directly. Consequently, k_{-D} was set to zero in the calculations and k_{-S} was determined as an independent parameter in addition to k_S. The fitted value of k_S was independent of pH indicating that the dissociation of the dinuclear phosphito complex to mononuclear complexes occurs as shown in equation 32:

$$Fe_2(OH)(HPO_3)^{3+} = Fe(OH)_2^+ + FeH_2PO_3^{2+}$$

$$v_{32} = k_{32}[Fe_2(OH)(HPO_3)^{3+}] - k_{-32}[Fe(OH)_2^+][FeH_2PO_3^{2+}] \quad (32)$$

It also follows that $k_{32} = k_S$. $Fe(OH)_2^+$ formed in equation 32 is present at low concentrations and it is mostly transformed into other mononuclear iron(III) species. This is reflected in the pH-dependence of k_{-S} which can be expressed as:

$$k_{-S} = \frac{K_2 k_{-32}}{[H^+]^2 + K_1[H^+] + K_2} \quad (33)$$

Rate constants determined with fitting are summarized in Table 14. The agreement between the experimental and fitted kinetic traces is illustrated in Figure 7.

Values for k_{-28} and k_{-29} can be estimated based on microscopic reversibility. It can be shown that $k_{-D} = k_{-28}[H^+] + k_{-29} \ll k_{32}$ at any pH explaining why k_{-D} values could not be fitted directly. This observation implies that the dissociation of

Table 14. Parameters determined in the iron(III) – phosphite ion system. T = 10.0 °C; μ = 1.0 M ($NaClO_4$).

k_{28}	$(3.3 \pm 0.3) \times 10^4$ $M^{-1}s^{-1}$
k_{29}	$(3.40 \pm 0.03) \times 10^5$ $M^{-1}s^{-1}$
k_{32}	0.18 ± 0.04 s^{-1}
k_{-32}	81 ± 15 $M^{-1}s^{-1}$
$\epsilon\{FeH_2PO_3^{2+}\}$	235 ± 14 $M^{-1}cm^{-1}$ [a]

a: 340 nm

$Fe_2(OH)(HPO_3)^{3+}$ into the hydroxo dimer and phosphite ion is much slower than the dissociation into mononuclear iron(III) complexes.

5.7.2. Hypophosphite Ion

Kinetic curves measured in the iron(III) – hypophosphite ion system show biphasic kinetics again (Figure 11). An absorbance decrease in the initial 0.1 s is followed by an absorbance increase on longer time scales, although the different phases of the reaction are not separated. The initial absorbance was practically the same in the presence and absence of hypophosphite ion suggesting that no instantaneous reaction occurs.

The initial rate method yielded the following orders a of reaction: 0.97 ± 0.03 with respect to hypophosphite ion, and 1.00 ± 0.01 with respect to $Fe_2(OH)_2^{4+}$. The stoichiometry of the first reaction could not be determined with the method used with phosphite ion (page 45) because the first step was not separated from the subsequent processes. It was assumed that the product is a 1:1 complex again which does not

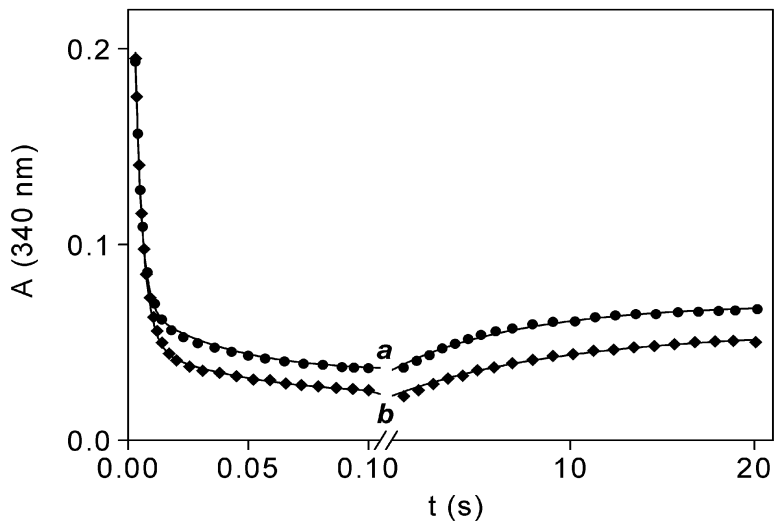

Figure 11. Measured and fitted kinetic curves in the iron(III) – hypophosphite ion system. Markers: measured points. Solid lines: fitted curves. [Fe(III)] = 2.59 mM; [P(I)] = 1.5 mM; pH = 1.12 (***a***), 0.84 (***b***); pH_{Fe} = 2.00 (***a***, ***b***); T = 10.0 °C; μ = 1.0 M ($NaClO_4$); optical path length 1 cm. Only about 10% of the measured points are shown for clarity.

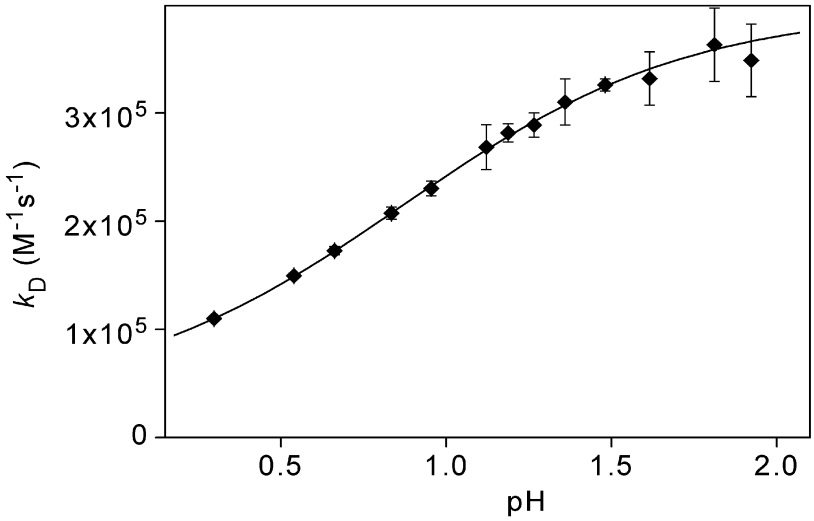

Figure 12. pH-dependence of k_D in the iron(III) – hypophosphite ion system. T = 10.0 °C; μ = 1.0 M ($NaClO_4$).

absorb at 340 nm. These assumptions were verified later by fitting the kinetic traces. The rate law for this reaction is in agreement with reaction 24 (page 44).

The pH-dependence of the first reaction was studied by calculating k_D values from the measured initial rates. The pH-dependence of k_D is shown in Figure 12 and can be interpreted with the following two pathways:

$$Fe_2(OH)_2^{4+} + H_3PO_2 = Fe_2(OH)(H_2PO_2)^{4+}$$

$$v_{34} = k_{34}[Fe_2(OH)_2^{4+}][H_3PO_2] - k_{-34}[Fe_2(OH)(H_2PO_2)^{4+}] \quad (34)$$

$$Fe_2(OH)_2^{4+} + H_2PO_2^- + H^+ = Fe_2(OH)(H_2PO_2)^{4+}$$

$$v_{35} = k_{35}[Fe_2(OH)_2^{4+}][H_2PO_2^-] - k_{-35}[Fe_2(OH)(H_2PO_2)^{4+}]/[H^+] \quad (35)$$

The following formula can be obtained for k_D:

$$k_D = \frac{k_{35} + k_{34}K_p[H^+]}{1 + K_p[H^+]} \quad (36)$$

where K_p is the protonation constant of dihydrogenhypophosphite ion (K_p = $[H_3PO_2]/[H_2PO_2^-]/[H^+]$). k_{34} and k_{35} were determined from this equation and were fixed at these values in the final calculations.

The results from the calculations showed that k_{-D} increased with increasing pH (Figure 13). On the basis of equations 34 and 35, a derivation for k_{-D} yields:

$$k_{-D} = k_{-34} + k_{-35}/[H^+] \quad (37)$$

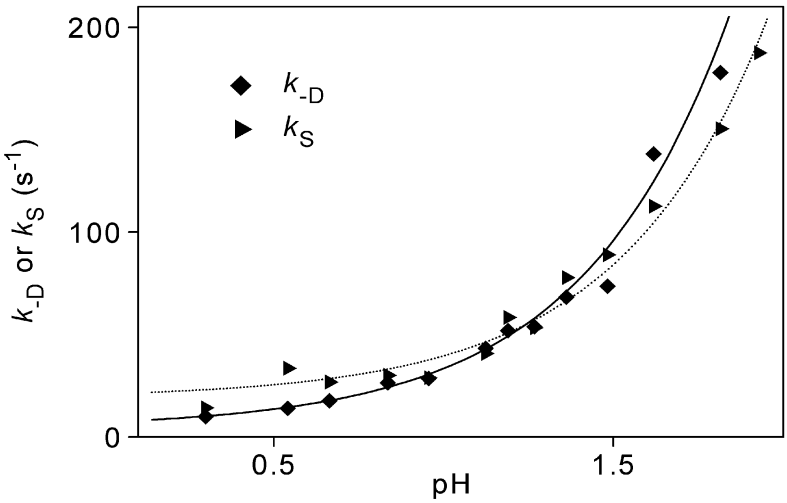

Figure 13. pH-dependence of k_{-D} and k_S in the iron(III) – hypophosphite ion system. T = 10.0 °C; μ = 1.0 M ($NaClO_4$).

k_S shows a pH-dependence similar to k_{-D} (Figure 13). This pH-dependence can be explained by the following equations:

$$Fe_2(OH)(H_2PO_2)^{4+} = FeOH^{2+} + Fe(H_2PO_2)^{2+}$$

$$v_{38} = k_{38}[Fe_2(OH)(H_2PO_2)^{4+}] - k_{-38}[FeOH^{2+}][Fe(H_2PO_2)^{2+}] \quad (38)$$

$$Fe_2(OH)(H_2PO_2)^{4+} = Fe(OH)_2^{+} + Fe(H_2PO_2)^{2+} + H^+$$

$$v_{39} = k_{39}[Fe_2(OH)(H_2PO_2)^{4+}]/[H^+] - k_{-39}[Fe(OH)_2^{+}][Fe(H_2PO_2)^{2+}] \quad (39)$$

The formula for k_S is given as:

$$k_S = k_{38} + k_{39}/[H^+] \quad (40)$$

It should be noted that the reverse step of reaction 35 and reaction 39 are written in simplified forms. The rate equation is interpreted as a fast deprotonation of the dinuclear complex followed by dissociation in the rate determining step similarly to reaction 11 of the hydrolytic cleavage. Rate constants determined with fitting are shown in Table 15. Fitted and measured curves are compared in Figure 11.

It is notable that the values of the rate constants, and especially the high values of k_{38} and k_{39} imply that the dinuclear complex $Fe_2(OH)(H_2PO_2)^{4+}$ is present only in the first few milliseconds of the reaction (Figure 14). The equilibrium between mononuclear and dinuclear forms of iron(III) is reached very rapidly, in less than 1 s. In agreement with these observations, the kinetic curves on longer time

scales (> 1 s) could be interpreted successfully by considering the reaction between mononuclear forms of iron(III) and hypophosphite ion only.

Table 15. Parameters determined in the iron(III) – hypophosphite ion system. T = 10.0 °C; μ = 1.0 M ($NaClO_4$).

k_{34}	$(2.9 \pm 0.1) \times 10^4$ $M^{-1}s^{-1}$
k_{35}	$(3.49 \pm 0.02) \times 10^5$ $M^{-1}s^{-1}$
k_{-34}	4.4 ± 0.6 s^{-1}
k_{-35}	2.9 ± 0.1 Ms^{-1}
k_{38}	19 ± 3 s^{-1}
k_{39}	2.06 ± 0.09 Ms^{-1}
$\epsilon\{FeH_2PO_2^{2+}\}$	70 ± 1 $M^{-1}cm^{-1}$ [a]

a: 340 nm

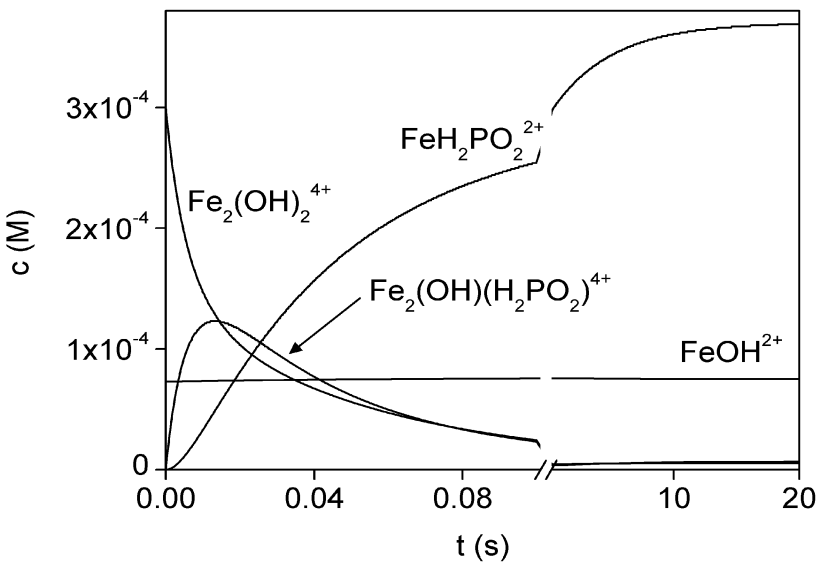

Figure 14. Calculated concentration profiles of iron(III) complexes during a typical kinetic run in the iron(III) – hypophosphite ion system. [Fe(III)] = 8.51 mM; [P(I)] = 0.50 mM; pH = 1.00; T = 10.0 °C; μ = 1.0 M ($NaClO_4$).

5.7.3. Selenite Ion

Selenite ion was reported to form polymeric species, e.g. $H(SeO_3)_2^{3+}$. However, the concentrations used in this work were sufficiently low to avoid the complications associated with the formation of the polymeric species.[172,188]

Kinetic traces here comprise a fast and a subsequent slow absorbance decrease (Figure 15). These phases were not fully separated, especially at higher pH and selenite ion concentration. The initial absorbance is practically the same in the presence and absence of selenite ion suggesting that no instantaneous reaction occurs.

The initial rate method gave the orders of reaction as 1.05 ± 0.02 with respect to selenite ion, and 1.06 ± 0.03 with respect to $Fe_2(OH)_2^{4+}$ at 340 nm. The stoichiometry of the first reaction could not be determined independently because the first step was not separated from the subsequent processes under all conditions. It was assumed that the product is a 1:1 complex of $Fe_2(OH)_2^{4+}$ and selenite ion and the complex has no absorption at 370 nm. This assumption was verified later by the calculations. The rate law is in agreement with reaction 24 (page 44).

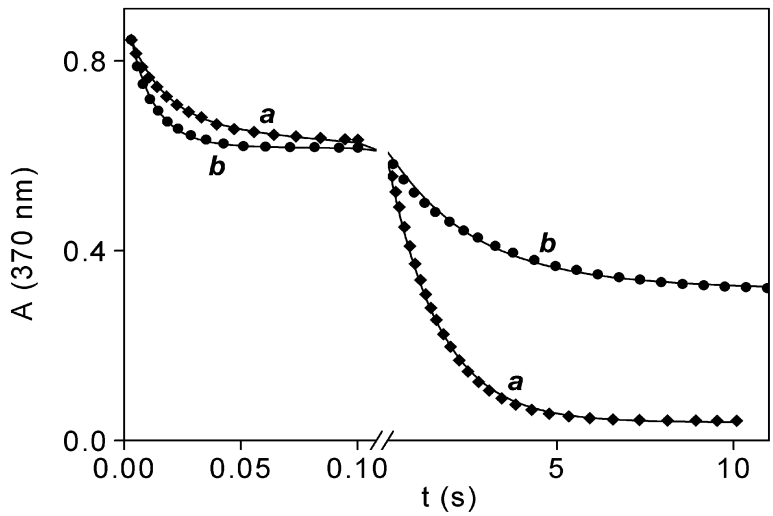

Figure 15. Measured and fitted kinetic curves in the iron(III) – selenite ion system. Markers: measured points. Solid lines: fitted curves. [Fe(III)] = 8.05 mM; [Se(IV)] = 0.50 mM; pH = 0.67 (***a***), 1.60 (***b***); pH_{Fe} = 2.20 (***a***, ***b***); T = 10.0 °C; μ = 1.0 M ($NaClO_4$); optical path length 1 cm. Only about 10% of the measured points are shown for clarity.

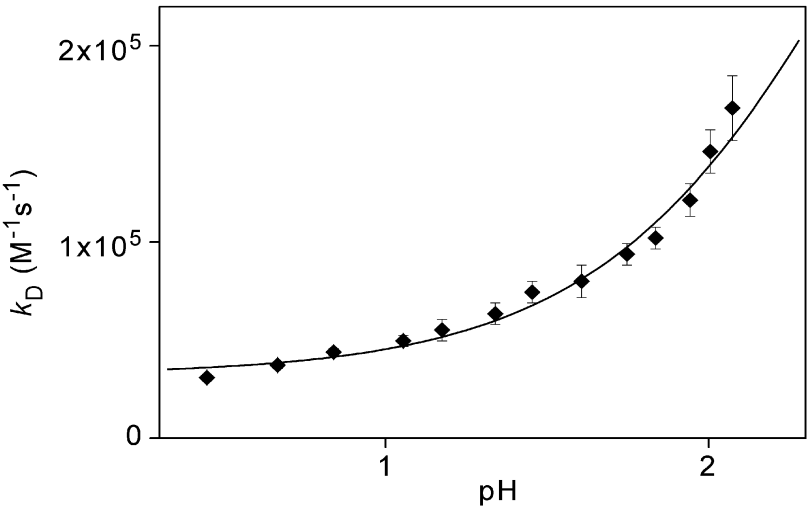

Figure 16. pH-dependence of k_D in the iron(III) – selenite ion system. T = 10.0 °C; μ = 1.0 M ($NaClO_4$).

The pH-dependence of the first reaction was studied by calculating k_D values from the initial rates at 370 nm. The pH-dependence of k_D is shown in Figure 16 and can be interpreted with the following two pathways:

$$Fe_2(OH)_2^{4+} + H_2SeO_3 = Fe_2(OH)(SeO_3)^{3+} + H^+$$

$$v_{41} = k_{41}[Fe_2(OH)_2^{4+}][H_2SeO_3] - k_{-41}[Fe_2(OH)(SeO_3)^{3+}][H^+] \quad (41)$$

$$Fe_2(OH)_2^{4+} + HSeO_3^- = Fe_2(OH)(SeO_3)^{3+}$$

$$v_{42} = k_{42}[Fe_2(OH)_2^{4+}][HSeO_3^-] - k_{-42}[Fe_2(OH)(SeO_3)^{3+}] \quad (42)$$

k_D can be expressed as:

$$k_D = \frac{k_{42} + k_{41}K_p[H^+]}{1 + K_p[H^+]} \quad (43)$$

where K_p is the protonation constant of hydrogenselenite ion (K_p = $[H_2SeO_3]/[HSeO_3^-]/[H^+]$). The values of k_{41} and k_{42} were determined from this equation and were included with fixed values in the calculations. It was found that the value of k_{-D} increased slightly with the decreasing pH. This is in agreement with the microscopic reversibility of reactions 41 and 42. k_{-D} can be given as:

$$k_{-D} = k_{-41}[H^+] + k_{-42} \quad (44)$$

The value of k_S, similarly to k_{-D}, increases linearly with $[H^+]$. This can be interpreted with a direct and a proton-assisted pathway for the dissociation of $Fe_2(OH)(SeO_3)^{3+}$ into mononuclear complexes :

Table 16. Parameters determined in the iron(III) – selenite ion system. T = 10.0 °C; μ = 1.0 M ($NaClO_4$).

k_{41}	$(2.7 \pm 0.1) \times 10^4$ $M^{-1}s^{-1}$
k_{42}	$(4.6 \pm 0.2) \times 10^5$ $M^{-1}s^{-1}$
k_{-41}	14 ± 7 $M^{-1}s^{-1}$
k_{-42}	26 ± 1 s^{-1}
k_{45}	0.64 ± 0.04 s^{-1}
k_{46}	6.8 ± 0.4 $M^{-1}s^{-1}$
$\epsilon\{FeHSeO_3^{2+}\}$	527 ± 20 $M^{-1}cm^{-1}$ [a]

a: 370 nm

$$Fe_2(OH)(SeO_3)^{3+} = Fe(OH)_2^{+} + FeHSeO_3^{2+}$$

$$v_{45} = k_{45}[Fe_2(OH)(SeO_3)^{3+}] - k_{-45}[Fe(OH)_2^{+}][FeHSeO_3^{2+}] \quad (45)$$

$$Fe_2(OH)_2X^{3+} + H^{+} = Fe(OH)^{2+} + FeHSeO_3^{2+}$$

$$v_{46} = k_{46}[Fe_2(OH)(SeO_3)^{3+}][H^{+}] - k_{-46}[Fe(OH)^{2+}][FeHSeO_3^{2+}] \quad (46)$$

Thus, k_S is given as:

$$k_S = k_{45} + k_{46}[H^{+}] \quad (47)$$

The values of estimated rate constants are summarized in Table 16. Fitted and measured curves are compared in Figure 15.

5.7.4. Sulfite ion

Aqueous sulfur(IV) has unique solution chemistry. There is no evidence for the existence of sulfurous acid, H_2SO_3, acidic sulfur(IV) solutions contain hydrated sulfur dioxide ($SO_2 \cdot nH_2O$).[9] In this work the commonly used simplified formula, $H_2O \cdot SO_2$, is adapted to emphasize that sulfur dioxide is a dibasic acid whose first dissociation process is:

$$H_2O \cdot SO_2 = HSO_3^{-} + H^{+} \quad (48)$$

Hydrogensulfite ion has two isomers containing O-bonded (SO_3H^{-}) or S-bonded (HSO_3^{-}) hydrogens.[189] This is the intermediate structural case between the isoelectronic species HPO_3^{2-} (P bonded hydrogen only) and $HClO_3$ (O bonded hydrogen only). The equilibrium constant for the reaction $HSO_3^{-} = SO_3H^{-}$ was determined by ^{17}O NMR to be 6.3 at 10 C° and μ = 1.0 M (NaCl).[189] However, the S and O-bonded isomers of hydrogensulfite ion interconvert very rapidly, and

hydrogensulfite ion can be regarded as a single species (denoted traditionally as HSO_3^-) for most practical kinetic considerations.[189] The existence of these isomers with hydrogensulfite ion also implies that the various protonated forms of sulfite ion can be both O-donor and S-donor ligands in complexes, and may also exhibit linkage isomerism.[190]

Hydrogensulfite ion can also dimerize to give $S_2O_5^{2-}$ ion.[191-193] The value of the corresponding equilibrium constant ($[S_2O_5^{2-}]/[HSO_3^-]^2 = 0.088\ M^{-1}$ in 1.0 M $NaClO_4$ at 25.0 ° C) is relatively low, and the dimeric form can be neglected at [S(IV)] < 0.1 M. The dimerization is relatively fast, although not instantaneous in the sense used in this study.[193]

$H_2O{\cdot}SO_2$ exchanges water molecules with the bulk solvent very rapidly,[193-195] and reaction 48 is expected to be diffusion controlled. Consequently, the oxygen exchange between sulfite ion and bulk water is also very rapid. This is exceptional among the ligands studied in this work because the O-exchange of all other ligands is much slower.

The significance of the iron(III) – sulfite ion reaction is outstanding and it has been studied extensively since the early 1930s.[196-198] The autoxidation of sulfite ion is efficiently catalyzed by iron(III) and this reaction is believed to be one of the major pathways leading to acid rain formation. The core of the catalytic cycle is the relatively fast redox reaction between sulfite ion and iron(III) which generates intermediates that react with dioxygen rapidly. Keeping the environmental impact of this process in mind, the redox reaction between iron(III) and sulfur(IV) was also studied in this work at metal ion excess. To our knowledge, such experimental conditions have not been used in previous studies.

Kinetic curves recorded at two wavelengths (340 and 430 nm) in the iron(III) – sulfite ion system are shown in Figure 17. At large iron(III) excess over sulfite ion, the same absorbance traces were recorded in the presence and absence of oxygen. It is notable that the initial absorbances at 430 nm are significantly different in the presence and absence of sulfite ion, indicating that an instantaneous reaction (phase I) between the reactants. The next, well separated phase is complete within 200 ms (phase II), whereas subsequent reactions do not reach equilibrium even after 15 minutes at 10.0 °C. At 340 nm a large absorbance decay was observed during phase

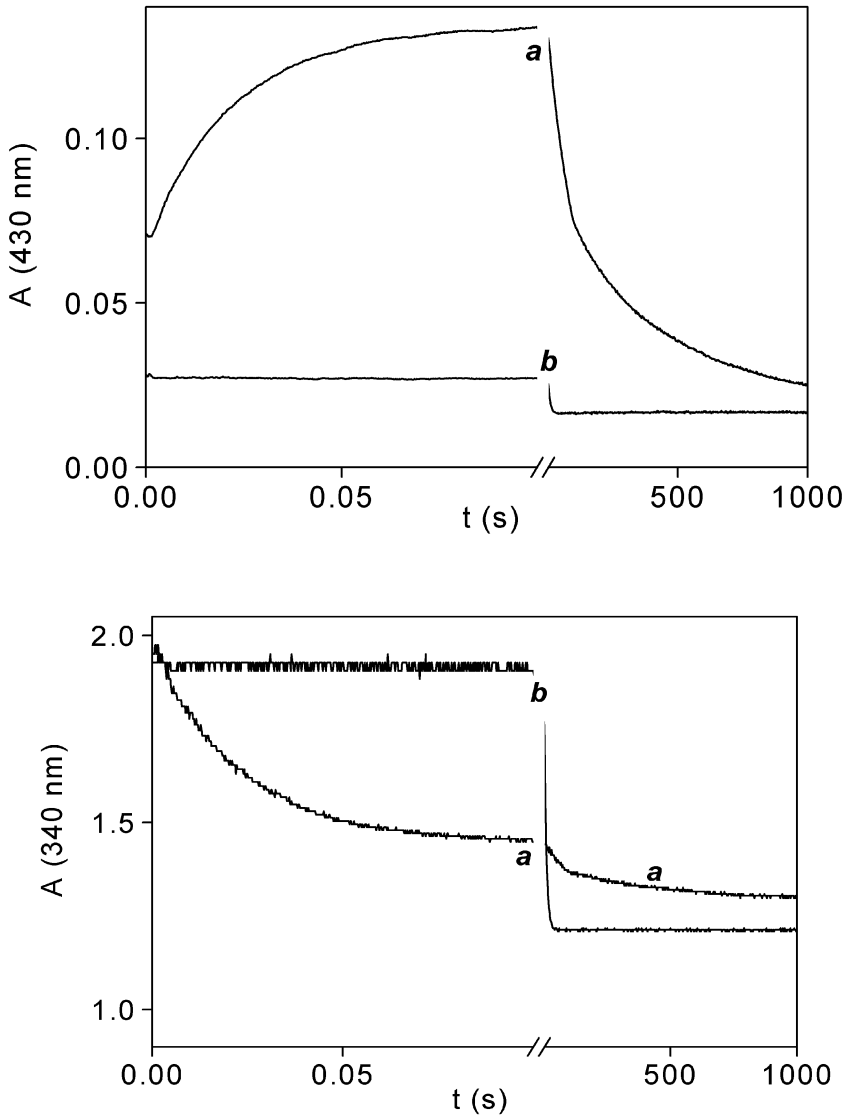

Figure 17. Typical kinetic traces in the iron(III) – sulfite ion system at 340 and 430 nm. [Fe(III)] = 20 mM; pH = 1.68; pH_{Fe} = 1.68; [S(IV)] = 0.50 mM (***a***) , 0 (***b***); T = 10.0 °C; μ = 1.0 M ($NaClO_4$).

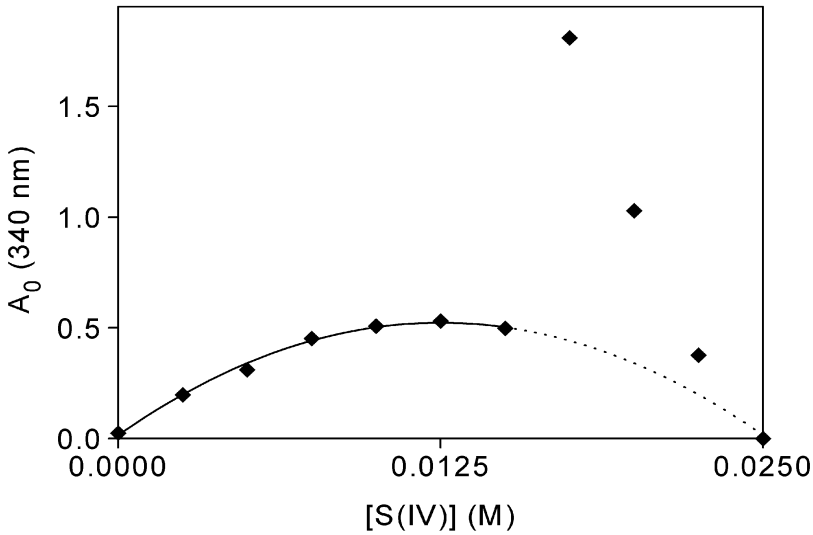

Figure 18. Job plot for phase I in the iron(III) – sulfite ion system at 430 nm. pH = 1.40; [Fe(III)] | + [S(IV)] = 25.0 mM; T = 10.0 °C; μ = 1.0 M ($NaClO_4$); optical path length 1 cm.

II, similarly to other systems studied in this work. However, an absorbance increase can be seen at 430 nm at the same time. It will be shown that a dinuclear complex, $Fe_2(OH)SO_3^{3+}$, is the product of phase II and has a significant absorbance at 430 nm.

Phase I was studied on the basis of the initial absorbance jump. The Job method[199] (Figure 18) showed that this spectral effect is due to the formation of a 1:1 complex between mononuclear forms of iron(III) and sulfite ion. The graph is asymmetric because of additional complex(es) with more than one sulfite ligand, most likely the bis-sulfito complex, formed at sulfite ion excess. Analysis at 25.0 °C showed that the equilibrium at iron(III) excess is represented by the following equation:

$$Fe^{3+} + HSO_3^- = FeSO_3^+ + H^+ \qquad K_{49} = \frac{[FeSO_3^+][H^+]}{[Fe^{3+}][HSO_3^-]} \qquad (49)$$

The value of K_{49} was determined at 25.0 °C and can be found in Table 9 (page 38). At 10.0 °C only a small conversion into $FeSO_3^+$ could be achieved and instead of K_{49} the product of the stability constant and the molar absorbance of the complex was determined; $\epsilon\{FeSO_3^+\}K_{49} = 281 \pm 8\ M^{-1}cm^{-1}$.

The extremely large rate of reaction 49 is unparalleled among the substitution reactions of iron(III) (Table 10, page 40). The reaction is much faster than predicted by the Eigen-Wilkins mechanism on the basis of the water exchange rate between mononuclear iron(III) forms and the bulk solvent. This extreme reactivity may indicate a mechanisms in which the complexation occurs via oxygen exchange on sulfite ion and not by substitution of a water molecule. According to this scenario, the oxygen of a coordinated water molecule replaces an oxygen in sulfite ion and the O–H bonds also rearrange between the complex and the bulk solvent at the same time. This interpretation is consistent with the very rapid oxygen exchange reported for sulfite ion.[193-195] Such a mechanism was proposed earlier for other complex formation reactions between metal ions and sulfite ion.[200,201] Finally, these conclusions are also supported by our observations in the chromium(III) – sulfite ion system. It was shown that the complex $CrSO_3^+$, contrary to earlier literature reports,[202] is also formed instantaneously with the inert $Cr(H_2O)_6^{3+}$.[203] In that case, the cleavage of the $Cr-OH_2$ bond is very slow and fast 'conventional' ligand substitution reactions can clearly be excluded.

The initial rate method provided information on phase II and yielded the orders of reaction as 0.97 ± 0.05 (1.03 ± 0.02) with respect to sulfite ion, and 0.92 ± 0.02 (0.95 ± 0.03) with respect to $Fe_2(OH)_2^{4+}$ at 430 nm (340 nm). The stoichiometry of phase II was determined from the concentration dependence of the amplitude of the absorbance change at 430 nm. The formation of a 1:1 complex was confirmed between $Fe_2(OH)_2^{4+}$ and sulfite ion:

$$K_{50} = \frac{[Fe_2(OH)(SO_3)^{3+}]}{[Fe_2(OH)_2^{4+}][HSO_3^-]} \tag{50}$$

The fitted value of K_{50} is shown in Table 17. The composition of $Fe_2(OH)(SO_3)^{3+}$ and the rate law for this step are in agreement with reaction 24 (page 44). It is worth noting that the chromium(III) analog of this dinuclear complex, $Cr_2(OH)(SO_3)^{3+}$, was reported in the literature.[200,204]

In the pH-dependent studies, k_D values were calculated by fitting the absorbance traces measured at 430 nm to the numerically integrated differential equation defined by the reversible reaction 24 (page 44). k_{-D} was forced to give the independently determined value of K_{50}. The pH-dependence of k_D is shown in Figure 19 and can be interpreted with the following two pathways:

$$Fe_2(OH)_2^{4+} + HSO_3^- = Fe_2(OH)(SO_3)^{3+}$$

$$v_{51} = k_{51}[Fe_2(OH)_2^{4+}][HSO_3^-] - k_{-51}[Fe_2(OH)(SO_3)^{3+}] \tag{51}$$

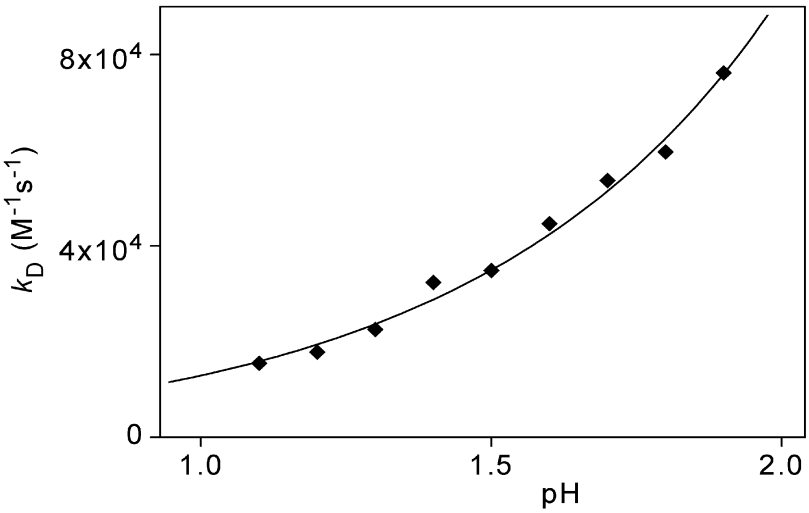

Figure 19. pH-dependence of k_D in the iron(III) – sulfite ion system. T = 10.0 °C; μ = 1.0 M ($NaClO_4$).

$$Fe_2(OH)_2^{4+} + SO_3^{2-} + H^+ = Fe_2(OH)(SO_3)^{3+}$$

$$v_{52} = k_{52}[Fe_2(OH)_2^{4+}][SO_3^{2-}] - k_{-52}[Fe_2(OH)(SO_3)^{3+}]/[H^+] \quad (52)$$

A derivation for k_D gives:

$$k_D = \frac{k_{51} + k_{52}/(K_{p1}[H^+])}{1 + K_{p2}[H^+]} \quad (53)$$

where K_{p2} is the protonation constant of hydrogensulfite ion ($K_{p2} = [H_2O{\cdot}SO_2]/[HSO_3^-]/[H^+]$), K_{p1} is the protonation constant of SO_3^{2-} ($K_{p1} = [HSO_3^-]/[SO_3^{2-}]/[H^+]$) (Table 8, page 36).

The redox reaction was taken into account during the final fitting. Reactions 54 and 55 were added to the model given in equations 24–27 (page 44) because they were shown to be the essential redox steps in the iron(III) – sulfite ion system under different conditions.[165]

$$FeSO_3^+ = Fe^{2+} + SO_3^{-\cdot}$$

$$v_{54} = k_{54}[FeSO_3^+] \quad (54)$$

$$Fe^{3+} + SO_3^{-\cdot} + H_2O = Fe^{2+} + SO_4^{2-} + 2H^+ \quad \text{fast} \quad (55)$$

This model interpreted the kinetic curves reasonably well. Attempts were made to include some kind of redox decomposition of $Fe_2(OH)(SO_3)^{3+}$ in the model, but such

Table 17. Parameters determined in the iron(III) – sulfite ion system. μ = 1.0 M ($NaClO_4$).

Parameter	10.0 ° C	25.0 ° C
k_{51}	$(4.5 \pm 0.3) \times 10^4$ $M^{-1}s^{-1}$	$(3.5 \pm 0.3) \times 10^5$ $M^{-1}s^{-1}$
k_{52}	$(2.1 \pm 0.2) \times 10^9$ $M^{-1}s^{-1}$	$\sim 4 \times 10^9$ $M^{-1}s^{-1}$
k_{54}	0.052 ± 0.012 s^{-1}	0.23 ± 0.04 s^{-1}
k_{56}	1.0 ± 0.3 s^{-1}	3.6 ± 0.8 s^{-1}
log K_{50}	3.37 ± 0.16	3.73 ± 0.11
ϵ $\{Fe_2(OH)(SO_3)^{3+}\}$	499 ± 65 $M^{-1}cm^{-1}$ [a]	549 ± 60 $M^{-1}cm^{-1}$ [a]

a: 430 nm

reaction steps were found to be marginal. The calculations showed that k_S was independent of pH implying that the dissociation of $Fe_2(OH)(SO_3)^{3+}$ occurs directly:

$$Fe_2(OH)(SO_3)^{3+} = FeOH^{2+} + FeSO_3^+$$

$$v_{56} = k_{56}[Fe_2(OH)(SO_3)^{3+}] - k_{-56}[FeOH^{2+}][FeSO_3^+] \quad (56)$$

A global fitting was also carried out based on the data measured at 10.0 °C. Several kinetic curves were fitted simultaneously to the model comprising reactions 49, 51, 52, 54, 55, and 56. Rate constants determined are shown in Table 17. It should be noted that the redox process was not complete within 15 minutes at 10.0 °C, but the stopped flow kinetic curves were only used in the calculations up to 1 minute. Thus, the measurements were repeated at 25.0 °C in order to inspect whether additional reactions needed to be taken into account at longer reaction times. The relevant parameters for the initial phase of the reaction were re-determined for this temperature as discussed before. In the final evaluation, kinetic curves were fitted individually to the same model that was used at 10.0 °C. It was concluded that the model was suitable for the interpretation of the whole process. Parameters determined at 25.0 °C are also shown in Table 17. Fitted and measured kinetic traces are compared in Figure 20.

Reaction 54 and the value obtained for k_{54} deserve some closer attention. This reaction is the key step in the redox process between iron(III) and sulfite ion. Although the corresponding rate constant was estimated earlier on the basis of model calculations,[165] the present study yielded the most straightforward results ever

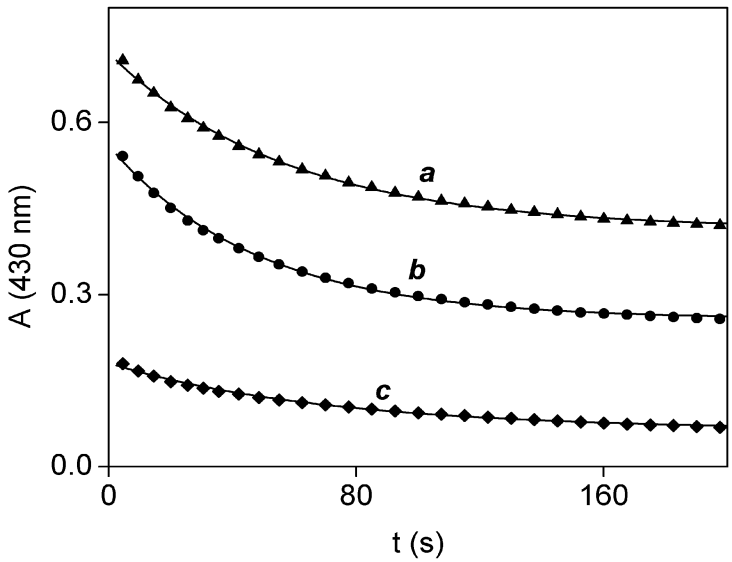

Figure 20. Measured and fitted curves in the iron(III) – sulfite ion system. Markers: measured points. Solid lines: fitted curves. [Fe(III)] = 75.0 mM, [S(IV)] = 1.00 mM, pH = 1.44, pH_{Fe} = 1.14 (***a***); [Fe(III)] = 50.0 mM, [S(IV)] = 1.00 mM, pH = 1.51, pH_{Fe} = 1.21 (***b***);[Fe(III)] = 34.8 mM, [S(IV)] = 2.00 mM, pH = 0.95; pH_{Fe} = 0.64 (***c***); T = 25.0 °C; μ = 1.0 M ($NaClO_4$). Only about 8% of the measured points are shown for clarity.

obtained on that process. The clarification of this point could be very helpful for further investigations on the iron(III) catalyzed autoxidation of sulfite ion.

In the view of the quite rapid redox reaction between iron(III) and sulfite ion, it is quite interesting that a crystal structure of an iron(III) hexasulfito complex, $(NH_4)_9[Fe(SO_3)_6]$, can be found in the literature.[205] In principle, a large excess of sulfite ion might inhibit the redox reaction with iron(III) provided that complexes with several sulfite ligands are inert to redox decomposition. However, kinetic data contradict this interpretation strongly.[165] Given the fact that the distinction between iron(II) and iron(III) is achieved through the presence or absence of a single N atom in this XRD study (hydrogens are invisible) and no further analytical data were reported, it is possible that the prepared salt is actually a complex of iron(II) and the XRD data need re-evaluation.

5.7.5. Phosphate and Arsenate Ions

These two ligands gave very similar results and are discussed together. Kinetic curves recorded in the iron(III) – arsenate ion system at two wavelengths are shown in Figure 21. The initial absorbance is practically the same in the presence and absence of arsenate ion suggesting that no instantaneous reaction occurs. A fast absorbance decrease (phase I) is followed by a slow increase (phase II) on longer time scales at 340 nm. Significant absorbance change does not occur in Phase I at 275 nm, where $FeH_2AsO_4^{2+}$ has a strong characteristic absorption band. Consequently, this mononuclear complex does not form in considerable amounts in the initial part of the reaction and the observations at 340 nm are consistent with the formation of a new complex.. Fully analogous curves were measured in the iron(III) – phosphate ion system.

On the basis of the initial rate method (Figure 22) the reaction was found to be first-order with respect to $Fe_2(OH)_2^{4+}$ as well as the ligand in both systems. The stoichiometry of phase I was confirmed by measuring the amplitude of absorbance change as a function of reactant concentrations (Figure 23). It was concluded that the product is a 2:1 complex of $Fe_2(OH)_2^{4+}$ and the ligand and this complex has no absorption at 340 nm. As the stoichiometry was unexpected, the Job method[199] was also used to confirm the results (Figure 24). The maximum at 2:1 $[Fe_2(OH)_2^{4+}]$: [L] ratio on the Job curve is in agreement with the previous conclusion about the stoichiometry.

The stoichiometry and the rate equation can be interpreted by adding the following reaction to the model given in equations 24–27:

$$Fe_2L + Fe_2(OH)_2^{4+} = Fe_4L \qquad K_{58} = \frac{[Fe_4L]}{[Fe_2(OH)_2^{4+}][Fe_2L]} \qquad (58)$$

Reaction 58 is a fast equilibrium as proved by later calculations.

The pH-dependence of phase I was studied by calculating k_D values from the measured initial rates at 340 nm in the iron(III) – arsenate ion system. In the iron(III) – phosphate ion system, k_D values were calculated by fitting the absorbance traces at 340 and 370 nm to the numerically integrated differential equation defined by reaction 24 (the reverse reaction could be neglected in the initial 200 ms). The results of pH-dependent studies are shown in Figure 25 and can be interpreted with the following pathways:

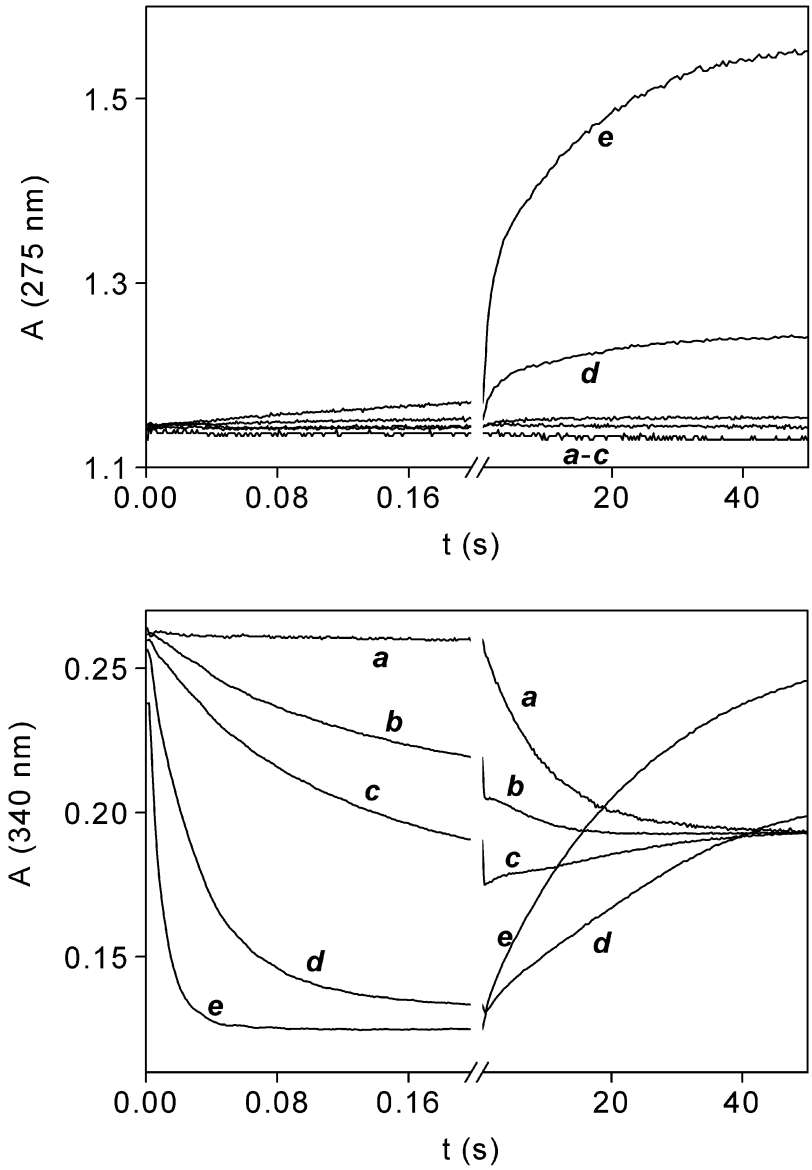

Figure 21. Typical kinetic curves in the iron(III) – arsenate ion system. [Fe(III)] = 4.50 mM: $[Fe_2(OH)_2^{4+}]_0$ = 0.050 mM; [As(V)] = 0 (***a***), 0.025 mM (***b***), 0.050 mM (***c***), 0.25 mM (***d***), 1.0 mM (***e***); pH = 1.60; pH_{Fe} = 1.60; T = 10.0 °C; μ = 1.0 M ($NaClO_4$); optical path length 1 cm (340 nm), 2 mm (275 nm).

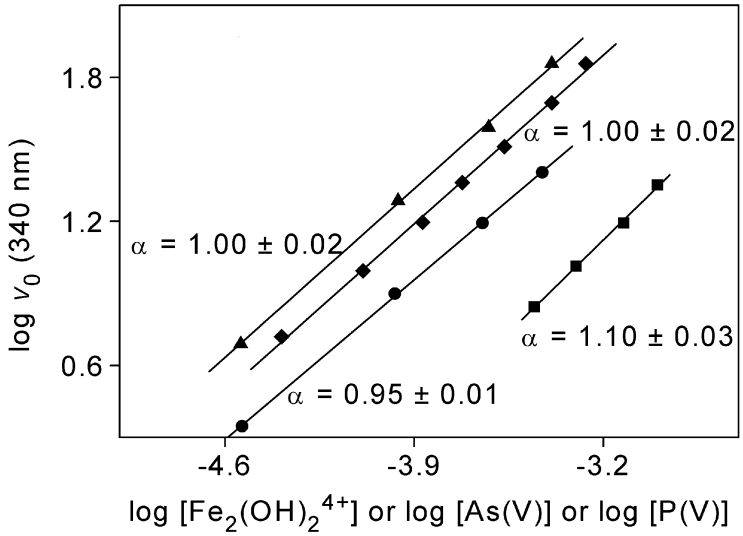

Figure 22. Initial rate method in the iron(III) – phosphate ion and arsenate ion systems. $[Fe_2(OH)_2^{4+}]_0 = 0.23$ mM (■) or $[P(V)]_0 = 0.75$ mM (●) and pH =1.68 for phosphate ion; $[Fe_2(OH)_2^{4+}]_0 = 0.41$ mM (▲) or [As(V)] =0. 50 mM (◆) and pH = 1.70 for arsenate ion; $T = 10.0$ °C; $\mu = 1.0$ M ($NaClO_4$); optical path length 1 cm; v_0 unit: AU·s^{-1}; concentration unit: M..

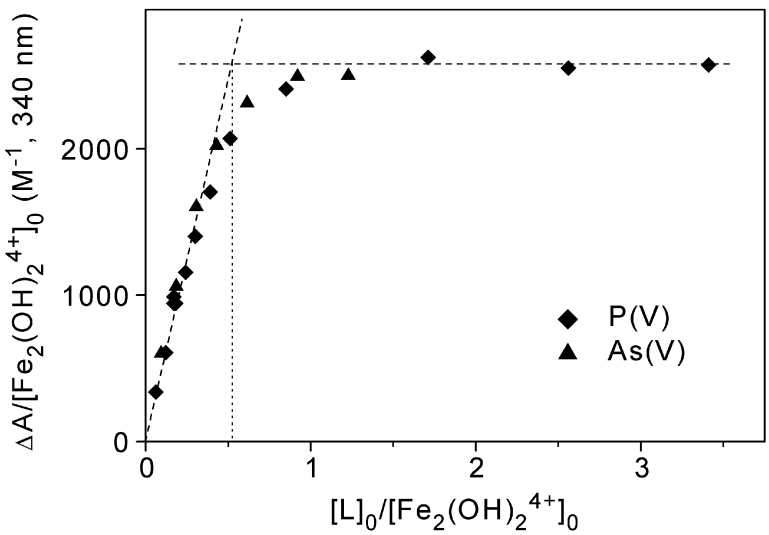

Figure 23. Normalized absorbance change in phase I as a function of the ligand/hydroxo dimer concentration ratio in the iron(III) – arsenate ion and phosphate ion systems. pH = 1.60 (phosphate ion), 1.70 (arsenate ion); T = 10.0 °C; $\mu = 1.0$ M ($NaClO_4$); optical path length 1 cm.

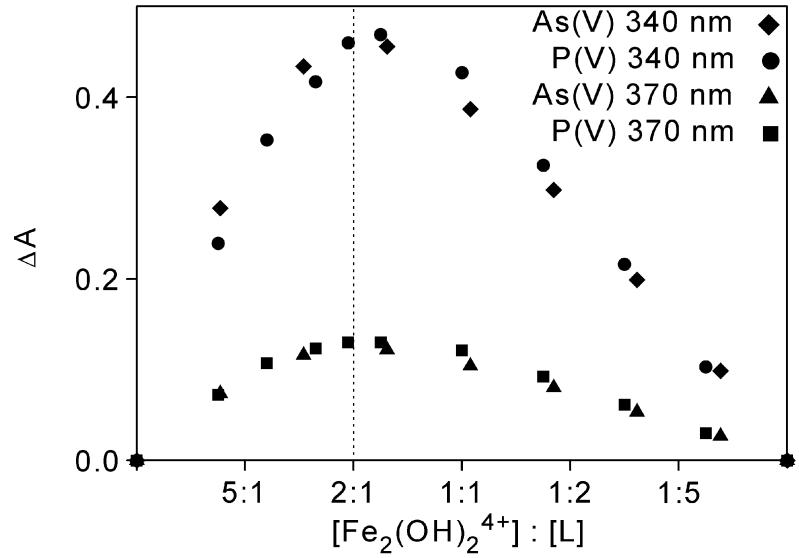

Figure 24. Job plot in the iron(III) – phosphate ion and arsenate ion systems at 340 and 370 nm. $[Fe_2(OH)_2^{4+}] + [P(V)] = 0.384$ mM; pH = 1.60 (phosphate ion); $[Fe_2(OH)_2^{4+}] + [As(V)] = 0.40$ mM; pH = 1.70 (arsenate ion); $T = 10.0$ °C; $\mu = 1.0$ M ($NaClO_4$); optical path length 1 cm.

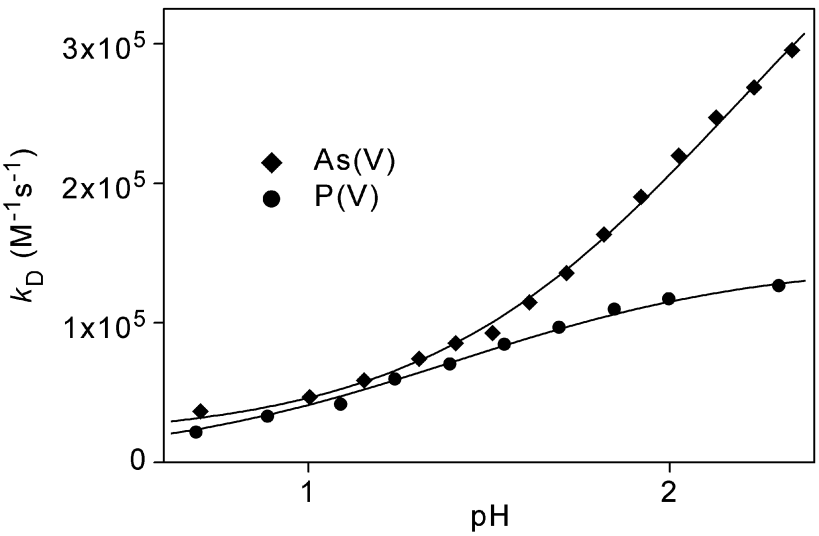

Figure 25. pH-dependence of k_D in the iron(III) – phosphate ion and arsenate ion systems. $T = 10.0$ °C; $\mu = 1.0$ M ($NaClO_4$).

$Fe_2(OH)_2^{4+} + H_3XO_4 = Fe_2(OH)(HXO_4)^{3+} + H^+$

$$v_{59} = k_{59}[Fe_2(OH)_2^{4+}][H_3XO_4] - k_{-59}[Fe_2(OH)(HXO_4)^{3+}][H^+] \quad (59)$$

$Fe_2(OH)_2^{4+} + H_2XO_4^- = Fe_2OH(HXO_4)^{3+}$

$$v_{60} = k_{60}[Fe_2(OH)_2^{4+}][H_2XO_4^-] - k_{-60}[Fe_2(OH)(HXO_4)^{3+}] \quad (60)$$

where X= P or As. A derivation for k_D gives:

$$k_D = \frac{k_{60} + k_{59}K_p[H^+]}{1 + K_p[H^+]} \quad (61)$$

where K_p is the protonation constant of dihydrogenphosphate or dihydrogenarsenate ions ($K_p = [H_3XO_4]/[H_2XO_4^-]/[H^+]$). k_{59} was too small to be determined in the phosphate ion system.

The evaluation of the full kinetic traces showed that k_S could not be determined with any acceptable precision and its significance was marginal. Attempts to obtain rate constants for reaction 58 were also unsuccessful. This reaction step could only be interpreted as a fast equilibrium. Very good fits were obtained with k_S fixed at zero. It is concluded that reaction 25 is unimportant and it was left out from the final model. Thus, only k_{-D} and K_{58} were fitted as free parameters. Both of these parameters were independent of pH. It follows that the composition of Fe_4L should be $Fe_4(XO_4)(OH)_2^{7+}$. In the iron(III) – phosphate ion system simultaneous fitting to all kinetic curves recorded at 340 and 370 nm were also carried out. It was concluded that no further reactions are needed to interpret the kinetic traces. Rate constants determined with fitting the kinetic traces are shown in Table 18. Fitted and measured curves for arsenate ion are compared in Figure 26.

Table 18. Parameters determined in the iron(III) – phosphate ion and arsenate ion systems. T = 10.0 °C; μ = 1.0 M ($NaClO_4$).

Parameter	P(V)	As(V)
k_{59}	– [a]	$(8 \pm 2) \times 10^3$ $M^{-1}s^{-1}$
k_{60}	$(1.44 \pm 0.02) \times 10^5$ $M^{-1}s^{-1}$	$(2.5 \pm 0.1) \times 10^5$ $M^{-1}s^{-1}$
k_{-59}	– [a]	26 ± 3 $M^{-1}s^{-1}$
k_{-60}	0.18 ± 0.03 s^{-1}	108 ± 16 s^{-1}
K_{58}	$(7 \pm 2) \times 10^4$ M^{-1}	$(6 \pm 2) \times 10^4$ $M^{-1}s^{-1}$
$\epsilon\{FeH_2XO_4^{2+}\}$	160 ± 30 $M^{-1}cm^{-1}$ [b] ~ 0 [c]	460 ± 50 $M^{-1}cm^{-1}$ [b]

a: too small to be determined; b: 340 nm; c: 370 nm

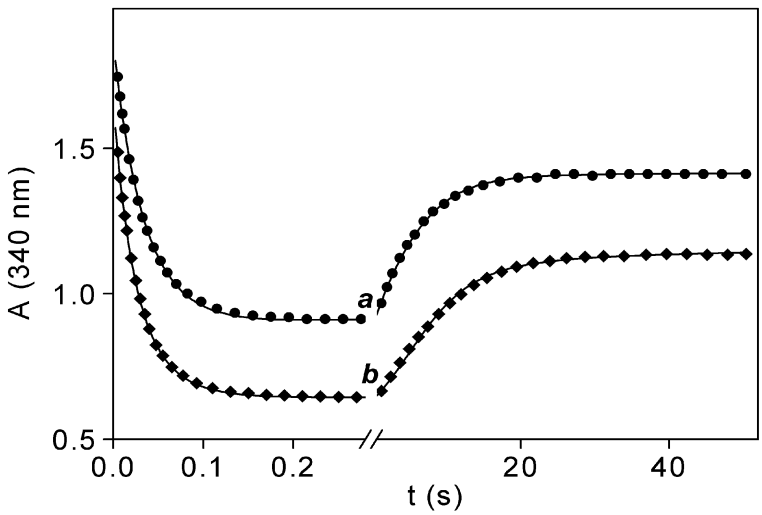

Figure 26. Measured and fitted kinetic curves in the iron(III) – arsenate ion system. Markers: measured points. Solid lines: fitted curves. [Fe(III)] = 78.9 mM (***a***), 44.9 mM (***b***); [As(V)] =0. 64 mM (***a***, ***b***); pH = 1.00 (***a***), 0.75 (***b***); pH_{Fe} = 1.00 (***a***), 0.75 (***b***); T = 10.0 °C; μ = 1.0 M ($NaClO_4$); optical path length 1 cm. Only about ~ 10% of the measured points are shown for clarity.

5.7.6. Arsenite Ion

Arsenite ion is present as H_3AsO_3 under acidic conditions. It has been pointed out that the structure is perhaps better expressed by the formula $As(OH)_3$.[206] The first formula is adapted in this work to indicate the overall composition only.

Iron (III) solutions have the same UV-vis spectra in the presence and absence of arsenite ion, i.e. possible complexation of iron(III) by arsenite ion cannot be detected by spectrophotometry. Nevertheless, arsenite ion catalyzes the dissociation of the hydroxo dimer.

Figure 27 shows experiments where an iron(III) solution was mixed with an acid solution with different arsenite ion concentrations. The reaction is first-order and it becomes faster with increasing arsenite ion concentration. The kinetic traces are identical regardless whether arsenite ion is initially added to the iron(III) (***b***) or the acid solution (***c***). This is a further piece of evidence that stable complexes, which would certainly influence the dissociation rate of $Fe_2(OH)_2^{4+}$ in case ***b***, do not form between the reactants. This conclusion is also supported by the observation that all

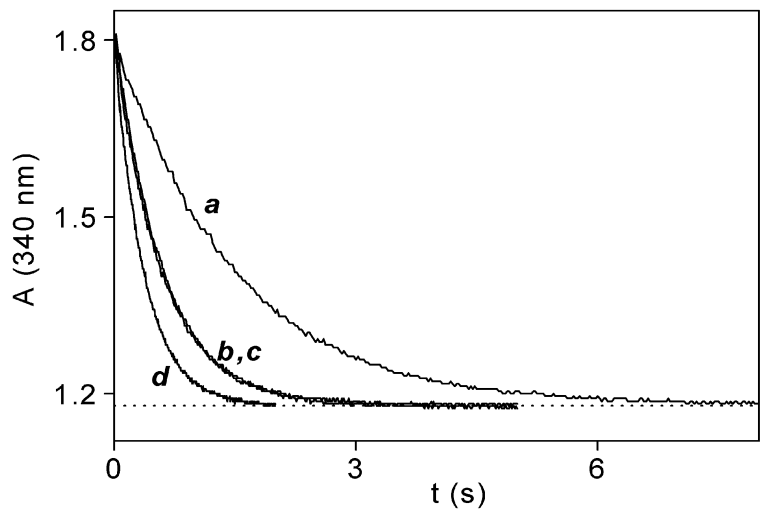

Figure 27. Kinetic traces demonstrating the catalytic effect of arsenite ion on the hydrolysis of iron(III). [Fe(III)] = 3.78 mM; [As(III)] = 0 (***a***), 0.50 mM pre-mixed with iron(III) solution (***b***), 0.50 mM pre-mixed with acid (***c***), 1.0 mM (***d***); pH = 1.96; pH_{Fe} = 1.98; T = 25.0 °C; μ = 1.0 M ($NaClO_4$); optical path length 1 cm. See text for a detailed explanation of the difference between experiment ***b*** and ***c***.

curves have the same initial and final absorbance values regardless of the actual concentration of arsenite ion.

As shown in Figure 28, the pseudo first-order rate constant, k_{obs}, is a linear function of the concentration of arsenite ion.

$$k_{obs} = k_{hdr} + k_{cat}[\mathrm{As(III)}] \quad (62)$$

k_{obs} was found to be independent of total iron(III) concentration below pH 1.7. The values of k_{cat} are plotted as a function of pH in Figure 29. The curve reaches some kind of limiting value at high acidities, has a minimum at about pH 1.8 and rises again at lower acidities. k_{cat} is slightly dependent on the total iron(III) concentration above pH 1.7. The shape of the curve in Figure 29 indicates that at least two catalytic pathways are operative. However, the observed pH-dependence cannot be assigned to any known protolytic equilibrium which involves the reactants. The lowest pK of arsenious acid (H_3AsO_3) was reported to be 9.23,[171] and our spectrophotometric measurements also confirmed the lack of any pH-dependent process with arsenite ion in the pH 0–2.0 region. The main hydrolytic reaction of iron(III) is the formation of $FeOH^{2+}$ in this pH range. However the observed effect cannot be assigned to the variation in [$FeOH^{2+}$] as a function of pH because a markedly different pH profile would be expected. It might be argued that the difference between the lowest and highest k_{cat} values is only about 50%, and some of the change might be due to variation in the medium because at high acidities significantly smaller amounts of $NaClO_4$ are used to set the ionic strength. In order to test this possibility, we carried out two series of experiments in somewhat different media: the first with always 1.00 M $NaClO_4$ added, i.e. $\mu > 1.0$ M at high acidities, and the second with smaller amounts of $NaClO_4$ to set the ionic strength exactly to 1.0 M. The corresponding rate constants agreed within 5% confirming that medium effects do not contribute to the noted pH dependence of k_{cat}.

The catalytic effect of arsenite ion implies a direct interaction between the hydroxo dimer and the ligand. It is assumed that a dinuclear complex, Fe_2As^{III}, is formed, which is similar to the ones described with the other ligands in this study.

$$Fe_2(OH)_2^{4+} + H_3AsO_3 = Fe_2As^{III}$$

$$v_{63} = k_{63}[Fe_2(OH)_2^{4+}][H_3AsO_3] - k_{-63}[Fe_2As^{III}] \quad (63)$$

While Fe_2As^{III} is not formed in detectable concentrations, it may open a catalytic pathway for the hydrolytic reaction via fast dissociation into mononuclear iron(III) species. The pH-dependence of k_{cat} strongly suggests that the dinuclear arsenito complex undergoes direct and proton-assisted dissociations.

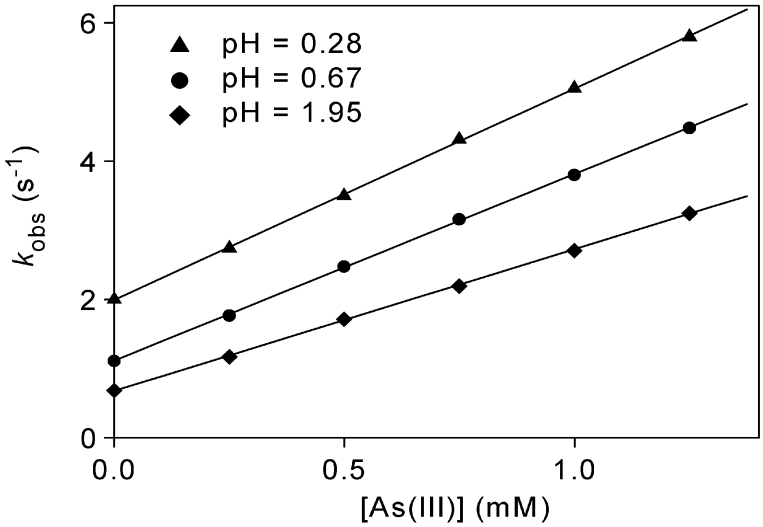

Figure 28. k_{obs} as a function of the concentration of arsenite ion. [Fe(III)] = 3.78 mM; T = 25.0 °C; μ = 1.0 M ($NaClO_4$).

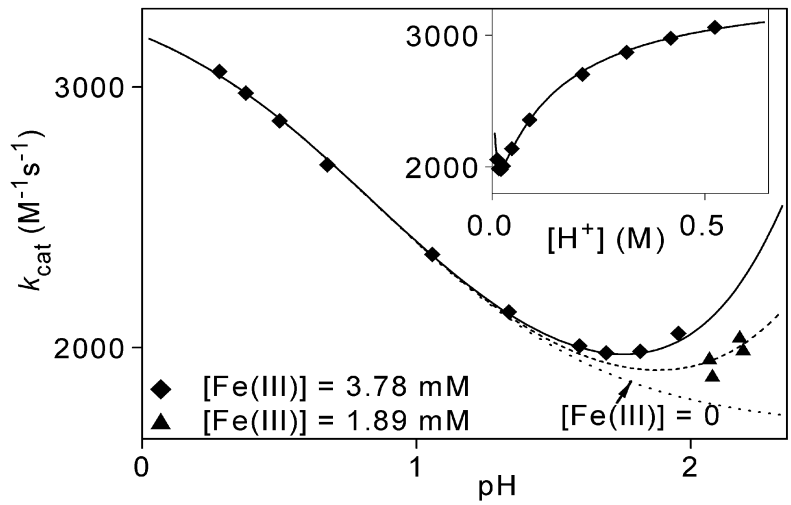

Figure 29. k_{cat} as a function of pH in the iron(III) – arsenite ion system. Inset: k_{cat} as a function of [H^+]. T = 25.0 °C; μ = 1.0 M ($NaClO_4$). Lines represent the best fit to equation 67.

$$Fe_2As^{III} = FeOH^{2+} + FeAs^{III}$$

$$v_{64} = k_{64}[Fe_2As^{III}] - k_{-64}[FeOH^{2+}][FeAs^{III}] \quad (64)$$

$$Fe_2As^{III} + H^+ = Fe^{3+} + FeAs^{III}$$

$$v_{65} = k_{65}[Fe_2As^{III}][H^+] - k_{-65}[Fe^{3+}][FeAs^{III}] \quad (65)$$

The scheme is completed by the dissociation of the mononuclear arsenito complex $FeAs^{III}$, which is always present at very low concentration levels. In order to be able to coordinate to the metal ion, H_3AsO_3 needs to release at least one proton and the corresponding reaction can be written as:

$$Fe^{3+} + H_3AsO_3 = FeAs^{III} + H^+ \qquad K_{66} = \frac{[FeAs^{III}][H^+]}{[Fe^{3+}][H_3AsO_3]} \quad (66)$$

Assuming that Fe_2As^{III} is in steady state, standard derivation on the basis of reactions 63–66 yields the following formula for k_{cat}:

$$k_{cat} = \frac{k_{63}k_{64}/k_{65} + k_{63}[H^+]}{(k_{-63} + k_{64})/k_{65} + [H^+]} + \frac{4[Fe_{tot}](k_{-63}k_{-64}/k_{65})K_1K_{66} + (k_{-63}k_{-65}/k_{65})K_{66}[H^+])}{(K_1 + [H^+] + K_2/[H^+])^2((k_{-63} + k_{64})/k_{65} + [H^+])} \quad (67)$$

Considering microscopic reversibility, $k_{-63}k_{-64}K_1K_{66}$ and $k_{-63}k_{-65}K_{66}$ can be replaced by $k_{63}k_{64}K_3$ and $k_{63}k_{65}K_3$, respectively. This leaves only three independent parameters, k_{63}, $k_{63}k_{64}/k_{65}$ and $(k_{-63} + k_{64})/k_{65}$. A fitting was also attempted with five independent parameters, but gave unsatisfactory results because of irresolvable cross correlation between the parameters. The parameters estimated with non-linear least squares fitting are listed in Table 19.

A closer look at the scheme described in reactions 63–66 and the values of the parameters reveals why k_{cat} reaches a limiting value at high acidity. At lower acidities reaction 64 is rate determining in the catalytic pathway. At higher acidities

Table 19. Parameters determined in the iron(III) – arsenite ion system. T = 25.0 °C; μ = 1.0 M ($NaClO_4$).

k_{63}	$(3.43 \pm 0.03) \times 10^3$ $M^{-1}s^{-1}$
$k_{63}k_{64}/k_{65}$	$(2.5 \pm 0.1) \times 10^2$ s^{-1}
$(k_{-63} + k_{64})/k_{65}$	0.149 ± 0.008 M
$K_{66}k_{-63}k_{-64}/k_{65}$	1.8×10^2 s^{-1} [a]
$K_{66}k_{-63}k_{-65}/k_{65}$	4.7 s^{-1} [b]

a: calculated as $(k_{63}k_{64}/k_{65})K_3/K_1$; b: calculated as $k_{63}K_3$

reaction 65 increases the dissociation rate of Fe_2As^{III}, and reaction 63 eventually becomes rate determining.

5.7.6. Sulfate Ion

Typical kinetic curves recorded in the iron(III) – sulfate ion system are shown in Figure 30. It is clearly seen that the initial absorbance measured in the presence of sulfate ion is significantly lower than in the corresponding experiment without the ligand. This initial absorbance jump is consistent with an instantaneous reaction (phase I), which was immeasurably fast even at 5.0 °C regardless of the initial concentrations. A detailed analysis proved that the absorbance jump is due to a direct reaction between $Fe_2(OH)_2^{4+}$ and sulfate ion. This is in agreement with the fact that the reaction of mononuclear iron(III) with sulfate was shown to be much slower in independent experiments (section 5.5.2., page 39). The amplitude of the absorbance jump increases with increasing sulfate ion concentration and the pH-dependence of ΔA correlates well with the shift in the HSO_4^-/SO_4^{2-} protolytic equilibrium (Figure 31). All results could be interpreted by assuming the formation of a dinuclear complex which has negligible absorption at 340 nm.

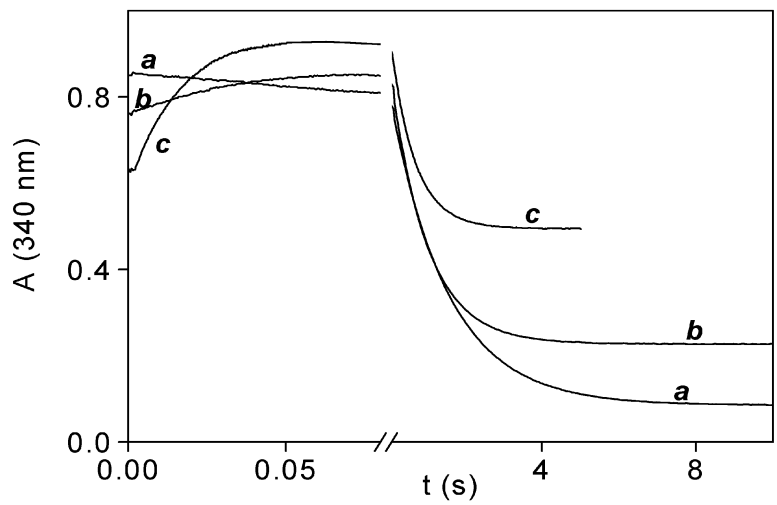

Figure 30. Kinetic traces in the iron(III) – sulfate ion system. [Fe(III)] = 3.0 mM; $[SO_4^{2-}]_T$ = 0 (***a***), 0.50 mM (***b***), 1.50 mM (***c***); pH = 1.12; pH_{Fe} = 2.00; T = 25.0 °C; μ = 1.0 M ($NaClO_4$); optical path length 1 cm.

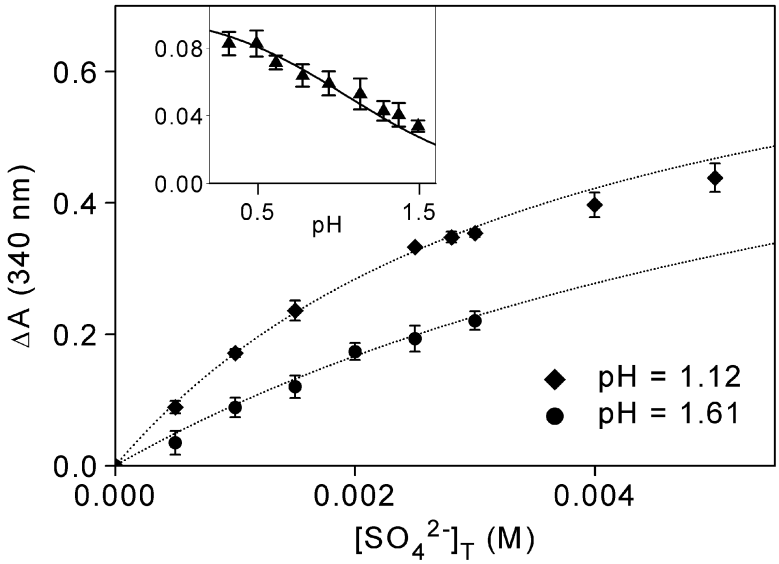

Figure 31. Initial absorbance jump as a function of sulfate ion concentration in the iron(III) – sulfate ion system ([Fe(III)] = 3.00 mM). Inset: Absorbance jump as a function of pH ([Fe(III)] = 5.00 mM; $[SO_4^{2-}]$ = 0.30 mM). T = 25.0 °C; μ = 1.0 M ($NaClO_4$); optical path length 1 cm. Lines: best fit to equation 68.

$$Fe_2(OH)_2^{4+} + HSO_4^- = Fe_2(OH)(SO_4)^{3+} \qquad K_{68} = \frac{[Fe_2(OH)(SO_4)^{3+}]}{[Fe_2(OH)_2^{4+}][HSO_4^-]} \qquad (68)$$

The value of K_{68} is given in Table 20. It should be noted that this is one of the limiting cases when our test method is not able to indicate the formation of a dinuclear complex because the reaction is instantaneous and does not contribute to the measured initial rate.

From the fact that the reaction is instantaneous, a lower limit, $k_{68} > 10^7\ M^{-1}s^{-1}$, can be estimated for the second-order formation rate constant, but it should be kept in mind that either HSO_4^- or SO_4^{2-} can be kinetically reactive in this step. The high k_{68} value is tentatively assigned to the pathway with sulfate ion because the deprotonated form of a ligand usually reacts faster in substitution reactions (further discussion in section 5.8., page 76).

As seen from Figure 30, there are two additional distinct phases (phase II and III) in the process. Analysis of phase II showed that this step could be interpreted as the formation of the mononuclear iron(III) sulfato complex $FeSO_4^+$.

$$Fe^{3+} + SO_4^{2-} = FeSO_4^+ \qquad K_{69} = \frac{[FeSO_4^+]}{[Fe^{3+}][SO_4^{2-}]} \tag{69}$$

The value of K_{69} is found in Table 9 (page 38). The kinetics of this phase was in excellent agreement with data obtained independently for the mononuclear complexation (section 5.5.2., page 39).

Phase III could be interpreted as equilibration between mononuclear and dinuclear forms of iron(III). This step always gave an excellent fit to an exponential function, but the pseudo first-order rate constants obtained were systematically and significantly larger than expected on the basis of equation 12 (page 27). This observation strongly suggests that sulfate ion catalyzes the hydrolysis iron(III). The catalytic effect could be interpreted by the dissociation of the dinuclear complex, which seems to be a commonly important step in most of the reactions studied here.

$$Fe_2(OH)SO_4^{3+} = FeOH^{2+} + FeSO_4^+$$

$$v_{70} = k_{70}[Fe_2(OH)(SO_4)^{3+}] - k_{-70}[FeOH^{2+}][FeSO_4^+] \tag{70}$$

Proton-assisted dissociation of $Fe_2(OH)(SO_4)^{3+}$, if it occurs at all, does not contribute to the measured rate and k_{obs} can be expressed as follows:

$$k_{obs} = k_a + 4k_{-a}[Fe_{mn}] \tag{71}$$

where k_a and k_{-a} are

$$k_a = \frac{k_H(1 + K_p[H^+]) + k_{70}K_{68}K_p[S(VI)][H^+]}{1 + K_p[H^+] + K_{68}K_p[S(VI)][H^+]} \tag{72}$$

$$k_{-a} = k_{-H} + \frac{k_{-70}K_{69}K_1[S(VI)][H^+]}{(1 + K_p[H^+])(K_1 + [H^+] + K_2/[H^+])^2} \tag{73}$$

where K_p is the protonation constant of sulfate ion ($K_p = [HSO_4^-]/[SO_4^{2-}]/[H^+]$), [S(VI)] is the concentration of uncomplexed sulfate ion (= $[HSO_4^-] + [SO_4^{2-}]$), which was calculated using the known equilibrium constants for each point. k_{-70} was

Table 20. Parameters determined in the iron(III) – sulfate ion system. T = 25.0 °C; μ = 1.0 M ($NaClO_4$).

K_{68}	$(6.0 \pm 0.1) \times 10^2$ M^{-1}
k_{70}	4.60 ± 0.06 s^{-1}
k_{-70}	200 $M^{-1}s^{-1}$ [a]
$\varepsilon\{FeSO_4^+\}$	1811 ± 8 $M^{-1}cm^{-1}$ [b]

a: calculated as $k_{70}K_3K_{68}K_p/(K_1K_{69})$
b: 340 nm

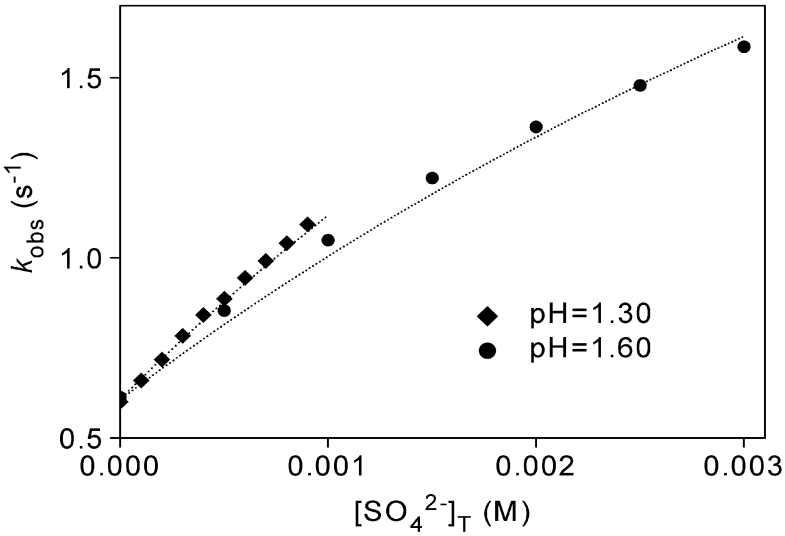

Figure 32. k_{obs} as a function of sulfate ion concentration in the iron(III) – sulfate ion system. Dashed lines represent the best fit to equations 71–73. [Fe(III)] = 5.00 mM for pH = 1.30; [Fe(III)] = 3.00 mM for pH = 1.60; T = 25.0 °C; μ = 1.0 M ($NaClO_4$).

replaced by $k_{70}K_3K_{68}K_p/(K_1K_{69})$ because of microscopic reversibility. The estimated parameters are listed in Table 20 and the best fit of the experimental k_{obs} values to equations 71–73 is illustrated in Figure 32.

5.8. Mechanistic and Structural Considerations

The results presented here prove the formation of transient di- and tetranuclear complexes between the iron(III) hydroxo dimer and simple inorganic ligands. With the exception of the arsenite ion system, the absorbance decay at the characteristic band of $Fe_2(OH)_2^{4+}$ could be used to obtain quantitative information on the equilibrium and kinetic features of these reactions. In the sulfite ion system, a relatively weak absorption band of the transient dinuclear complex could also be identified.

Table 21 summarizes the rate constants determined for the direct complex formation reactions of the hydroxo dimer with different protonated forms of various ligands. Significant differences are not found between the corresponding rate

Table 21. Rate constants for the reactions $Fe_2(OH)_2^{4+} + H_xL \rightarrow Fe_2L$ $T = 10.0$ °C; $\mu = 1.0$ M ($NaClO_4$).

Ligand (H_nL)	k ($M^{-1}s^{-1}$)		
	H_nL	$H_{n-1}L^-$	$H_{n-2}L^{2-}$
H_3PO_2	2.9×10^4	3.5×10^5	–
H_3PO_3	3.3×10^4	3.4×10^5	–
H_3PO_4	$< 1 \times 10^4$	1.4×10^5	–
H_3AsO_3	3.4×10^3 [a]	–	–
H_3AsO_4	8×10^3	2.5×10^5	–
$H_2O{\cdot}SO_2$	$< 5 \times 10^3$	4.5×10^4	2.1×10^9
H_2SO_4	–	– [b]	$> 1.0 \times 10^7$
H_2SeO_3	2.7×10^4	4.6×10^5	–

a: 25.0 °C; b: no data, any value $< 10^6$ does not contradict the results

constants of the neutral as well as the uninegative forms of the ligands implying that specific interactions are not operative in these reactions. Accordingly, the results suggest that these reactions are controlled by the properties of the metal center(s) and they proceed via a dissociative interchange (I_d) mechanism. Thus, $k = k_{ex}K_{ip}$ applies, where k is the rate constant of the complex formation reaction, k_{ex} is the rate constant of the water exchange between the hydroxo dimer and the bulk water, and K_{ip} is the ion pair stability constant between the reactants. The 10 to 30 times difference between the rate constants of the two forms of the same ligand is consistent with this interpretation. The noted difference can conveniently be explained in terms of the charge products of the reactants as the Fuoss equation[207] predicts the following stability constants for ion pair formation with a tetrapositive ion (10.0 °C and $\mu = 1.0$ M): $K_{ip} = 0.32$ M^{-1} (neutral ligand), $K_{ip} = 2.8$ M^{-1} (uninegative ligand). The confirmation of these considerations would require a well-defined k_{ex} value for the hydroxo dimer. However, the determination of this water exchange rate constant does not seem to be feasible because of experimental limitations. Apparently the same interpretation does not apply for the dinegative SO_3^{2-} ion. In this case, the Fuoss equation predicts $K_{ip} = 24$ M^{-1}, which would be consistent with a difference of approximately one order of magnitude between the rate constants of the HSO_3^- and

SO_3^{2-} forms. The reason for the very high second-order rate constant of the SO_3^{2-} ion pathway is unclear, and may possibly be related to the unique chemistry of aqueous sulfite ion.

The formation of $Fe_2(OH)(SO_4)^{3+}$ was instantaneous, and only a lower limit could be determined for the corresponding rate constant. HSO_4^- and SO_4^{2-} are always present in comparable concentrations and it is very likely that the SO_4^{2-} path is predominant in the formation of this complex as deprotonation of a ligand typically enhances its reactivity. It should be added that dinegative forms of other ligands, such as HPO_4^{2-} or SeO_3^{2-}, might be similarly reactive. However, these forms are always present at extremely low concentration levels under the conditions applied, and the contributions of their reactions to the overall rate is negligible.

Thorough structural characterization of the identified di- and tetranuclear intermediates seems to be beyond experimental limitations because the lifetime of these species does not exceed a few seconds in solution. For the same reason, preparation of solid salts of these complexes is looks rather unfeasible. The results obtained here allow only general conclusions for the structures of the di- and tetranuclear complexes. In this respect, it is noteworthy that only oxoanions ($H_lXO_m^{n-}$) form such complexes and direct reactions were not observed between $Fe_2(OH)_2^{4+}$ and ligands which are otherwise fairly good complexing agents for mononuclear iron(III) forms. While the bent O–X–O moiety of an oxoanion may coordinate to two metal centers simultaneously, similar coordination modes can be excluded with ligands such as N_3^-, SCN^-, Cl^-. The geometry, most probably the appropriate O–X–O angle, appears to be a key factor because the formation of analogous complexes could not be found with some ligands that also contain the O–X–O motif, e.g. acetate ion and its derivatives. In accordance with these considerations, the core structures shown in Scheme 4 are proposed for $Fe_4(PO_4)(OH)_2^{7+}$ and $Fe_2(OH)(SO_3)^{3+}$. It seems likely that all other di- and tetranuclear intermediates have similar structures.

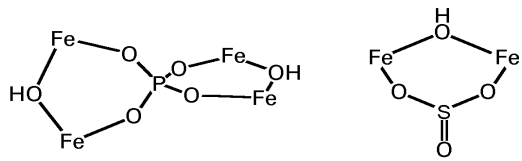

Scheme 4. Proposed core structures for $Fe_4(PO_4)(OH)_2^{7+}$ and $Fe_2(OH)(SO_3)^{3+}$.

On the basis of an XRD study, a structure very similar to those shown in Scheme 4 was reported for the core $Fe_4(\mu_4\text{-}OHO)(\mu\text{-}OH)_2^{7+}$ recently.[208] Other examples supporting our assumptions can be found in the literature where all four oxygen atoms of a phosphate ion are coordinated to different iron(III) centers.[209,210] However, these structural analogies should not be overvalued because the solid state structures determined for iron(III) complexes are so versatile that XRD support for almost any structural motif can be found in the literature.

The odd feature of $Fe_4(XO_4)(OH)_2^{7+}$ complexes is their relatively high stability despite the large overall positive charge. It seems to be very plausible that the +7 charge is localized mainly on the four iron atoms. Repulsive forces between the positively charged metal centers should destabilize the tetranuclear complex. The existence of these species may indicate that the coordinated water molecules somehow offset the effects of repulsion. It should be added that the average charge of an iron atom is somewhat smaller in the teranuclear and most of the dinuclear complexes than in $Fe_2(OH)_2^{4+}$. The smaller average charge may be a stabilizing factor, too. It is notable that this effect is absent in the case of $Fe_2(OH)(H_2PO_2)^{4+}$ and $Fe_2(OH)(H_2AsO_3)^{4+}$, which only have very short lifetimes.

Another interesting point in this study is that the rate constants k_{-D} and k_S have very similar pH-dependences whithin each system. Both of these rate constants refer to a monomolecular decomposition of Fe_2L. The products are $Fe_2(OH)_2^{4+}$ and L in the k_{-D} path (equation 24, page 44), FeL and Fe_{mn} in the k_S path (equation 25, page 44). The results suggest that the same intermediates are involved in these processes. These intermediates may be similar to species ***b***, ***d***, and ***f*** in Scheme 3 (page 29) in that they contain only one hydroxo bridge, in addition to a ligand that is coordinated to a single metal center. This intermediate may decompose either through the dissociation of the ligand giving the hydroxo dimer and a free ligand, or the cleavage of the hydroxo bridge resulting in the formation of two mononuclear complexes.

6. Summary

This dissertation summarizes detailed studies on the direct ligand substitution reactions of the iron(III) hydroxo dimer, $Fe_2(\mu\text{-}OH)_2(H_2O)_8^{4+}$, with hypophosphite, phosphite, phosphate, arsenite, arsenate, sulfite, sulfate, and selenite ions carried out mainly by the stopped flow method.

Hydrolytic equilibria of aqueous iron(III) were studied with UV-vis spectrophotometry and stability constants for $FeOH^{2+}$ and $Fe_2(OH)_2^{4+}$ were determined for the conditions applied in this study. The kinetics of the formation and dissociation of the hydroxo dimer was investigated and a previously proposed mechanism was improved to interpret kinetic data at higher pH.

Dinuclear and mononuclear forms of aqueous iron(III) cannot be separated, and the spectral effects usually provide little support to decide which form reacts with a particular ligand. A method was developed to confirm the direct ligand substitution reactions of $Fe_2(OH)_2^{4+}$ based on a comparison of initial rates measured in two complementary kinetic experiments. Protonation constants of the studied ligands were determined. The equilibrium and kinetics of the formation of mononuclear iron(III) complexes in these systems were characterized.

The detailed studies established that di- or, in the case of phosphate and arsenate ions, tetranuclear intermediates form in these reactions, and the final products are mononuclear iron(III) complexes. Quantitative information on the multinuclear intermediates could be obtained by monitoring the absorbance change at the characteristic band of the hydroxo dimer. The intermediates $Fe_4(PO_4)(OH)_2^{7+}$, $Fe_4(AsO_4)(OH)_2^{7+}$, $Fe_2(OH)(SO_3)^{3+}$, $Fe_2(OH)(SeO_3)^{3+}$, $Fe_2(OH)(HPO_3)^{3+}$, $Fe_2(OH)(SO_4)^{3+}$, $Fe_2(OH)(H_2PO_2)^{4+}$, $Fe_2(OH)(H_2AsO_3)^{4+}$, $Fe_2(OH)(HPO_4)^{3+}$, $Fe_2(OH)(HAsO_4)^{3+}$ were identified in the studied systems. The rate constants of the dominant reaction paths were determined in each reaction. The validity of the models were tested by calculations. Neutral forms of ligands were usually found to react an order of magnitude slower with $Fe_2(OH)_2^{4+}$ than the uninegative forms, and the rate constants are very similar for different ligands. This was interpreted in the terms of a dissociative interchange mechanism and the differences in the rate constants were explained by considering the differences in the stabilities of the ion pairs formed between the reactants.

Arsenite ion does not form any detectable complexes with iron(III), but markedly catalyzes the dissociation of $Fe_2(OH)_2^{4+}$ into mononuclear species. A kinetic model was proposed for this reaction which postulates the formation of a dinuclear arsenito complex at low concentration levels.

In the sulfite ion system, the redox reaction between iron(III) and sulfur(IV) was also studied. It was shown that the presence or absence of oxygen does not influence the kinetic traces at high iron(III) excess. The redox decomposition of the mononuclear complex $FeSO_3^+$ was found to be the key step and its rate constant could be determined more reliably than in previous studies.

Although direct structural information could not be obtained for the di- and tetranuclear intermediates, the reactivity patterns suggest that they contain a bridging ligand unit in addition to one hydroxo bridge. Matrix rank analysis of time-resolved spectral data were used to show that the di- and tetranuclear intermediates, with the exception of $Fe_2(OH)(SO_3)^{3+}$, do not have significant absorption in the wavelength range 300–450 nm.

7. Összefoglalás

Ezen doktori értekezés témája a vas(III) hidroxodimer, $Fe_2(\mu\text{-}OH)_2(H_2O)_8^{4+}$, ligandumszubsztitúciós reakcióinak kinetikája és mechanizmusa hipofoszfit-, foszfit-, foszfát-, arzenit-, arzenát-, szulfit-, szulfát-, és szelenitionnal. A kinetikai vizsgálatok nagy részét *stopped flow* (megállított áramlásos) módszerrel végeztük fotometriás detektálással a 270–450 nm-es hullámhossztartományban.

Megvizsgáltuk a vas(III) hidrolízisének egyensúlyát és kinetikáját. Megállapítottuk, hogy a vizes oldatban reprodukálhatóan tanulmányozható koncentrációtartományban a Fe^{3+}, $FeOH^{2+}$ és a $Fe_2(OH)_2^{4+}$ komplexek vannak jelen számottevő koncentrációban. Meghatároztuk a hidroxokomplexek stabilitási állandóit és az egyes vas(III)komplexek UV-látható spektrumát az általunk használt körülmények mellett. A hidroxodimer bomlásának és keletkezésének kinetikáját is tanulmányoztuk. Az eredmények alapján javasoltuk a korábban kidolgozott, kétlépéses mechanizmus kiegészítését egy harmadik lépéssel, ami elsősorban viszonylag nagyobb pH (> 1,8) esetén jelentős.

A vas(III)ion vizes oldatában található egy- és kétmagvú formák egymástól elválaszthatatlanok, így gyakran nehéz annak eldöntése, hogy melyik forma reakciójához rendelhető a fotometriásan detektált abszorbanciaváltozás egy-egy konkrét esetben. Ezért teszteljárást dolgoztunk ki a hidroxodimer ligandumszubsztitúciós reakcióinak azonosítására. A módszer két, egymást kiegészítő kinetikai kísérletben mért kezdeti abszorbanciaváltozás-sebesség összehasonlításán alapul. A két kísérletben ugyanolyan végösszetételű reakcióelegyet állítunk elő úgy, hogy a hidroxodimer kiindulási koncentrációja jelentősen különbözik. A két kezdeti sebesség hányadosa így jelzőszámként használható, amelynek 1.0-tól eltérő értéke azt mutatja, hogy a ligandumszubsztitúciós reakcióban az $Fe_2(OH)_2^{4+}$ közvetlen reaktánsként vesz részt. Mintegy 30 szervetlen ligandum esetében vizsgáltuk meg, hogy közvetlenül reagálnak-e a hidroxodimerrel. Az így azonosított reakciók kinetikáját részletesen tanulmányoztuk. Az esetek többségében megbízható vizsgálatokat csak 10.0 °C-on tudtunk végezni a *stopped flow* módszerrel, mert szobahőmérséklet közelében a folyamatok túl gyorsak voltak.

Meghatároztuk a kiválasztott ligandumok protonálódási állandóit és megvizsgáltuk, hogy a ligandumok és a vas(III)ion között végbemegy-e redoxireakció. A szulfition esetében a vas(III)ion redukciója viszonylag gyors volt. Kiemelkedő fontossága miatt ebben az esetben a redoxifolyamatok kinetikai leírását is célul tűztük ki. A többi rendszer közül az arzenition és a hipofoszfition esetén

tapasztaltuk a vas(III)ion redukálódását vas(II)ionná, de ezen folyamatok igen lassúak voltak, így nem zavarták a ligandumszubsztitúciós vizsgálatokat.

A vizsgált ligandumok vas(III)ionokkal egymagvú komplexeket képeznek, amelyekről kimutattuk, hogy nagy vas(III)felesleg mellett is jelentős mértékben keletkeznek. Irodalmi előzményekre támaszkodó spektrofotometriás eljárásokkal, külön kísérletsorozatban tanulmányoztuk ezen komplexek keletkezésének egyensúlyát és kinetikáját valamennyi ligandummal. A vizsgálatokat kellően kicsi teljes vas(III)koncentráció használatával végeztük, így a hidroxodimer koncentrációja és reakciói elhanyagolhatóak voltak. Az így nyert moláris abszorbanciákat, egyensúlyi és sebességi állandókat felhasználtuk a hidroxodimer reakcióinak értelmezése során.

Az értekezés fő részét a vas(III)felesleg mellet végzett részletes kinetikai vizsgálatok alkotják. A mérési eredmények kiértékeléséhez több reakciórendszer tapasztalatai alapján a következő általános modellt állítottuk fel:

$Fe_2(OH)_2^{4+} + L = Fe_2L$

$v_D = k_D[Fe_2(OH)_2^{4+}][L]_T - k_{-D}[Fe_2L]$

$Fe_2L = FeL + Fe_{mn}$

$v_S = k_S[Fe_2L] - k_{-S}[FeL][Fe_{mn}]$

$Fe_{mn} + L = FeL$

$v_M = k_M[Fe_{mn}][L]_T - k_{-M}[FeL]$

$Fe_2(OH)_2^{4+} = 2Fe_{mn}$

$v_H = k_H[Fe_2(OH)_2^{4+}] - k_{-H}[Fe_{mn}]^2$

Az egyenletekben Fe_2L kétmagvú vas(III)komplexet, míg FeL egymagvú vas(III)-komplexet jelöl. Ezen komplexek sztöchiometriai összetételét minden esetben meghatároztuk. Az arzenát- és foszfátionok esetében négymagvú köztitermékek keletkezését tapasztaltuk, és ennek értelmezésére a modellt a következő reakcióval egészítettük ki:

$Fe_2L + Fe_2(OH)_2^{4+} = Fe_4L$

Ezt a reakciót csak gyors előegyensúlyként lehetett kezelni a számítások során. Így az oda- és visszairányú reakciók sebességi állandójára nem kaptunk kinetikai információt, viszont a egyensúlyi állandót mind arzenát-, mind foszfátionnal meghatároztuk.

A modellben szereplő összes sebességi állandó függ a pH-tól. A v_M-re és v_H-ra vonatkozó egyenletekben szereplő sebességi állandókat független módszerrel határoztuk meg. k_D-t általában a görbék kezdeti szakaszából a teljes modell alkalmazása nélkül is ki tudtuk számítani. A pszeudo-elsőrendű görbékre alapozott, hagyományos kinetikai kiértékelési módszer csak a szulfátion és az arzenition

esetében volt alkalmazható. Ezekben az esetekben a kinetikai paramétereket a pszeudo-elsőrendű sebességi állandóra (k_{obs}) levezetett összefüggések alapján k_{obs} kísérleti értékeinek illesztésével határoztuk meg. Más rendszerekben a k_{-D}, k_S és k_{-S} sebességi állandókat az abszorbancia–idő görbéknek a modell által meghatározott differenciálegyenlet-rendszerre történő közvetlen illesztésével számítottuk a *ZiTa* vagy a *SCIENTIST* számítógépes programok segítségével. Az egyes sebességi állandók pH-függése alapján azonosítottuk a ligandumok különböző protonált formáival kapcsolatos reakcióutakat. Várakozásainknak megfelelően a ligandumok deprotonálódása minden esetben növelte a reakcióképességet.

A kvantitatív eredmények túlnyomó részét az $Fe_2(OH)_2^{4+}$ jellemző abszorpciós sávján végzett mérések alapján nyertük. A következő köztitermékeket azonosítottuk: $Fe_4(PO_4)(OH)_2^{7+}$, $Fe_4(AsO_4)(OH)_2^{7+}$, $Fe_2(OH)(SO_3)^{3+}$, $Fe_2(OH)(SeO_3)^{3+}$, $Fe_2(OH)(HPO_3)^{3+}$, $Fe_2(OH)(SO_4)^{3+}$, $Fe_2(OH)(H_2PO_2)^{4+}$, $Fe_2(OH)(H_2AsO_3)^{4+}$, $Fe_2(OH)(HPO_4)^{3+}$, $Fe_2(OH)(HAsO_4)^{3+}$. Az utolsó három részecske közvetlenül nem detektálható, jelenlétükre a kinetikai sajátságokból lehetett következtetni. A szulfitionnal képződő kétmagvú köztitermék, amelynek összetétele $Fe_2(OH)(SO_3)^{3+}$, kivételesnek bizonyult olyan szempontból, hogy ennek saját abszorpciós sávját tudtuk azonosítani 430 nm körül, így az $Fe_2(OH)_2^{4+}$ abszorpciós sávján végzett vizsgálatokat nagyon hasznos adatokkal tudtuk kiegészíteni. Az idő függvényében felvett UV-látható spektrunok alapján mátrixranganalízissel igazoltuk, hogy az $Fe_2(OH)(SO_3)^{3+}$ kivételével az egyes rendszerekben képződő két- és négymagvú köztitermékeknek nincsen jelentős elnyelése a 300 nm feletti hullámhossztartományban.

A szulfition és vas(III)ion közötti redoxireakciót is részletesen tanulmányoztuk nagy vas(III)felesleg mellett. Azt tapasztaltuk, hogy ilyen körülmények között a kinetikai görbék lefutására az oxigén jelenléte vagy annak kizárása nincsen hatással. A redoxireakció kulcslépése az egymagvú szulfitokomplex redoxibomlása:

$$FeSO_3^+ = Fe^{2+} + SO_3^{\cdot-}$$

Ez a reakció a sebességmeghatározó lépés a teljes redoxifolyamatban. Az általunk használt módszerrel a korábbi becsléseknél sokkal megbízhatóbban meg tudtuk határozni a folyamat sebességi állandóját. Kísérleti eredményeink szerint az $Fe_2(OH)(SO_3)^{3+}$ komplex közvetlenül nem vesz részt redoxireakcióban.

Arzenitionnal nem képződött detektálható vas(III)komplex, azonban az arzenition katalizálja a hidroxodimer képződését és bomlását. Ezt a kísérleti tapasztalatot úgy értelmeztük, hogy a korábbiakkal analóg komplexek itt is keletkeznek, csak sokkal kisebb koncentrációban.

Szulfátionnal a kétmagvú köztitermék képződése a *stopped flow* készülék holtidején, vagyis 1 ms-on belül végbement még 5.0 °C-on is bármely kiindulási

koncentrációknál, így erre a reakcióra kinetikai információt nem nyertünk, az abszorbanciaváltozások amplitúdója alapján azonban a megfelelő egyensúlyi állandót meg tudtuk határozni.

Azt tapasztaltuk, hogy az egyes ligandumok hidroxodimerrel való reakciójára vonatkozó másodrendű sebességi állandók elsősorban a reaktáns ligandum töltésétől függnek, s a különböző ligandumok azonos töltésű formáihoz tartozó sebességi állandók csak kevéssé különböznek egymástól. Az azonos ligandumok semleges és egyszeresen negatív formáihoz tartozó sebességi állandók közötti eltérés minden esetben egy nagyságrend körülinek adódott. Ezen eredmények jól értelmezhetők egy I_d típusú mechanizmussal. A sebességi állandók különbségét a reaktánsok közötti ionpárok stabilitásának különbsége magyarázza.

A két- és négymagvú köztitermékek szerkezetét közvetlenül vizsgálni nem tudtuk. Azonban az $Fe_2(OH)_2^{4+}$ reaktivitási jellegzetességei alapján valószínűsíthető, hogy ezen komplexekben a ligandum O–X–O részlete az egyik OH csoportot helyettesítve hídként kapcsol össze két vas(III)centrumot, amelyek a másik hidroxidionon keresztül is összekapcsolódnak.

8. References

The language of the original publication (when different from English) is given in parentheses after the reference. Abbreviations used: F: French, G: German, H: Hungarian, J: Japanese, P: Portuguese, R: Russian. When the original publication was not available to the author of this dissertation, works in which citations were found are given after the reference.

1. Andersson, K. K.; Gräslund, A. *Adv. Inorg. Chem.* **1995**, *43*, 359-408 and references therein.
2. Solomon, E. I. *Inorg. Chem.* **2001**, *40*, 3656-3669 and references therein.
3. Moënne-Loccoz, P.; Richter, O. M. H.; Huang, H. W.; Wasser, I. M.; Ghiladi, R. A.; Karlin, K. D.; de Vries, S. *J. Am. Chem. Soc.* **2000**, *122*, 9344-9345.
4. Neves, A.; Rossi, L. M.; Vencato, I.; Haase, W.; Werner, R. *J. Chem. Soc., Dalton Trans.* **2000**, 707-712.
5. Neves, A.; Terenzi, H.; Horner, R.; Horn Jr., A.; Szpoganicz, B.; Sugai, J. *Inorg. Chem. Commun.* **2001**, *4*, 388-391. Abstract on htttp:\\www.chemweb.com.
6. Harms, D.; Meyer, J.; Westerheide, L.; Krebs, B.; Karst, U. *Anal. Chim. Acta* **1999**, *401*, 83-90.
7. Nishino, S.; Hosomi, H.; Ohba, S.; Matsushima, H.; Tokii, T.; Nishida, Y. *J. Chem. Soc., Dalton Trans.* **1999**, 1509-1513.
8. Zhang, X.; Anderson, T. M.; Chen, Q.; Hill, C. L. *Inorg. Chem.* **2001**, *40*, 418-419.
9. Greenwood, N. N.; Earnshaw, A. *Chemistry of the Elements*; Pergamon Press: Oxford, U.K., 1984.
10. Richens, D. T. *Chemistry of Aqua Ions*; John Wiley & Sons: Chichester, U.K., 1997.
11. Burgess, J. *Metal Ions in Solution*; Ellis Horwood Ltd.: Chichester, U.K., 1978.
12. Cannon, R. D. *Electron Transfer Reactions*; Butterworth and Co. Ltd.: London, U.K., 1980.

13. *Mechanistic Aspects of Inorganic Reactions*; ACS Symposium Series No. 198; Rorabacher, D. B.; Endicott, J. F., Eds; Comstock, M. J., Series Ed.; American Chemical Society: Washington, D. C., U.S.A., 1982.

14. Wilkins, R. G. *Kinetics and Mechansism of Reactions of Transition Metal Complexes*; 2nd ed., VCH Publishers Inc.: New York, NY, U.S.A., 1991.

15. Sylva, R. N. *Rev. Pure Appl. Chem.* **1972**, *22*, 115-131. Cited in refs. 10, 22, 29, 37, 49, 52, 66, 77, no record found in Chemical Abstracts.

16. Cotton, S. A. *Coord. Chem. Rev.* **1972**, *8*, 184-223.

17. Flynn Jr., C. M. *Chem. Rev.* **1984**, *84*, 31-41.

18. Byrne, R. H.; Luo, Y. R.; Young, R. W. *Marine Chem.* **2000**, *70*, 23-35.

19. Cornell, R. M.; Giovanoli, R.; Schneider, W. *J. Chem. Tech. Biotechnol.* **1989**, *46*, 115-134. Cited in ref. 10 and Chemical Abstracts **1989**, *111*, 246631g.

20. Pykhteev, O. Y.; Efimov, A. A.; Moskvin, L. N. *Russ. J. Appl. Chem.* **1999**, *72*, 9-20 or *Zh. Prikl. Khim.* **1999**, *72*, 11-21 (R).

21. Hedström, B. O. A. *Arkiv Kemi* **1953**, *6*, 1-16.

22. Khoe, G. H.; Brown, P. L.; Sylva, R. N.; Robins, R. G. *J. Chem. Soc., Dalton Trans.* **1986**, 1901-1906.

23. Ciavatta, L.; Grimaldi, M. *J. Inorg. Nucl. Chem.* **1975**, *37*, 163-169.

24. Rabinowitch, E.; Stockmayer, W. H. *J. Am. Chem. Soc.* **1942**, *64*, 335-347.

25. Siddall, T. H.; Vosburgh, W. C. *J. Am. Chem. Soc.* **1951**, *73*, 4270-4272.

26. Mulay, L. N.; Selwood, P. W. *J. Am. Chem. Soc.* **1955**, *77*, 2693-2701.

27. Milburn, R. M.; Vosbourgh, W. C. *J. Am. Chem. Soc.* **1955**, *77*, 1352-1355.

28. Milburn, R. M. *J. Am. Chem. Soc.* **1957**, *79*, 537-540.

29. Knight, R. J.; Sylva, R. N. *J. Inorg. Nucl. Chem.* **1975**, *37*, 779-783.

30. Behar, B.; Stein, G. *Isr. J. Chem.* **1969**, *7*, 827-830.

31. Popa, G.; Luca, C.; Iosif, E. *Z. Phys. Chem. (Leipzig)* **1963**, *222*, 49-53 (G).

32. Hair, N. J.; Beattie, J. K. *Inorg. Chem.* **1977**, *16*, 245-250.

33. Beattie, J. K.; Best, S. P.; Skelton, B. W.; White, A. H. *J. Chem. Soc., Dalton Trans.* **1981**, 2105-2111.

34. Armstrong, R. S.; Beattie, J. K.; Best, S. P.; Braithwaite, G. P.; Del Favero, P.; Skelton, B. W.; White, A. H. *Aust. J. Chem.* **1990**, *43*, 393-398.

35. Sham, T. K.; Hastings, J. B.; Perlman, M. L. *Chem. Phys. Lett.* **1981**, *83*, 391-396.

36. Best, S. P.; Forsyth, J. B. *J. Chem. Soc., Dalton Trans.* **1990**, 395-400.

37. Herdman, G. J.; Neilson, G. W. *J. Phys.: Condens. Matter* **1992**, *4*, 627-638.

38. Magini, M. *J. Inorg. Nucl. Chem.* **1978**, *40*, 43-48.

39. Martin, R. L.; Hay, P. J.; Pratt, L. R. *J. Phys. Chem. A* **1998**, *102*, 3565-3573.

40. Schröder, D.; Bärsch, S.; Schwarz, H. *J. Phys. Chem. A* **2000**, *104*, 5101-5110.

41. Johnson, D. A.; Nelson, P. G. *Inorg. Chem.* **1999**, *38*, 4949-4955.

42. Acklin, P. *Helv. Chim. Acta* **2000**, *83*, 677-686.

43. Martinez, P.; van Eldik, R.; Kelm, H. *Ber. Bunsenges. Phys. Chem.* **1985**, *89*, 81-86.

44. Nadtochenko, V. A.; Kiwi, J. *Inorg. Chem.* **1998**, *37*, 5233-5238.

45. Pozdnyakov, I. P.; Glebov, E. M.; Plyusnin, V. F.; Grivin, V. P.; Ivanov, Y. V.; Vorobyev, D. Y.; Bazhin, N. M. *Pure Appl. Chem.* **2000**, *72*, 2187-2197.

46. Benkelberg, H. J.; Warneck, P. *J. Phys. Chem.* **1995**, *99*, 5214-5221.

47. Kopylovich, M. N.; Iponova, N. A.; Baev, A. K.; Kirillov, A. M. *Russ. J. Phys. Chem.* **2000**, *74*, 1268-1270 or *Zh. Fiz. Khim.* **2000**, *74*, 1409-1411 (R).

48. Feitknecht, W.; Michaelis, W. *Helv. Chim. Acta* **1962**, *45*, 212-224 (G).

49. Knight, R. J.; Sylva, R. N. *J. Inorg. Nucl. Chem.* **1974**, *36*, 591-597.

50. Biedermann, G.; Schindler, P. *Acta. Chem. Scand.* **1957**, *11*, 731-740.

51. Lamb, A. B.; Jacques, A. G. *J. Am. Chem. Soc.* **1938**, *60*, 1215-1225.

52. Feitknecht, W.; Giovanoli, R.; Michaelis, W.; Müller, M. *Z. Anorg. Allg. Chem.* **1975**, *417*, 114-124 (G).

53. Schugar, H.; Walling, C.; Jones, R. B.; Gray, H. B. *J. Am. Chem. Soc.* **1967**, *89*, 3712-3720.

54. Thompson, M.; Connick, R. E. *Inorg. Chem.* **1981**, *20*, 2279-2285.

55. Spiccia, L.; Stoeckli-Evans, H.; Marty, W.; Giovanoli, R. *Inorg. Chem.* **1987**, *26*, 474-482.

56. Merakis, T.; Murphy, A.; Spiccia, L.; Beguin, A.; Marty, W. *Helv. Chim. Acta* **1989**, *72*, 993-995.

57. Crimp, S. J.; Spiccia, L.; Krouse, H. R.; Swaddle, T. W. *Inorg. Chem.* **1994**, *33*, 465-470.

58. Ardon, M.; Plane, R. A. *J. Am. Chem. Soc.* **1959**, *81*, 3197-3198.

59. Daniele, P. G.; Rigano, C.; Sammartano, S.; Zelano, V. *Talanta* **1994**, *41*, 1577-1582.

60. Morrison, T. I.; Reis Jr., A. H.; Knapp, G. S.; Fradin, F. Y.; Chen, H.; Klippert, T. E. *J. Am. Chem. Soc.* **1978**, *100*, 3262-3264.

61. Magini, M.; Saltelli, A.; Caminiti, R. *Inorg. Chem.* **1981**, *20*, 3564-3565.

62. Morrison, T. I.; Shenoy, G. K.; Nielsen, L. *Inorg. Chem.* **1981**, *20*, 3565-3566.

63. Thich, J. A.; Ou, C. C.; Powers, D.; Vasiliou, B.; Mastropaolo, D.; Potenza, J. A.; Schugar, H. J. *J. Am. Chem. Soc.* **1976**, *98*, 1425-1433.

64. Borer, L.; Thalken, L.; Ceccarelli, C.; Glick, M.; Zhang, J. H.; Reiff, W. M. *Inorg. Chem.* **1983**, *22*, 1719-1724.

65. Johansson, G. *Acta Chem. Scand.* **1962**, *16*, 403-420.

66. Knudsen, J. M.; Larsen, E.; Moreira, J. E.; Nielsen, O. F. *Acta. Chem. Scand.* **1975**, *A 29*, 833-839.

67. Carrano, C. J.; Spartalian, K. *Inorg. Chem.* **1984**, *23*, 1993-1994.

68. Meagher, A. *Inorg. Chim. Acta* **1988**, *146*, 19-23.

69. Ujihira, Y.; Suzuki, Y. *Bunseki Kagaku* **1974**, *23*, 1028-1035 (J).

70. Vértes, A.; Ranogajec-Komor, M.; Gelencsér, P. *Acta Chim. (Budapest)* **1973**, *77*, 55-67.

71. Pan, H. K.; Yarusso, D. J.; Knapp, G. S.; Pineri, M.; Meagher, A.; Coey, J. M. D.; Cooper, S. L. *J. Chem. Phys.* **1983**, *79*, 4736-4745.

72. Schugar, H. J.; Rossman, G. R.; Gray, H. B. *J. Am. Chem. Soc.* **1969**, *91*, 4564-4566.

73. Cattrall, R. W.; Murray, K. S.; Peverill, K. I. *Inorg. Chem.* **1971**, *10*, 1301-1304.

74. Murray, K. S. *Coord. Chem. Rev.* **1974**, *12*, 1-35 and references therein.

75. Espenson, J. H.; Dustin, D. F. *Inorg. Chem.* **1969**, *8*, 1760-1763.

76. Fábián, I.; Gordon, G. *Inorg. Chem.* **1991**, *30*, 3994-3999.

77. Wilhelmy, R. B.; Patel, R. C.; Matijević, E. *Inorg. Chem.* **1985**, *24*, 3290-3297.

78. Below, J. F.; Connick, R. E.; Coppel, C. P. *J. Am. Chem. Soc.* **1958**, *80*, 2961-2967.

79. Lee, T. S.; Kolthoff, I. M.; Leussing, D. L. *J. Am. Chem. Soc.* **1948**, *70*, 3596-3600.

80. Fogg, P. G. T.; Hall, R. J. *J. Chem. Soc. (A)* **1971**, 1365-1370.

81. Grace, M. R.; Swaddle, T. W. *Inorg. Chem.* **1992**, *31*, 4674-4678.

82. Pandey, R. N.; Smith, W. MacF. *Can. J. Chem.* **1972**, *50*, 194-200.

83. Pouli, D.; Smith, W. MacF. *Can. J. Chem.* **1960**, *38*, 567-575.

84. Strahm, U.; Patel, R. C.; Matijević, E. *J. Phys. Chem.* **1979**, *83*, 1689-1695.

85. Accascina, F.; Cavasino, F. P.; Di Dio, E. *Trans. Faraday Soc.* **1969**, *65*, 489-495.

86. Carlyle, D. W.; Espenson, J. H. *Inorg. Chem.* **1967**, *6*, 1370-1376.

87. Seewald, D.; Sutin, N. *Inorg. Chem.* **1963**, *2*, 643-645.

88. Davis, G. G.; Smith, W. MacF. *Can. J. Chem.* **1962**, *40*, 1836-1845.

89. Espenson, J. H.; Helzer, S. R. *Inorg. Chem.* **1969**, *8*, 1051-1053.

90. Biruš, M.; van Eldik, R. *Inorg. Chem.* **1991**, *30*, 4559-4563.

91. Hasinoff, B. B. *Can. J. Chem.* **1979**, *57*, 77-82.

92. Martinez, P.; van Eldik, R. *Ber. Bunsenges. Phys. Chem.* **1985**, *89*, 728-734.

93. Grant, M.; Jordan, R. B. *Inorg. Chem.* **1981**, *20*, 55-60.

94. Swaddle, T. W.; Merbach, A. E. *Inorg. Chem.* **1981**, *20*, 4212-4216.

95. Helm, L.; Merbach, A. E. *Coord. Chem. Rev.* **1999**, *187*, 151-181 and references therein.

96. Hemmes, P.; Rich, L. D.; Cole, L. C.; Eyring, E. M. *J. Phys. Chem.* **1971**, *75*, 929-932.

97. Hynes, M. J.; Ó Coinceanainn, M. *J. Inorg. Biochem.* **2001**, *85*, 131-142.

98. Qureshi, M. S.; Kazmi, S. A. *J. Chem. Soc. Pak.* **1998**, *20*, 175-178.

99. Kislenko, V. N.; Oliinyk, L. P. *Rus. J. Gen. Chem.* **2000**, *70*, 570-573 or *Zh. Obshchei Khim.* **2000**, *70*, 611-614 (R).

100. Sommer, B. A.; Margerum, D. W. *Inorg. Chem.* **1970**, *9*, 2517-2521.

101. Po, H. N.; Sutin, N. *Inorg. Chem.* **1971**, *10*, 428-431.

102. Wendt, H. *Z. Elektrochem.* **1962**, *66*, 235-239 (G).

103. Wendt, H. *Inorg. Chem.* **1969**, *8*, 926-927.

104. Lutz, B.; Wendt, H. *Ber. Bunsenges. Phys. Chem.* **1970**, *74*, 372-380.

105. Conocchioli, T. J.; Hamilton Jr., E. J.; Sutin, N. *J. Am. Chem. Soc.* **1965**, *87*, 926-927.

106. Sisley, M. J.; Jordan, R. B. *Inorg. Chem.* **1991**, *30*, 2190-2195.

107. Chatlas, J.; Jordan, R. B. *Inorg. Chem.* **1994**, *33*, 3817-3822.

108. Sisley, M. J.; Jordan, R. B. *Inorg. Chem.* **1995**, *34*, 6015-6023.

109. Biruš, M.; Kujundžić, N.; Pribanić, M. *Inorg. Chim. Acta* **1981**, *55*, 65-69.

110. Xu, J.; Jordan, R. B. *Inorg. Chem.* **1988**, *27*, 1502-1507.

111. Secco, F.; Venturini, M. *Polyhedron* **1999**, *18*, 3289-3293.

112. Secco, F.; Venturini, M.; Fanelli, N. *Ann. Chim. (Rome)* **1999**, *89*, 129-136.

113. Løgager, T.; Holcman, J.; Sehested, K.; Pedersen, T. *Inorg. Chem.* **1992**, *31*, 3523-3529.

114. Ondrus, M. G.; Gordon, G. *Inorg. Chem.* **1972**, *11*, 985-989.

115. Bacchi, A.; Ivanovic-Burmazovic, I.; Pelizzi, G.; Andjelkovic, K. *Inorg. Chim. Acta* **2001**, *313*, 109-119.

116. Sowrey, F. E.; Tilford, C.; Wocadlo, S.; Anson, C. E.; Powell, A. K.; Bennington, S. M.; Montfrooij, W.; Jayasooriya, U. A.; Cannon, R. D. *J. Chem. Soc., Dalton Trans.* **2001**, 862-866.

117. Chen, W. H.; Wei, H. H.; Lee, G. H.; Wang, Y. *Polyhedron* **2001**, *20*, 515-521.

118. Gao, E. Q.; Yin, L. H.; Tang, J. K.; Cheng, P.; Liao, D. Z.; Jiang, Z. H.; Yan, S. P. *Polyhedron* **2001**, *20*, 669-673.

119. Seddon, E. J.; Yoo, J.; Folting, K.; Huffman, J. C.; Hendrickson, D. N.; Christou, G. *J. Chem. Soc., Dalton Trans.* **2000**, 3640-3648.

120. Aneetha, H.; Panneerselvam, K.; Liao, T. F.; Lu, T. H.; Chung, C. S. *J. Chem. Soc., Dalton Trans.* **1999**, 2689-2694.

121. Raptopoulou, C. P.; Tangoulis, V.; Psycharis, V. *Inorg. Chem.* **2000**, *39*, 4452-4459.

122. Westerheide, L.; Müller, F. K.; Than, R.; Krebs, B.; Dietrich, J.; Schindler, S. *Inorg. Chem.* **2001**, *40*, 1951-1961.

123. Hagadorn, J. R.; Que Jr., L.; Tolman, W. B. *J. Am. Chem. Soc.* **1999**, *121*, 9760-9761.

124. He, C.; Barrios, A. M.; Lee, D.; Kuzelka, J.; Davydov, R. M.; Lippard, S. J. *J. Am. Chem. Soc.* **2000**, *122*, 12683-12690.

125. Lee, D.; Lippard, S. J. *J. Am. Chem. Soc.* **2001**, *123*, 4611-4612.

126. Kwak, B.; Lah, M. S. *Bull. Korean. Chem. Soc.* **2000**, *21*, 65-68.

127. Mandel, A.; Schmitt, W.; Womack, T. G.; Bhalla, R.; Henderson, R. K.; Heath, S. L.; Powell, A. K. *Coord. Chem. Rev.* **1999**, *190-192*, 1067-1083 and references therein.

128. Furutachi, H.; Ohyama, Y.; Tsuchiya, Y.; Hashimoto, K.; Fujinami, S.; Uehara, A.; Suzuki, M.; Maeda, Y. *Chem. Let.* **2000**, 1132-1133.

129. Arii, H.; Nagatomo, S.; Kitagawa, T.; Miwa, T.; Jitsukawa, K.; Einaga, H.; Masuda, H. *J. Inorg. Biochem.* **2000**, *82*, 153-162.

130. Krutz Jr., D. M. *Chem. Rev.* **1990**, *90*, 585-606 and references therein.

131. Wilkinson, E. C.; Dong, Y.; Que Jr., L. *J. Am. Chem. Soc.* **1994**, *116*, 8394-8395.

132. Sutton, J. *Nature* **1952**, *169*, 71-72.

133. Pascal, J. L.; Favier, F. *Coord. Chem. Rev.* **1998**, *178-180*, 865-902 and references therein.

134. Fábián, I.; Gordon, G. *Inorg. Chem.* **1992**, *31*, 2144-2150.

135. Gordon, G.; Tewari, P. H. *J. Phys. Chem.* **1966**, *70*, 200-204.

136. Everett, K. G.; Skoog, D. A. *Anal. Chem.* **1971**, *43*, 1541-1547.

137. Covington, A. K.; Bates, R. G.; Durst, R. A. *Pure Appl. Chem.* **1983**, *55*, 1467-1476.

138. Irving, H. M.; Miles, M. G.; Pettit, L. D. *Anal. Chim. Acta* **1967**, *38*, 475-488.

139. Pócsi, I.; Fábián, I. *J. Chem. Soc., Dalton Trans.* **1988**, 2231-2233.

140. Tonomura, B.; Nakatani, H.; Ohnishi, M.; Yamaguchi-Ito, J.; Hiromi, K. *Anal. Biochem.* **1978**, *84*, 370-383.

141. Lente, G. *Komplexképződés a vas(III) – szulfition reakció kezdeti szakaszában*; M.Sc. Thesis, Lajos Kossuth University: Debrecen, Hungary, 1997 (H).

142. Applied Photophysics SX.18MV Stopped Flow Reaction Analyser User Handbook, Hardware Section, Last Revised: 6th August 19998.

143. Dickson, P. N.; Margerum, D. W. *Anal. Chem.* **1986**, *58*, 3153-3158.

144. Dunn, B. C.; Meagher, N. E.; Rorabacher, D. B. *J. Phys. Chem.* **1996**, *100*, 16925-16933.

145. Lin, C.; Rorabacher, D. B. *J. Phys. Chem.* **1974**, *78*, 305-308.

146. Meagher, N. E.; Rorabacher, D. B. *J. Phys. Chem.* **1994**, *98*, 12590-12593.

147. Paul, C.; Kirschner, K.; Haenisch, G. *Anal. Biochem.* **1980**, *101*, 442-448.

148. Peintler, G.; Nagy, A.; Horváth, A. K.; Körtvélyesi, T.; Nagypál, I. *Phys. Chem. Chem. Phys.* **2000**, *2*, 2575-2586.

149. Lente, G.; Fábián, I. *unpublished results*.

150. Zékány, L.; Nagypál, I. in *Computational Methods for the Determination of Formation Constants*; Legett, D. J., Ed.; Plenum Press: New York, 1985, pp. 291-299.

151. *SCIENTIST*, version 2.0; Micromath Software: Salt Lake City, UT, USA, 1995.

152. *ZiTa*, version 4.1. by Peintler, G.; Attila József University: Szeged, Hungary, 1997.

153. Ainsworth, S. *J. Phys. Chem.* **1961**, *65*, 1968-1972.

154. Coleman, J. S.; Varga, L. P.; Mastin, S. H. *Inorg. Chem.* **1970**, *9*, 1015-1020.

155. Hugus Jr., Z. Z.; El-Awady, A. A. *J. Phys. Chem.* **1971**, *75*, 2954-2957.

156. Katakis, D. *Anal. Chem.* **1965**, *37*, 876-878.

157. Wallace, R. M. *J. Phys. Chem.* **1960**, *64*, 899-901.

158. Wallace, R. M.; Katz, S. M. *J. Phys. Chem.* **1964**, *68*, 3890-3892.

159. Peintler, G.; Nagypál, I.; Jancsó, A.; Epstein, I. R.; Kustin, K. *J. Phys. Chem. A* **1997**, *101*, 8013-8020.

160. Maeder, M.; Zuberbühler, A. D. *Anal. Chem.* **1990**, *62*, 2220-2224.

161. *Matlab for Windows*, Version 4.2c1; The Mathworks Inc.: Natick, MA, USA, 1994.

162. Espenson, J. H. *Chemical Kinetics and Reaction Mechanisms*; McGraw-Hill Inc.: New York, NY, U.S.A., 1995.

163. Sillén, L. G.; Martell, A. E. *Stability Constants of Metal Ion Complexes*; Special Publication No. 17, Chemical Society: London, 1964 and Supplement 1, 1971 and references therein.

164. *Stability Constants of Metal-Ion Complexes, Part A.; Inorganic Ligands*; IUPAC Chemical Data Series No. 21; Högfeldt, E., Ed.; Pergamon: Oxford, U.K., 1982 and references therein.

165. Brandt, C.; Fábián, I.; van Eldik, R. *Inorg. Chem.* **1994**, *33*, 687-701.

166. Morris, D. F. C.; Hedger, T. J.; Watson, P. A. *J. Inorg. Nucl. Chem.* **1971**, *33*, 2077-2083.

167. Buist, G. J.; Lewis, J. D. *Chem. Commun.* **1965**, 66-67.

168. Kren, R. M.; Dodgen, H. W.; Nyman, C. J. *Inorg. Chem.* **1968**, *7*, 446-451.

169. Taylor, J. E. *J. Phys. Chem. A* **1998**, *102*, 2172-2176.

170. Campbell, M. J. M.; Nyman, C. J. *Inorg. Chem.* **1962**, *1*, 842-844.

171. Britton, H. T. S.; Jackson, P. *J. Chem. Soc.* **1934**, 1048-1055.

172. Arnek, R.; Barcza, L. *Acta Chem. Scand.* **1972**, *26*, 213-217.

173. Khoe, G. H.; Robins, R. G. *J. Chem. Soc., Dalton Trans.* **1988**, 2015-2021.

174. Frei, V.; Podlahová, J.; Podlaha, J. *Collection Czechoslov. Chem. Commun.* **1964**, *29*, 2587-2596 (G).

175. Tartar, H. V.; Garretson, H. H. *J. Am. Chem. Soc.* **1941**, *63*, 808-816.

176. Grzybowski, A. K. *J. Phys. Chem.* **1958**, *62*, 555-559.

177. Frydman, M.; Nilsson, G.; Rengemo, T.; Sillén, L. G. *Acta Chem. Scand.* **1958**, *12*, 878-884.

178. Sellers, P.; Sunner, S.; Wadsö, I. *Acta Chem. Scand.* **1964**, *18*, 202-206.

179. Masalovich, V. M.; Agasyan, P. K.; Nikolaeva, E. R. *Zh. Neorgan. Khim.* **1966**, *11*, 272-277 (R).

180. Hamada, S.; Ishikawa, Y.; Shirai, T. *Nippon Kagaku Zasshi* **1965**, *86*, 1042-1046 (J). Cited in ref. 163 and Chemical Abstracts **1966**, *64*, 10739g.

181. Filatova, L. N. *Zh. Neorg. Khim.* **1974**, *19*, 3335-3339 (R).

182. Kraft, J.; van Eldik, R. *Inorg. Chem.* **1989**, *28*, 2297-2305.

183. Pilipenko, A. T.; Ivashchenko, L. N. *Zh. Obshchei Khim.* **1956**, *26*, 656-660 (R).

184. Galal-Gorchev, H.; Stumm, W. *J. Inorg. Nucl. Chem.* **1963**, *25*, 567-574.

185. Filatova, L. N.; Chepelevetskii, M. L. *Zh. Neorg. Khim.* **1966**, *11*, 1662-1668 (R).

186. Holroyd, A.; Salmon, J. E. *J. Chem. Soc.* **1957**, 959-963.

187. Ciavatta, L.; Iuliano, M.; Porto, R. *Ann. Chim. (Rome)* **1992**, *82*, 447-461.

188. Barcza, L.; Sillén, L. G. *Acta Chem. Scand.* **1971**, *25*, 1250-1260.

189. Horner, D. A.; Connick, R. E. *Inorg. Chem.* **1986**, *25*, 2414-2417.

190. Nyberg, B.; Larsson, R. *Acta Chem. Scand.* **1973**, *27*, 63-70.

191. Golding, R. M. *J. Chem. Soc.* **1960**, 3711-3716.

192. Connick, R. E.; Tam, T. M.; von Deuster, E. *Inorg. Chem.* **1982**, *21*, 103-107.

193. Betts, R. H.; Voss, R. H. *Can. J. Chem.* **1970**, *48*, 2035-2041.

194. Tolmachev, Y. V.; Scherson, D. A. *J. Phys. Chem. A* **1999**, *103*, 1572-1578.

195. Bishenden, E.; Donaldson, D. J. *J. Phys. Chem. A* **1998**, *102*, 4638-4642.

196. Pezza, H. R.; Lopes, C. F. F.; Suárez-Iha, M. E. V.; Coichev, N. *Quim. Nova* **1999**, *22*, 529-540 (P) and references therein.

197. Brandt, C.; van Eldik, R. *Chem. Rev.* **1995**, *95*, 119-190 and references therein.

198. Bäckström, H. L. J. *Z. Phys. Chem.* **1934**, *25B*, 122-138 (G).

199. Job, P. *Ann. Chim.* **1928**, *9*, 113-203 (F).

200. Carlyle, D. W.; King, E. L. *Inorg. Chem.* **1970**, *9*, 2333-2339.

201. van Eldik, R.; von Jouanne, J.; Kelm, H. *Inorg. Chem.* **1982**, *21*, 2818-2820.

202. Moritzen, P. A.; El-Awady, A. A.; Harris, G. M. *Inorg. Chem.* **1985**, *24*, 313-318.

203. Magalhães, M. E. A.; Lente, G.; Fábián, I. *Highly labile sulphito complexes of chromium(III)*; poster presented at the 34th International Conference on Coordination Chemistry, July 9-14, 2000, Edinburgh, UK.

204. Choi, S. N.; Carlyle, D. W. *Inorg. Chem.* **1974**, *13*, 1818-1823.

205. Larsson, L. O.; Niinistö, L. *Acta Chem. Scand.* **1973**, *27*, 859-867.

206. Loehr, T. M.; Plane, R. A. *Inorg. Chem.* **1968**, *7*, 1708-1714.

207. Fuoss, R. M. *J. Am. Chem. Soc.* **1958**, *80*, 5059-5061.

208. Boudalis, A. K.; Lalioti, N.; Spyroulias, G. A.; Raptopoulou, C. P.; Terzis, A.; Tangoulis, V.; Perlepes, S. P. *J. Chem. Soc., Dalton Trans.* **2001**, 955-957.

209. Li, M. X.; Jin, S. L.; Liu, H. Z.; Xie, G. Y.; Chen, M. Q.; Xu, Z.; You, X. Z. *Polyhedron* **1998**, *17*, 3721-3725.

210. Zima, V.; Lii, K. H. *J. Chem. Soc., Dalton Trans.* **1998**, 4109-4112.

Scientific Publications of Gábor Lente

(in reverse chronological order)

Publications connected to this dissertation

6. Gábor Lente, István Fábián
Ligand Substitution Kinetics of the Iron(III) Hydroxo Dimer with Simple Inorganic Ligands
submitted to *Inorg. Chem.*

5. Gábor Lente, István Fábián
Kinetics and Mechanisms of the Oxidation of Sulfur(IV) by Iron(III) at Metal Ion Excess
submitted to *J. Chem. Soc., Dalton Trans*., invited paper in a 2002 issue connected to the conference Dalton Discussion 4.

4. Gábor Lente, István Fábián
A simple test to confirm the ligand substitution reactions of the hydrolytic iron(III) dimer
Reaction Kinetics and Catalysis Letters, **2001**, *73*, 117–125.

3. Gábor Lente, M. Elizabeth A. Magalhaes, István Fábián
Kinetics and Mechanism of Complex Formation Reactions in the Iron(III)–Phosphate Ion System at Large Iron(III) Excess. Formation of a Tetranuclear Complex
Inorganic Chemistry, **2000**, *39*, 1950–1954.

2. Gábor Lente, István Fábián
A New Reaction Path in the Dissociation of the $Fe_2(\mu\text{-}OH)_2(H_2O)_8^{4+}$ Complex
Inorganic Chemistry, **1999**, *38*, 603–605.

1. Gábor Lente, István Fábián
The Early Phase of the Iron(III) Sulfite Ion Reaction. The Formation of a Novel Iron(III)–Sulfito Complex
Inorganic Chemistry, **1998**, *37*, 4204–4209.

Publications not connected to this dissertation

6. Gábor Lente, James H. Espenson
Kinetics and Mechanism of Oxygen Transfer to Methyl(oxo)dithiolato-rhenium(V) Complexes
Inorganic Chemistry, **2000**, *39*, 4809–4814.

5. Gábor Lente, Xiao-Peng Shan, Ilia A. Guzei, James H. Espenson
Syntheses and Structures of Rhenium(IV) and Rhenium(V) Complexes with Ethanedithiolato Ligands
Inorganic Chemistry, **2000**, *39*, 3572–3576.

4. Gábor Lente, Ilia A. Guzei, James H. Espenson
Kinetics and Mechanism of the Monomerization of a Re(V) Dithiolato Dimer with Monodentate Ligands. Electronic and Steric Effects
Inorganic Chemistry, **2000**, *39*, 1311–1319.

3. Gábor Lente, Josemon Jacob, Ilia A. Guzei, James H. Espenson
Kinetics and Crystallographic Studies of the Ligand Monomerization of a Dithiolato(methyl)(oxo)rhenium(V) Dimer
Inorganic Reaction Mechanisms, **2000**, *2*, 169–177.

2. Josemon Jacob, Gábor Lente, Ilia A. Guzei, James H. Espenson
Monomerization of a Rhenium(V) Dimer by Ligation
Inorganic Chemistry, **1999**, *38*, 3762–3763.

1. Gábor Lente, A. Mark Dobbing, David T. Richens
Kinetic Studies of Water Exchange and Substitution by NCS^- on the Sulfur-capped Triangular Ion $[Mo_3(\mu_3\text{-}S)(\mu\text{-}O)_3(OH_2)_9]^{4+}$
Inorganic Reaction Mechanisms, **1998**, *1*, 3–16.

REACTIONS OF THE IRON(III) HYDROXO DIMER WITH INORGANIC LIGANDS

(A VAS(III) HDIROXODIMER REAKCIÓI SZERVETLEN LIGANDUMOKKAL)

Értekezés a doktori (Ph.D.) fokozat megszerzése érdekében
a *Kémia* tudományágban

Írta: *Lente Gábor* okleveles *vegyész*

Készült a Debreceni Egyetem *Kémiai* doktori iskolája
(*Koordinációs kémiai* programja) keretében

Témavezető: *Dr. Fábián István*

A doktori szigorlati bizottság:

elnök: Dr. .....
tagok: Dr. .....
Dr. .....

A doktori szigorlat időpontja: .....

Az értekezés bírálói:

Dr. .....
Dr. .....
Dr. .....

A bírálóbizottság:

elnök: Dr. .....
tagok: Dr. .....
Dr. .....
Dr. .....
Dr. .....

Az értekezés védésének időpontja: .....